

FACULDADE DE ENGENHARIA DA UNIVERSIDADE DO PORTO

Optical surface roughness measurement techniques for industrial applications

Frederico Preto Direito



Mestrado Integrado em Engenharia Mecânica

Supervisor: Dr. Paulo Tavares

Second Supervisor: Prof. Mário Vaz

March 9, 2021

Optical surface roughness measurement techniques for industrial applications

Frederico Preto Direito

Mestrado Integrado em Engenharia Mecânica

March 9, 2021

Abstract

Surface roughness is a material surface's property that affects the component behavior, internally, affecting mechanical properties, and externally, possibly affecting the performance of the system in which the component is included. The most common surface roughness methods require contact with the material, damaging the surface, if the material is softer than the contacting instrument, and are restricted to a single line profile. As such, it is necessary for supplementary methods to be developed, in order to measure surface roughness without damaging the material's surface, and acquire information from the whole surface. Optical techniques for surface roughness measurements are a subject on the rise, as they don't need any contact to perform the measurements, while measuring the whole surface, not merely a single line profile. These techniques also remain affordable, compared to other common non-contact methods such as Scanning Probe Microscopy and Electron Microscopy methods, which require expensive hardware and software. The referred optical techniques contain one fundamental shortcoming: as these usually require multiple captures of the same reflection pattern, and the minimal displacement causes this pattern to change, any vibration may render the measurement inaccurate. There are special methods to eliminate vibration influence, but these usually come at a price.

The present work aims to develop an affordable and effective optical surface roughness measurement technique that is to be employed in an industrial environment. As such, a single capture method is picked, speckle pattern analysis. Speckle pattern analysis is originally a technique that also required multiple captures but, with some adaptation, transforming it to a single capture method was feasible. Allied to Haralick's parameters, that translate image information into statistical properties, it is possible to accurately obtain the surface roughness value. Maintaining the economic factor in mind, a method has been developed.

Two different software packages were experimented with, Matlab and MVTec's Halcon, in order to obtain a more diverse set of results. The system components were usual optical paraphernalia, such as a laser beam, a collimator with an integrated pin hole, and an optical lens, with a monochromatic camera to capture the images. Algebraic manipulation of the image information on the softwares was performed in order to transform a black and white image into statistical properties, which received further treatment. The chosen method to ascertain the quality of the measurements was a linear regression with the different values obtained.

In the end, with the proper calibration, measurements with a negligible error ratio were achieved, with an R-squared value of almost 1 in some cases. The value range in which the measurement is possible was approximately between the dozens of nanometers to roughly one hundred micrometers. It is then concluded that, as long as the surface that is to be examined possesses a surface roughness value inside of the range set in calibration, an accurate and precise estimation of its surface roughness will be obtained.

Keywords: surface roughness measurement, optical techniques, contactless techniques, speckle pattern analysis, Haralick's parameters

“To become good at anything you have to know how to apply basic principles. To become great at it, you have to know when to violate those principles.”

Garry Kasparov

“We can only see a short distance ahead, but we can see plenty there that needs to be done.”

Alan Turing

Acknowledgements

We are currently living in trying times, as the Covid-19 pandemic is happening. The development of this thesis started while the outbreak was already a constant in our lives, but nevertheless this has been a period of adaptation and constant struggle.

The thesis I am presenting is a product of hard work and dedication, even with the outside factors that escape my control. However, the merit of this project isn't all my own. There is a select group of people that helped me along the path that today brings me here.

To those who shaped, molded, and made me into what I am today, or helped me in any way or form, this section is dedicated to you.

To the Engineering Faculty of the University of Porto, and University of Porto in general, for allowing the wonderful ride that these last five years and a half have been. I will probably never find another academic institution like this one, and I will dearly treasure all the moments I spent here for the rest of my life.

To Dr. Paulo Tavares and Prof. Mário Vaz, for their availability, guidance, counseling, experience, and constant support throughout the thesis development period, even to answer to my ridiculously out of work hours e-mails or Team's messages.

To my friends, which are too many to list, for always being there to support and help me, no matter the subject or hour; for allowing me to enjoy myself in the company of those whom I hold dear; for all the good laughs and conversations we ever had. I hold all my friendships with great care and always will for the future to come, and I hope you keep allowing me to be around you.

To my girlfriend, for being who she is; for caring about me unconditionally; for handling all my bad moods and tiredness; for allowing me to live through things I hadn't experienced yet.

And finally, to my family, for being a constant pillar of support on my academic pursues, no matter how difficult times may be; for teaching me all the virtues and qualities that I currently possess (the bad personality traits are purely my own fault, my parents and sisters are angels); for showing me that there is always more to life than books and computers; for everything.

Life is full of hardships, but going on is easier if you're surrounded by those you love.

Frederico Preto Direito

Contents

1	Introduction	1
1.1	Motivation	2
1.2	Objectives	3
1.3	Structure / Organization	4
1.4	Host	4
2	Surface Roughness	7
2.1	Defining Surface Roughness	8
2.2	The Importance of Surface Roughness	12
2.3	Surface Roughness Measurement	14
2.3.1	Mechanical Profilometer Method	14
2.3.2	Optical Methods	15
2.3.3	Scanning Probe Microscopy Methods	15
2.3.4	Fluid Methods	18
2.3.5	Electrical Methods	19
2.3.6	Electron Microscopy Methods	19
2.3.7	Comparison of the Methods	21
3	Optical Techniques	23
3.1	Speckle Patterns	24
3.2	Interferometry	24
3.3	Image Analysis	27
3.3.1	Analysis Statistics	27
3.4	Softwares	32
3.5	Optical Methods	32
3.5.1	Taper-Sectioning Method	33
3.5.2	Light-Sectioning Method	33
3.5.3	Specular Reflection Methods	34
3.5.4	Diffuse Reflection (Scattering) Methods	35
3.5.5	Speckle Pattern Method	38
3.5.6	Optical Interference Method	38
3.5.7	Choosing a Method	43
4	Methodology	45
4.1	Physical Assembly	45
4.2	Samples	49
4.2.1	Rugotest No. 3	49
4.2.2	Paint Comparator	50

4.3	Captured Images	51
4.4	Adjustments to Speckle Pattern Techniques	53
4.5	Image processing	55
4.5.1	Matlab	56
4.5.2	MVTec Halcon	61
4.5.3	Excel	67
4.6	Conclusion	68
5	Results and Discussion	69
5.1	Evaluation Framework	69
5.2	Possible influence on the result's quality	72
5.3	Measurement Results	74
5.3.1	Surface group 1 - Paint Comparator	75
5.3.2	Surface group 2 - Rugotest No. 3 (coarse grain)	81
5.3.3	Surface group 3 - Rugotest No. 3 (fine grain)	87
5.3.4	Surface group 4 - Paint Comparator and Rugotest No. 3 (coarse grain)	93
5.3.5	Surface group 5 - Paint Comparator and Rugotest No. 3 (fine grain)	100
5.4	Results Discussion	107
6	Conclusions and Future Work	109
6.1	Future Work	111
6.1.1	Components	112
6.1.2	System operation	113
	References	117
A	Technical Datasheet for the Paint Comparator	123
B	Technical Datasheet for the Rugotest No. 3	129
C	Developed scripts for Matlab's image analysis	133
D	Developed scripts for MVTEC Halcon's image analysis	147
D.1	MVTEC Halcon's script	147
D.2	Matlab's script	154

List of Figures

2.1	Different degrees of roughness on a surface [16].	8
2.2	Roughness and Waviness in a surface [18].	9
2.3	"SEM micrograph of a stylus trace on a turned aircraft aluminum alloy" [16].	9
2.4	Single line surface profile [17].	10
2.5	Origin of a crack on a surface defect [30].	13
2.6	Graphical representation of already pointed out profilometer's lack of resolution, providing results with poor accuracy.	15
2.7	STM apparatus proposed by Binning and Rohrer [44].	16
2.8	Surface reconstruction from an STM scan [46].	17
2.9	STM or AFM tip close to a sample [45].	18
2.10	Illustration of the probe for pneumatic gaging [48].	19
2.11	Surfaces captured by an electron microscope [51].	20
2.12	Surface map performed by Backscattered Electron Signals [52].	21
3.1	Reflection of a light beam, credits given in the image.	24
3.2	Speckle pattern [54].	25
3.3	Results of wave superimposition in (a) waves with the same phase (b) waves with a phase difference of half a wavelength.	25
3.4	Schematic of a Michelson interferometer [56].	26
3.5	Interferometry fringes (credits to openstax CNX).	27
3.6	Grayscale Matrix [61].	28
3.7	Gray-Tone Spatial-Dependence matrix structure, in any given direction [61].	29
3.8	Gray-Tone Spatial-Dependence matrix for the horizontal direction [61].	29
3.9	Gray-Tone Spatial-Dependence matrix for the (a) 45° direction. (b) 90° direction. (c) 135° direction [61].	29
3.10	Example of a light slit for the light-sectioning method [63].	34
3.11	High-reflectance diffuse integrated sphere [69].	36
3.12	Angular distribution mechanism developed by Vorburger [73].	37
3.13	Example of an interferometer for fringe creation, the Twyman-Green interferometer [78].	39
3.14	Adapted Twyman-Green interferometer for PSI analysis [81].	40
3.15	Fringe patterns from (a) plane surfaces (b) spherical surfaces [81].	40
3.16	Example of an algorithm for PSI analysis [81].	41
3.17	Example of a CSI instrument (credits to the NPL - "A National Measurement Good Practice Guide", No.108).	42
3.18	Schematic of the obtained information from the CSI process (credits to the NPL - "A National Measurement Good Practice Guide", No.108).	43
4.1	Source of coherent light, the laser.	46

4.2	The Collimator + Pinhole component (a) Pinhole (b) Mounted component	47
4.3	The light beam (a) Unfiltered (b) Filtered with the collimator and pinhole setup.	47
4.4	Biconvex lens (a) Mounted in the assembly (b) Unmounted	48
4.5	Camera and lens setup (a) Mounted in the assembly (b) Camera (c) Lens	48
4.6	System disposition (a) Laser turned off (b) Laser turned on	49
4.7	Rugotest No. 3.	50
4.8	Paint Comparator.	51
4.9	Speckle pattern example, with a distance of 4 cm and maximum iris range.	52
4.10	Speckle pattern example, with a distance of 4 cm and an iris range of F16.	52
4.11	Output of the Matlab script for speckle pattern analysis.	61
4.12	Text file generated in MVTec Halcon.	65
5.1	Contrast measurements obtained from the Comparator surfaces' analysis, at a distance of 12cm and iris range F22.	70
5.2	Linear regression performed on the data set from Contrast measurements obtained from the Comparator surfaces' analysis, at a distance of 12cm and iris range F22.	71
5.3	Contrast measurements obtained from the Comparator surfaces' analysis, at a distance of 8cm and maximum iris range.	72
5.4	Linear regression performed on the data set from Contrast measurements obtained from the Comparator surfaces' analysis, at a distance of 8cm and maximum iris range.	73
5.5	Evolution of the different Haralick's parameters with distance, for all iris ranges, for the Matlab analysis of surface group 1.	77
5.6	Evolution of the different Haralick's parameters with distance, for all iris ranges, for the MVTec's Halcon analysis of surface group 1.	80
5.7	Evolution of the different Haralick's parameters with distance, for all iris ranges, for the Matlab analysis of surface group 2.	83
5.8	Evolution of the different Haralick's parameters with distance, for all iris ranges, for the MVTec's Halcon analysis of surface group 2.	86
5.9	Evolution of the different Haralick's parameters with distance, for all iris ranges, for the Matlab analysis of surface group 3.	89
5.10	Evolution of the different Haralick's parameters with distance, for all iris ranges, for the MVTec's Halcon analysis of surface group 3.	92
5.11	Evolution of the different Haralick's parameters with distance, for all iris ranges, for the Matlab analysis of surface group 4.	95
5.12	Evolution of the different Haralick's parameters with distance, for all iris ranges, for the MVTec's Halcon analysis of surface group 4.	99
5.13	Evolution of the different Haralick's parameters with distance, for all iris ranges, for the Matlab analysis of surface group 5.	102
5.14	Evolution of the different Haralick's parameters with distance, for all iris ranges, for the MVTec's Halcon analysis of surface group 5.	106
6.1	Rough sketch of a behavioral GRAFCET that describes the functioning of the system. . .	116

List of Tables

3.1	Optical methods comparison [17].	43
4.1	Analysis Groups	54
5.1	Evaluation of the quality of the obtained R-squared values for the Matlab analysis of surface group 1.	75
5.2	R-squared values obtained from Matlab analysis of surface group 1.	76
5.3	Evaluation of the quality of the obtained R-squared values for the MVTEC's Halcon analysis of surface group 1.	78
5.4	R-squared values obtained from Halcon analysis of surface group 1.	79
5.5	Evaluation of the quality of the obtained R-squared values for the Matlab analysis of surface group 2.	81
5.6	R-squared values obtained from Matlab analysis of surface group 2.	82
5.7	Evaluation of the quality of the obtained R-squared values for the MVTEC's Halcon analysis of surface group 2.	84
5.8	R-squared values obtained from Halcon analysis of surface group 2.	85
5.9	Evaluation of the quality of the obtained R-squared values for the Matlab analysis of surface group 3.	87
5.10	R-squared values obtained from Matlab analysis of surface group 3.	88
5.11	Evaluation of the quality of the obtained R-squared values for the MVTEC's Halcon analysis of surface group 3.	90
5.12	R-squared values obtained from Halcon analysis of surface group 3.	91
5.13	Evaluation of the quality of the obtained R-squared values for the Matlab analysis of surface group 4.	93
5.14	R-squared values obtained from Matlab analysis of surface group 4.	94
5.15	Evaluation of the quality of the obtained R-squared values for the MVTEC's Halcon analysis of surface group 4.	96
5.16	R-squared values obtained from Halcon analysis of surface group 4.	98
5.17	Evaluation of the quality of the obtained R-squared values for the Matlab analysis of surface group 5.	100
5.18	R-squared values obtained from Matlab analysis of surface group 5.	101
5.19	Evaluation of the quality of the obtained R-squared values for the MVTEC's Halcon analysis of surface group 5.	103
5.20	R-squared values obtained from Halcon analysis of surface group 5.	105

List of Algorithms

4.1	Matlab analysis - General variable initialisation	57
4.2	Matlab analysis - Storing the images in Matlab's memory	57
4.3	Matlab analysis - Cropping of the introduced images	57
4.4	Matlab analysis - Calculation of the Intensity for each image	57
4.5	Matlab analysis - Creation of the Gray Level Co-occurrence Matrices for each image	58
4.6	Matlab analysis - Calculation of Contrast and Energy for each image	58
4.7	Matlab analysis - Vector concatenation for each statistical parameter, for each surface section's group analysis	59
4.8	Matlab analysis - Plotting of the graphics for individual group analysis control . .	59
4.9	Matlab analysis - Linear regression for each parameter for the Comparator	60
4.10	Matlab analysis - Concatenation of each parameter's linear regression errors for the Comparator	60
4.11	Matlab analysis - Matrix creation for all linear regression analysis' error	60
4.12	MVTec's Halcon analysis - Storing the images in Halcon's memory	61
4.13	MVTec's Halcon analysis - Cropping of the introduced images	62
4.14	MVTec's Halcon analysis - Calculation of the Intensity for each image	62
4.15	MVTec's Halcon analysis - Creation of the Gray Level Co-occurrence Matrices in all four directions and calculation of Contrast and Energy for each direction . . .	63
4.16	MVTec's Halcon analysis - Calculation of the average Energy and Contrast with values from the four established directions	63
4.17	MVTec's Halcon analysis - Concatenation of the vectors containing information about each image, and generation of the text file containing them	63
4.18	MVTec's Halcon analysis - Opening the text files generated by Halcon in Matlab's environment	64
4.19	MVTec's Halcon analysis - Obtaining the surface information from the text file .	65
4.20	MVTec's Halcon analysis - Vectors containing surface roughness values for each section group were created	65
4.21	MVTec's Halcon analysis - Concatenation of the parameters values for each image into vectors	65
4.22	MVTec's Halcon analysis - Plotting of the graphics for individual group analysis control	66
4.23	MVTec's Halcon analysis - Linear regression for each parameter for the Comparator	66
4.24	MVTec's Halcon analysis - Concatenation of each parameter's linear regression errors for the Comparator	67
4.25	MVTec's Halcon analysis - Matrix creation for all linear regression analysis' error	67
C.1	Matlab script in its entirety for Matlab analysis	133
D.1	Halcon script in its entirety for MVTec's Halcon analysis	147
D.2	Matlab script in its entirety for MVTec's Halcon analysis	154

Abbreviations and Symbols

Abbreviations

AA	Arithmetic Average
AD	Angular Distribution
AFM	Atomic Force Microscopy
BES	Backscattered Electron Signal
CLA	Center Line Average
DCT	Discrete Cosine Transform
GLCM	Gray Level Co-occurrence Matrix
GRAFCET	Graphe Fonctionnel de Commande, Étapes Transitions
INEGI	Institute of Science and Innovation in Mechanical and Industrial Engineering
LVD	Linear Variable Differential Transformer
PSI	Phase Shifting Interferometry
PZT	Piezo electric material (Lead zirconate titanate)
RMS	Root Mean Square
RTO	Research and Technology Organization
SPM	Scanning Probe Microscopy
STM	Scanning Tunneling Microscopy
TIS	Total Integrated Scatter
UMAI	Advanced Monitoring and Structural Integrity Unit

Symbols

σ	Surface roughness variance
λ	Light's wavelength
θ_i	Beam's angle of incidence
ϕ	Desired Phase
I	Intensity Distribution
I_O	Object beam intensity
I_R	Reference beam intensity
K	Kurthosis
L	Length of the measured profile
m	Mean line of surface height
R	Specular reflectance in the angle of incidence
R_0	Total reflectance of the rough surface
R_a	Arithmetic mean deviation of the assessed profile
R_{ku}	Kurthosis
R_p	Maximum peak height
R_{pm}	Average peak-to-mean height
R_q	Root mean square
R_{sk}	Skewness
R_t	Maximum peak-to-valley height
R_v	Maximum valley depth
R_z	Average peak-to-valley height
R-squared	Indicator of the linear regression's quality
Sk	Skewness

Chapter 1

Introduction

The present project aims to develop a contactless method for surface roughness measurements, using optic analysis techniques and image processing software, such as Matlab and MVTec Halcon, in an industrial setting. The initial intent is to analyze samples with a known surface roughness, using a system whose key components are a laser, that shines a coherent light beam on the sample, and a camera, for image capture. In order to achieve the best possible accuracy, and considering the environment in which the system is to be implemented, a number of experiments with diverse optic analysis methods and components have been set, while also varying the different factors that might impact the measurement, such as the distances between sample and camera, as well as the iris range, which corresponds to the camera's lens aperture, ultimately responsible for the registered speckle size. The experimental setup has been kept as simple as possible, to promote the industrial ease of deployment and acceptance. The captured images will then be analysed and deconstructed in statistical properties that have been previously established, whose variations will be studied and compared to the known surfaces, calculating a direct relation between the reflected light's statistical properties and the sample's surface roughness. Additionally, and considering once again the industrial environment, an attempt to automate the whole process, from calibrating to obtaining the sample's surface roughness, will be discussed.

This chapter will brief the reader on the current undertaking, stating the motivation and reasoning behind the development of this project and the main objectives to be attained. It also presents the order in which the dissertation was structured, with a short characterization of each chapter, establishing a clear overview of the topics that are to be approached. At the end of this chapter, a short description of the setting of this work as proposed by the host institution, INEGI (Institute of Science and Innovation in Mechanical and Industrial Engineering), will be presented, along with the limitations endured during the experimental work, mostly due to the SARS-COV2 outbreak that imposed severe restrictions on the work.

1.1 Motivation

Surface roughness is an important characteristic in every mechanical element or system, as it possesses a great effect on general material's mechanical properties, behaviour and surface finish, which is important for commercial objectives. [1–6]. As such, measuring surface roughness for product quality control, is a standard and vital procedure in today's industry. These procedures can be divided into two main groups: contact (mechanical) and non-contact approaches [7, 8].

The most common approach to measure surface roughness is the mechanical profilometer, a contact method, which consists on tracing the surface of the element in interest with a stylus instrument [9]. The pen's diamond head constantly oscillates due to the height difference in the measured surface, generating electrical outputs that are sent to the processing unit, thus arithmetically calculating the surface roughness of the sample. As it's been said, this is the most common method of measuring roughness, although it possesses several disadvantages, such as its measurement precision, which is limited by the diameter of the tip of the pen, as the tip may not be able to access the full profile of deep valleys (low points); the state of the product's surface finish, as it may be susceptible to damage by running the stylus pen through the material, if it's sensitive to any kind of contact with other surfaces; and the efficiency of this process, which features a low cadence, as the pen has to slowly travel through the surface, from one end to the other. This approach to measuring roughness is also limited to a 1-dimensional measurement, as a 2-dimensional measurement would require a very large number of runs, as you'd need to cover the whole surface with a small pen to obtain an accurate measurement.

Due to the drawbacks and limitations of the presented mechanical method, the main one being the possibility of damaging the measured element's surface, there has been a rise on the interest of optical systems and other techniques to measure surface roughness in recent years, giving birth to the non-contact approaches [10]. These optical methods usually consist on shining a coherent light source on the surface of the element, through a physical mechanism composed of elements to reflect or divide the light beam (such as mirrors and beam splitters) and manipulate the diameter of the beam, creating light speckles when the light rays are scattered as they hit the sample's surface. These light speckles are captured using a camera and analyzed afterwards with the use of image processing software, to estimate the surface roughness by comparing the statistic properties of light variations with the surface roughness variation.

The first attempt of estimating the roughness with optical methods was performed in 1972, by Sprague [11], finding the correlation between the contrast of light speckles, which is a statistic property of the captured image, and the material's surface roughness. In 1978, Asakura [12] largely expanded this initial discovery with a series of experiments dedicated to studying the statistical properties of light speckles variations and correlating the values to the surface roughness. Thus, the first optical methods for surface roughness measurements were established, based on the principles of interferometry and formation of light speckles. Although similar and based on the same principles, Asakura's and Sprague's methods were different. With the development of other optical approaches to surface roughness measurement, they ended up complementing each

other's [13].

In current times, computer's processing power has largely evolved, thus overcoming the issues related to computational burden and leading into newer forms of analysis of the light speckles, faster and more precise. With the rise of the subject of biomechanics, and biomaterials being more and more common, the non-contact approaches have been gaining attraction on today's industry, as these biomaterials are usually quite sensitive to contact with other surfaces, making it impossible or quite difficult to measure the roughness without damaging the material with contact methods. Nevertheless, these are usually only utilized in experimental environments, and are also usually quite expensive, even though the research on the subject has been expanding. This project focuses on developing an optical approach to the measurement of surface roughness that is affordable, capable of a quick cadence and can accurately estimate the surface roughness of the any sample's surface in the order of the micrometer, for industrial applications such as found in the metallurgical or paint industries.

1.2 Objectives

The main objective of this project has been already presented above, as the development of an optical approach to measure the surface roughness of any surface, that fits in a production line. Ergo, this process must possess a high cadence, obtain precise results and be as affordable as possible. More specifically, the main objectives of the present project can be summarized in the following keypoints:

- Define which optical technique or techniques the development of the non-contact approach will be based on;
- Develop and refine a functioning physical mechanism based on the defined optical techniques that will enable the use of the technique in an industrial setting, shining a laser beam on the sample that is to be measured and capture the generated light speckles;
- Develop a script based on the image processing software that will estimate the surface roughness through the use of different statistic properties and is easily deployed in an industry setting;
- Validate the system by testing it on surfaces whose surface roughness had been previously measured;
- Refine both the physical mechanism and the virtual processing in order to obtain the most accurate measurements possible;
- Explore the possibility of an automated system in order to calibrate and integrate the mechanism in an industrial environment.

1.3 Structure / Organization

The present dissertation will be organized in the following order:

- **Chapter 2** states the importance of surface roughness in today's industry, presenting several applications in which surface roughness directly affects the properties of the material and the system in which it's used, as well as the available contact and contactless measurement methods;
- **Chapter 3** briefly reviews important knowledge regarding light dispersion, ranging from the basics of speckle formation to interferometry, while also presenting important concepts for image processing, that are thoroughly used in the development of the project, through image processing softwares. Followingly, an introduction of the possible optical techniques and physical systems for the study of interferometry in general is performed, detailing which can be applied to the measurement of surface roughness while explaining their operation, as well as justifying the choice for the current work
- **Chapter 4** fully presents the established methodology developed in the project, demonstrating its implementation, first by introducing the physical setup, listing every component present in the mechanism while also stating its function; secondly by introducing the image processing softwares in Matlab and MVTec Halcon, as well as the scripts developed in order to obtain the statistical properties of the captured images, with a step-by-step explanation;;
- **Chapter 5** presents the results obtained from the stated methodology, comparing both image processing softwares, Matlab and MVTec Halcon, as well as discussing its adequacy in an industry environment, considering the underlying factors that affected the measurements, such as distances and iris range, evaluating the accuracy of the method;
- **Chapter 6** states the final conclusions from the developed project, as well as pointing out further work which can be done in order to improve the results obtained regarding the project, such as them the physical mechanism, the developed software, or both. There is also a section dedicated to the exploration of the possibility of automating the system, presenting the planification developed for the referred purpose, in the form of GRAFCET, as well as stating the technical requirements and components necessary to build an automated system, depending on the degree of automation that is requested, resulting in an upgrade of the methodology that was presented in Chapter 4;

1.4 Host

The present project was proposed by UMAI (Advanced Monitoring and Structural Integrity Unit), as the author was ending a one year internship in this unit of INEGI, the Institute of Science and Innovation in Mechanical and Industrial Engineering, which is a Research and Technology Organization (RTO) with the mission to transfer technology to the industry. Possessing a team

dedicated to working with optical techniques and image processing, the proposed project perfectly fit UMAI's objectives and competences, as the necessary equipment for the project development had already been previously acquired for multiple other projects.

The work was developed in the midst of the Covid-19 outbreak, and even though INEGI's - and, more specifically, UMAI's - installations quickly adapted to the pandemic conditions, the project still ended up suffering some delays and time restraints due to obligatory lockdowns and remote working.

Chapter 2

Surface Roughness

The physical property that stands at the core of this work is surface roughness. Therefore, prior to the introduction of more in-depth concepts that will refer to surface roughness, it is important to have a deep understanding of this physical phenomenon, how it's quantified, how it influences the materials and mechanical systems in general, and how it can be measured.

The present chapter starts by explaining what Surface Roughness is, introducing physical phenomena that create the disparity in height on the surface finish; an historical framework to further understand the importance of quantifying roughness; what kind of influence it might have on mechanical systems, either advantageous or disadvantageous; and, finally, how it is usually measured, in a broad coverage of the diverse measurement methods.

From this review, it is intended to provide the basic foundations required to delve deeper into the development of the project, establishing the importance of surface roughness, and fully comprehending the physical phenomena that allows the optical analysis in surface roughness measurement.

2.1 Defining Surface Roughness

A solid material will always have a degree of irregularity or deviation at its surface, independently of how it was fabricated. No machining or surface finish method can completely nullify these surface irregularities, which can range from actual shape deviations to the order of interatomic distances. Thus, no perfectly flat surface exists [14, 15].

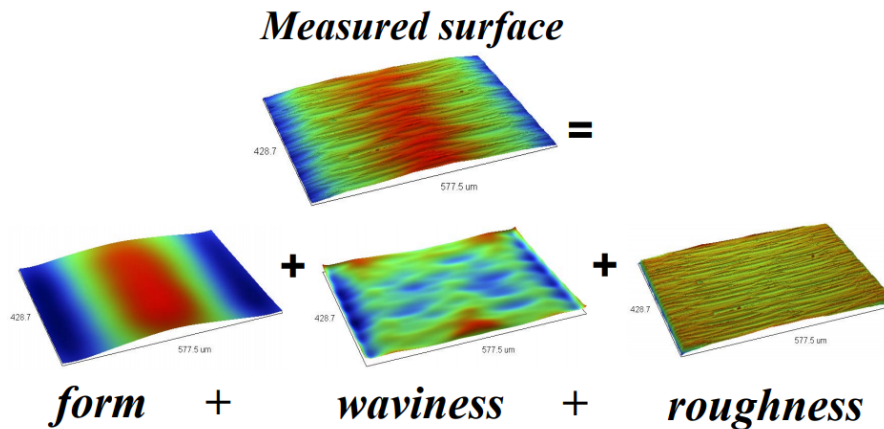


Figure 2.1: Different degrees of roughness on a surface [16].

In 1994, David Whitehouse [15] points out three different surface irregularity classes: Roughness, Waviness and Errors of Form. In 1999, Bharat Bhushan [14, 17] adapts the irregularity classes Whitehouse had established, advancing five different degrees of surface irregularities, still used to this day. Presented in growing order of wavelengths, these were:

- Surface Roughness, also called micro or nano-roughness, which is commonly caused by the manufacturing process. These irregularities can be caused by, for example, a tool mark left on the surface during the fabrication of the material, as it might be observed in Figure 2.3 or marks left by the surface finish processes, such as grinding or polishing;
- Surface Waviness (also called macro-roughness), is a defect that can be caused by an improper manufacturing process. These irregularities can be caused by, for example, a vibration between the workpiece and the mechanism that is performing the manufacturing process;
- Lay, which is the principal direction of the predominant surface pattern, ordinarily determined by the production method;
- Flaws, which are unwanted interruptions in the texture of the sample's surface;
- Errors of form, gross deviations from the planned shape of the sample's surface, which can be caused by many different factors, such as thermal distortion or errors in slideways. Errors of form may or may not be considered as part of the surface texture.

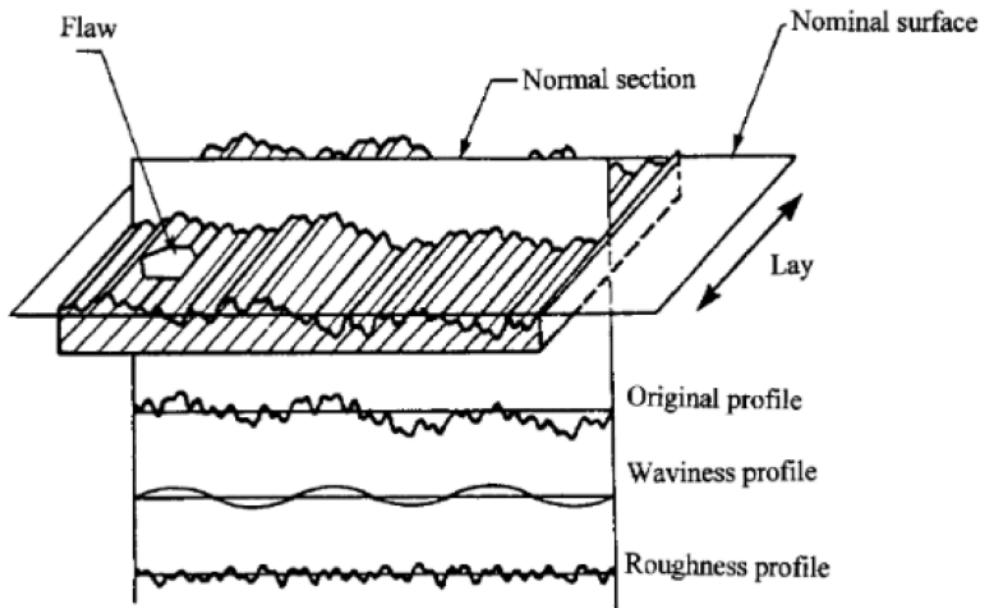


Figure 2.2: Roughness and Waviness in a surface [18].

It is not entirely correct to approach these classes of irregularities as completely independent from each other, even though the causes for their formation are majorly different [15, 19]. For the sake of convenience, surface roughness, or micro-roughness, will be described and assessed, as if it was completely independent, and no other type of deviation is present in the sample's surface. Thus, waviness, lays, flaws and errors of form will be ignored and treated as if they don't influence micro-roughness.

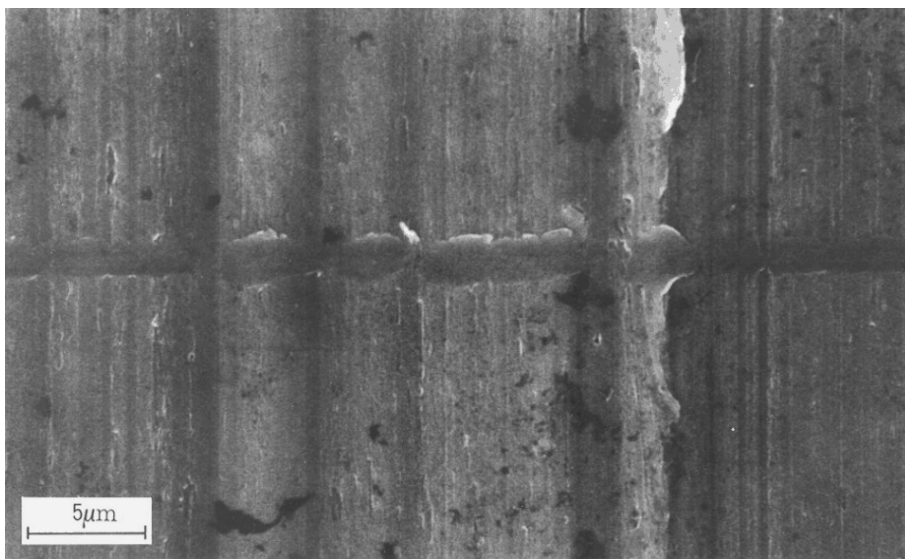


Figure 2.3: "SEM micrograph of a stylus trace on a turned aircraft aluminum alloy" [16].

Then, micro-roughness will now be focused. To correctly access micro-roughness, depending on the chosen measurement method, the measurements are either made in a single line profile across the sample's surface, or in multiple parallel lines profiles, these being called surface maps. A single line profile usually looks like the one represented in Figure 2.4, containing high points, which are called asperities or peaks, and low points, called valleys. Two lines can also be observed: the reference line, which is the origin of the height measurements, and the mean line, which is the average height of the surface, i.e., the sum of the areas delimited by the height profile below the line is equal to the sum of the areas above the line [14, 15].

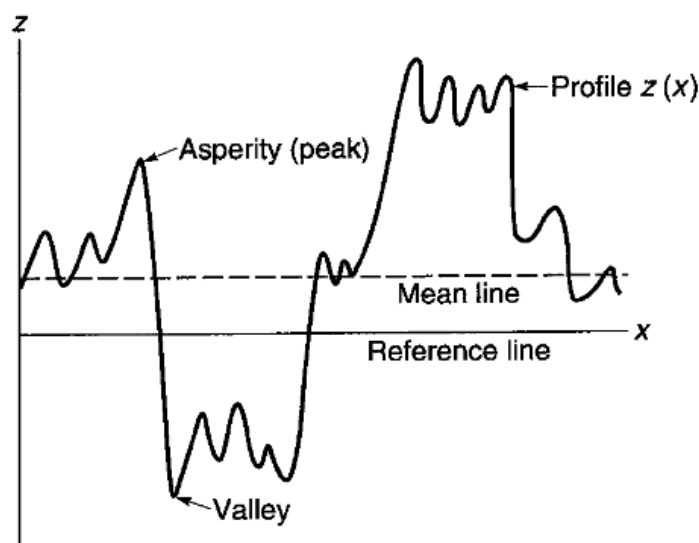


Figure 2.4: Single line surface profile [17].

With these concepts established, the statistical height descriptors of a surface, or the properties that quantify surface roughness, can be introduced. The most commonly used ones are the center-line average (CLA, or R_a , also known as arithmetic average), the standard deviation or variance (σ), and the root mean square (RMS or R_q) [20]. If the function is a probability distribution, the zeroth moment is the total probability (i.e., one), the first moment is the expected value, the second central moment is the variance, the third standardized moment is the skewness (Sk , or R_{sk}), and the fourth standardized moment is the kurtosis (K , or R_{ku}). The last two referred parameters, skewness and kurtosis, are then mainly utilized in the study of the amplitude probability distribution and other density functions of the height profile of a surface, which won't be focused on during this project.

There are multiple other properties that can help describe a material's surface roughness, such as R_t , the maximum peak to valley height, R_p , or maximum peak height, the distance between the highest asperity and the mean line, R_v , or maximum valley depth, the distance between the mean line and the lowest valley, R_z , or average peak to valley height, the distance between the

averages of five highest asperities and the five lowest valleys, and R_{pm} , or average peak-to-mean height, the distance between the averages of the five highest asperities and the mean line [14, 17, 21]. Specifically, this set of five properties is only required for highly technical applications, as sometimes the average roughness just isn't enough to accurately describe the surface, given that it is calculated as an average deviation in the vertical axis. For applications where the maximum height of asperities and minimum depth for valleys is important, such as for tribological purposes, these properties might be used as they provide that information [22, 23].

Among all the properties presented, the center-line average or R_a , is the far more common one, even though it might be due to historical reasons - the first profilometers only had the capacity to calculate the average height, and nothing else [24]. As it's been referred, the center line-average is the arithmetic mean of the absolute value of the height values, measured from the mean line, which is usually enough information for general applications. Assuming L is the length of the measured profile along direction x , the center-line average can be calculated by:

$$R_a = CLA = AA = \frac{1}{L} \int_0^L |z - m| dx \quad (2.1)$$

where

$$m = \frac{1}{L} \int_0^L z dx \quad (2.2)$$

Assuming again that L is the length of the measured profile, and m is calculated as in equation 2.2, variance can be calculated by:

$$\sigma^2 = \frac{1}{L} \int_0^L (z - m)^2 dx \quad (2.3a)$$

$$= R_q^2 - m^2 \quad (2.3b)$$

where σ is the standard deviation and R_q , or the root mean square, is the square root of the arithmetic mean of the square of the height disparity, measured from the reference line, is calculated by:

$$R_q^2 = RMS^2 = \frac{1}{L} \int_0^L (z^2) dx \quad (2.4)$$

In the special case that m coincides with the reference line, i.e., m equals zero, then the variance is equal to the root mean square.

Another note to add is that for the usual material surfaces' used in mechanical engineering (Gaussian surfaces), R_a and σ have a relation that can be approximated to

$$\sigma \approx \sqrt{\frac{\pi}{2}} R_a \approx 1.25 R_a \quad (2.5)$$

Even though the current project won't focus on skewness and kurtosis, as it's been referred, the equations to calculate these properties, respectively, are still established as

$$Sk = \frac{1}{\sigma^3 L} \int_0^L (z-m)^3 dx \quad (2.6)$$

$$K = \frac{1}{\sigma^4 L} \int_0^L (z-m)^4 dx \quad (2.7)$$

On a final note, it's important to refer that, for surface maps, any average roughness parameter can be calculated in a similar mathematical approach to the one presented here for a surface profile [14, 17].

2.2 The Importance of Surface Roughness

In this section, there will be a brief presentation of several applications where surface roughness is an extremely important property, as it greatly affects whatever result that is expected to achieve [25]. These cases were chosen as they greatly differ in the scientific area they are applied to, ranging from mechanical fields, such as fatigue strength, to the most unexpected areas, such as heat transfers.

Starting with properties commonly found in mechanical engineering fields, there have been a lot of findings directly relating the average surface roughness (R_a) and many mechanical properties, such as tensile strength [26], or fatigue strength [27, 28], the later highlighted as the most important one. It is well known surface topology plays a great role in fatigue resistance. Several studies have been made in hopes of isolating the effect of surface roughness on the propagation of fatigue cracks. When being tested for fatigue resistance, most materials would start showing cracks exactly at the roots of the most pronounced valleys of the surface. Any type of surface indentation functions as a stress concentrator, fomenting the origin of such cracks. Furthermore, it could be shown that the material would start suffering from the propagation of these cracks a lot more if the valleys had high deepness values, as expected. Thus, it can be easily concluded that higher R_a values translate into worse fatigue resistance. In fact, a method of testing the material in order to avoid any fatigue cracks on the surface of any material caused by surface roughness was developed. It consisted of making a single micrometric notch on the sample, simulating a single valley on the surface, proceeding with the usual tests. The sample with the artificial micrometric notch had always a lower fatigue strength than any specimen of the same material with natural surface roughness, setting the threshold for fatigue resistance [27–30].

Still in the field of mechanical engineering, another property that is greatly affected by surface roughness is adhesion; in this case, diverse literature suggests that surface roughness is a beneficial factor that contributes to adhesion [31, 32]. In fact, surface roughness enables polymeric adhesives to form a better adhesive bond with the material's surface, resulting in a higher fracture energy of the joint. This can be explained by the increase of the spreading coefficient, that results from surface roughness, as it raises the contact area between the material and the adhesive. However, if

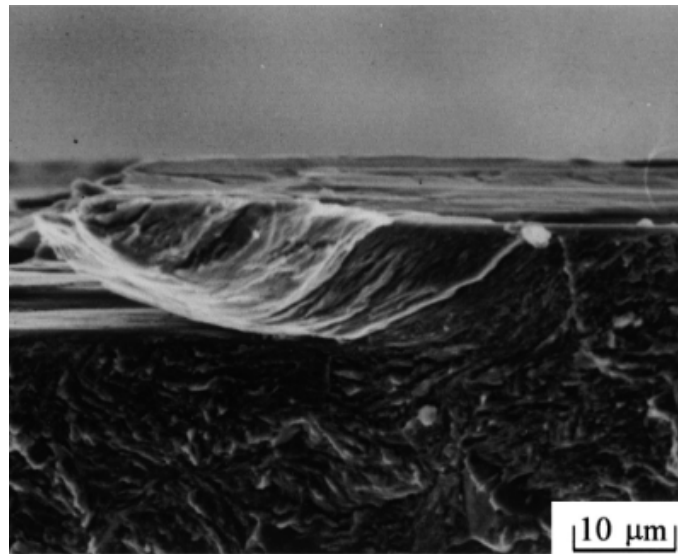


Figure 2.5: Origin of a crack on a surface defect [30].

the adhesive is not spread correctly, the formation of pores in the narrowest valleys may happen. Thus, one must be careful with artificial surface roughening for adhesion purposes, as it may have an adverse effect, if not handled carefully.

In the field of heat transfers, surface roughness is also a quite important property. Two examples will be given, one of a boiling system, the other of air heating.

The process of heating a container with liquid inside is in itself a classic example of the process of boiling, a common heat transfer problem. At the surface that is being heated, bubble formations can be observed, due to its surface roughness. This bubble formation can be directly related to heat transfer coefficients, i.e., the formation of bubbles at the heated surface directly affects the heat transfer that is being studied, translating into an indirect relation between surface roughness and the heat transfer process; surface roughness promotes heat transfer through the increase in bubble formation, again due to the increase in effective area [33].

Another example of heat transfer process that is affected by surface roughness are the solar thermal systems. In these systems, an air flow is heated by solar radiation, raising its temperature in the process. It's been concluded that raising the surface roughness or altering surface roughness geometry in the surface of the tube where exists the airflow greatly increases the efficiency of the system, by raising the heat transfer coefficients while not slowing the velocity of airflow by a significant amount. In general, surface roughness is a beneficial factor in heat transfer applications, and as it was pointed out in relation to adhesion applications, the creation of artificial surface roughness or even manipulating surface roughness geometry is quite common [34].

As it has been shown, there are several many other applications where surface roughness is an important factor, from the most different scientific and technological fields (materials' mechanical properties, heat transfers, adhesion, atomic dispersion, fluid mechanics, etc.), not always directly affecting the final outcome, but also indirectly affecting other properties that are intrinsic to the

final result, in negative or positive ways [35–38]. Hence, the historical interest in the manipulation of surface roughness, reducing it through processes of grinding or polishing in case it's unwanted, or raising it using sandblasting or sanding processes.

2.3 Surface Roughness Measurement

As it has been already referred, there is a large diversity of surface roughness measurement methods. Historically, the mechanical profilometer was the first one to be refined, and is to this day the most commonly used method. To compensate for its shortcomings, other methods were introduced throughout the years, creating several different options [39]. A brief presentation of some of the options will be listed, explaining its functioning and limitations, starting with the mechanical profilometer.

2.3.1 Mechanical Profilometer Method

The most common method, as well as the most documented, the mechanical profilometer, is preferred due to its economic cost and capacity for obtaining quick results. For most of the applications, the information provided by this process might be enough, as it provides a quick, and accurate, feedback on the general state of the surface finish, up to a degree. Most of the literature about surface roughness usually contains a brief exposure of this method, as it is a cornerstone in surface roughness measurement [11, 13–15, 17].

Mechanical profilometers provide measurements in one dimension, operating by moving a stylus at a constant speed through a surface, from one end to another in a single line - the movement performed in the x axis. A diamond tip is the component that makes contact with the surface, oscillating vertically, according to the surface topology - the movement performed in the y axis. That vertical movement is transformed into a digital signal through the use of external electronics, being amplified and communicated to a separate computer that registers the information given by the stylus. Depending on the envisaged resolution of the measurement, additional electronics or position sensors might be added, such as an LVDT sensor. The information recorded by the computer will result in a graphic where the x axis corresponds to the length of the surface that was measured, and the y axis corresponds to the surface's height. The resulting line, which will be called profile, is a good representation of the surface topology.

However, the mechanical profilometer possesses three important shortcomings:

- The need for contact - the stylus must come into contact with the material surface. In case the material is softer than the stylus head, the material's surface might be damaged;
- The resolution - as the measurement is made with the stylus, it can only 'fit' in valleys that are wider than the stylus head's diameter. If the valley is narrower than the stylus' head, the measurement won't be accurate. A graphical representation may be observed in Figure 2.6;

- The restriction to a single line profile - to obtain a reading, the stylus must travel from one end of the surface to the other, restricting the readings to a single line profile. In case we need to make a surface map, we'd need to run as many tests as needed to cover the whole surface, which is quite an efficient process.

As such, it has been necessary to develop other surface roughness measurement methods that can compensate these shortcomings [13, 17].

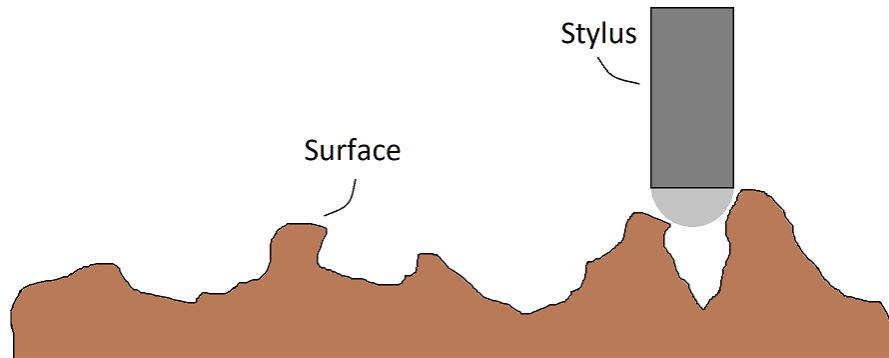


Figure 2.6: Graphical representation of already pointed out profilometer's lack of resolution, providing results with poor accuracy.

2.3.2 Optical Methods

Optical methods are approaches that generally consist on focusing a light wave on a sample's surface, and capturing the resulting reflection with a camera. These captured images are then analyzed and converted into a matrix of grayscale values, to calculate pre-established statistical properties using those grayscale values, which are, in turn, used to calculate surface roughness. They generally fix all three of the mechanical profilometer shortcomings, as there is usually no need for contact with the material's surface; the resolution, although also limited, is higher than that of the profilometer; and it measures the surface as a whole and not only a single line profile, allowing surface maps to be easily built [13, 17, 39].

These methods will be further explained in Chapter 3, after addressing the required Optical concepts.

2.3.3 Scanning Probe Microscopy Methods

There are two main techniques related to Scanning Probe Microscopy (SPM) methods: Scanning Tunneling Microscopy, or STM, and Atomic Force Microscopy, or AFM [17, 40, 41].

STM is based on the principle of electron tunneling (proposed by Giaver in 1960 [42]), which states that if a potential difference is applied between two metals that are separated by a thin insulating film, the electrons will penetrate the film, creating a tunneling current, if the surfaces are no further apart than 10 nm. Modern STM instruments utilize vacuum as the thin insulating

film, allowing the electrons to easily create a tunneling current, as suggested initially by Gerd Binnig, Heinrich Rohrer and their colleagues [43, 44]. Combined with lateral scanning down to 1nm, these instruments have vertical resolutions of the atomic scale (1\AA), due to the exponential relation between the measured tunneling current and the distance between the two surfaces. These instruments usually possess a sharp metal tip acting as an electrode, which is brought to a distance smaller than 1 nm to the surface that is to be measured, that acts as the second electrode. The created tunneling current is usually in the range of 0.2 to 1 nA, which can be easily measured. These complex instruments can usually work in two modes, constant current or constant height; in constant current mode, the sharp metal tip moves horizontally and vertically to keep the measured current at an equal value through the whole scanning, its movement being recorded, giving a profile of the surface at the end of the scan; in constant height mode, the metal tip only moves horizontally, keeping its vertical position constant, the variation of the measured tunneling current being recorded and, with a quick post-measurement processing, the profile of the surface is easily calculated.

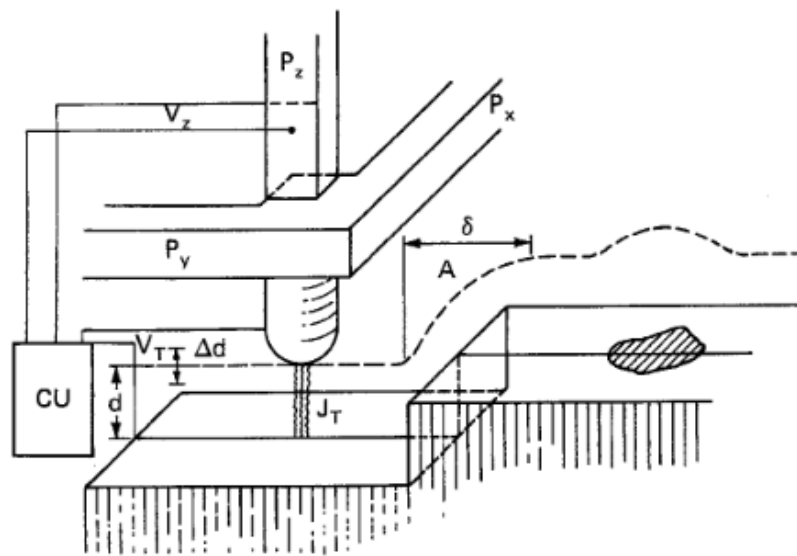


Figure 2.7: STM apparatus proposed by Binnig and Rohrer [44].

AFM, also proposed by Binnig in 1985 [45], fixes the major shortcoming of the STM technique, which is the fact that the material whose surface roughness is being measured must be an electrical conductor. AFM, while slightly worsening the atomic resolution levels of measurement in STM, was developed to scan any type of material surface, electrical conductor or not. Instead of having a sharp metal tip, it has a very flexible cantilever beam with an ultrasmall mass at the end. This ultrasmall mass, which usually comes in the form of a sharp tip, with radius ranging from 5 to 50 nm, comes in contact with the surface to be measured. While the scan happens, atomic interaction will cause small forces to manifest, in the order of the nN, which will cause deflections in the cantilever beam, in the order of the tenth of the nm, that can be picked up by tunneling,

capacitive or even optical detectors. These displacements can then be translated into variation of height at the sample's surface. Usually, in these operations, it is the tip that is being scanned, i.e., it is the material that is being moved, in order to stop any kind of vibrations from being recorded in the cantilever, as it would greatly affect the measurement results.

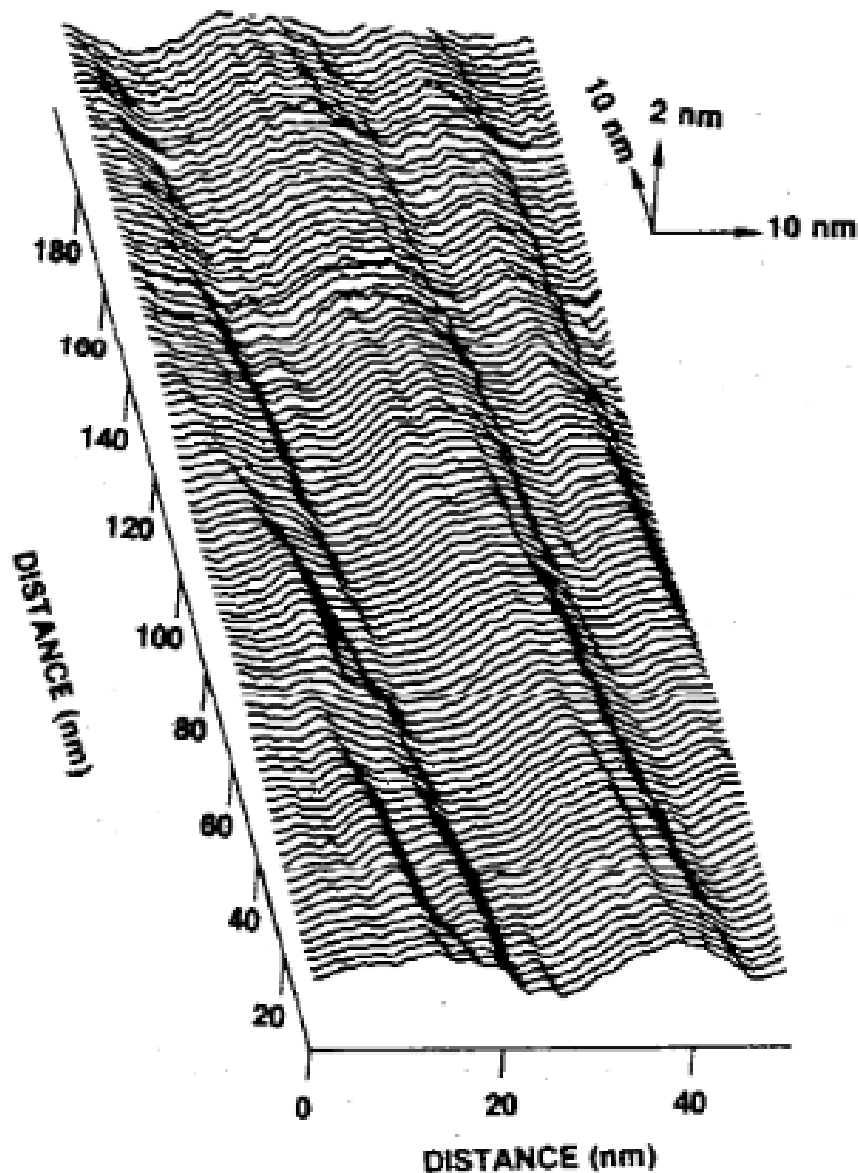


Figure 2.8: Surface reconstruction from an STM scan [46].

If needed, AFM can also operate without any contact between the tip and the material's surface. In this mode of operation, the tip is brought within a few nanometers from the surface, where the Van der Waals attractive forces between atoms is present, resulting in small deflections of the cantilever. This technique is named "attractive force imaging", or "noncontact imaging", as opposed to the contact method, also called "repulsive" or "contact" mode, and is rarely used outside

of research environments, as it is very slow and difficult to perform.

In sum, Scanning Probe Microscopy methods are an excellent alternative to the mechanical profilometer, as they compensate for all of its shortcomings, but require a huge initial investment, as the mechanisms and instruments used to perform these techniques are quite expensive.

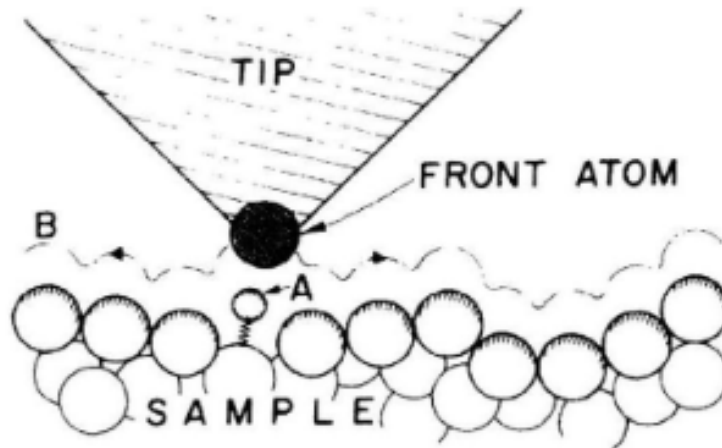


Figure 2.9: STM or AFM tip close to a sample [45].

2.3.4 Fluid Methods

Fluid methods are normally only used in continuous inspection procedures, such as those in quality control. These methods require no contact with any surface, and are usually very fast. In general, these techniques are performed by placing the surface which roughness is to be measured in a container such that there exists a fluid flow between two ends of a container, flowing over the sample material. The time it takes for the container to empty, i.e., for the fluid to escape through the container's gap, is empirically correlated to the surface roughness. From fluid methods, two techniques can be highlighted: the hydraulic method and the pneumatic gaging method.

In the hydraulic method, the container is set vertically in a way that the gap is on the bottom side. The container is then filled with water, and the gap is placed in contact with the sample material. The time it takes for the container to be fully emptied is then translated into a surface roughness. This method is adequate for large roughness patterns, such as the one present in road surfaces, which was one of the first and principal applications for this method. The earliest references to this method date back to 1960, proposed by Schultz [47].

For lower roughness values, there exists the pneumatic gaging method. The instrument is exactly the same, only the physical property to be correlated with roughness changes, as the container will always be filled with air. In this method, the property that correlates with surface roughness is the pneumatic pressure that is measured inside the container. This method was initially proposed by R. W. Woolley in 1991, as a high resolution, fast, non-contacting method for surface topography assessment [48].

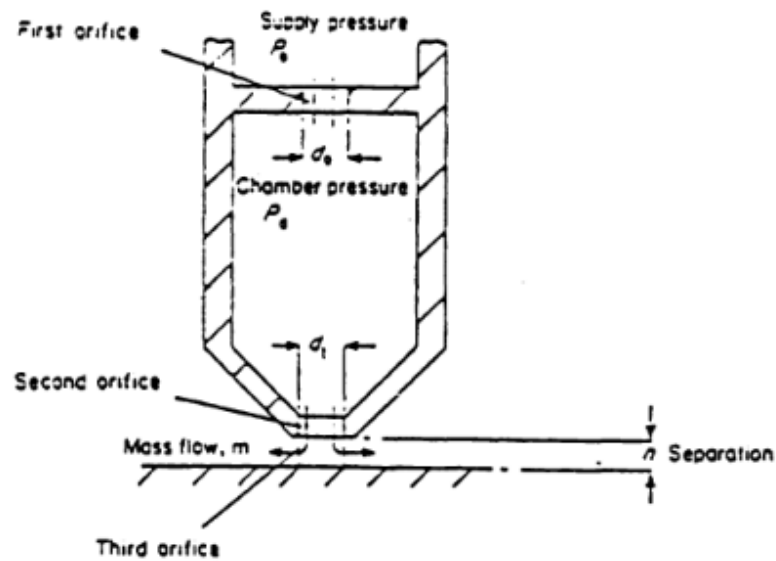


Figure 2.10: Illustration of the probe for pneumatic gaging [48].

These methods aren't commonly used, and it can't be said they compensate for the contact or resolution shortcomings in the mechanical profilometer method, but they provide a rough estimate of surface roughness throughout the whole surface and not only from a single line profile.

2.3.5 Electrical Methods

The only electrical method that exists consists on analysing the capacitance between two conducting elements, these being the instrument and the sample's surface [49]. Thus, this method requires the measured surface to be a conducting element. The measured capacitance can be directly correlated to the distance between two elements, so, as the instrument moves forward at a constant height, the variation of capacitance translates into the variation of the surface height. This way, an accurate representation of a single line profile is easily achieved. The patent for the instrument was registered in 1993, by David R. McMurtry and David K. Thomas [50].

This method is also not commonly used, even less than the fluid methods, as it is also restricted to a single line profile, as the mechanical profilometer.

2.3.6 Electron Microscopy Methods

There are three different techniques that can be highlighted in electron microscopy methods, these being Scanning Electron Microscopy, Integrating of Backscattered Signals and Stereomicroscopy.

The reflection electron microscopy technique is quite simple: macroscopic and microscopic surface features are captured using a digital camera, and then analyzed, as initially proposed by

Halliday in 1955 [51]. Although simple, this process is quite incomplete, due to the difficulty on obtaining quantitative data, because the images are only captured from one perspective, it becomes difficult to analyze the whole surface, because asperities might cover parts of the surface. In preparation for this technique, the specimens must also be placed in vacuum and insulated with a conductive coating, with materials such as gold or carbon, a step usually accomplished by sputtering the material over the object surface. In case this step is not conducted properly, the electrons from the incident beam don't have a conductive route to exit the sample and form a strong static field, that prevents the visualization of the sample.

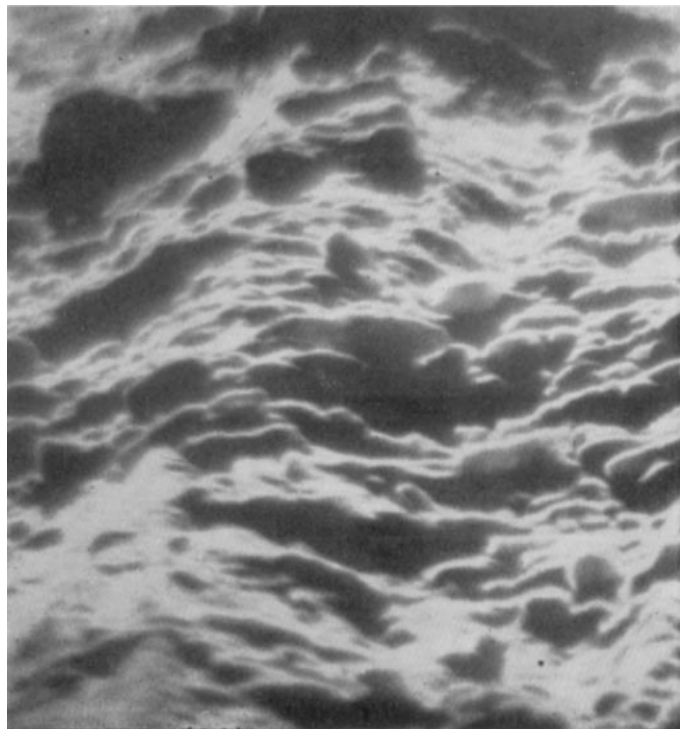


Figure 2.11: Surfaces captured by an electron microscope [51].

Integration of Backscattered Signals is a technique that involves analyzing backscattered electron signals (BES), an upgrade to the scanning electronic microscopy technique, developed by Sato and O-Hori in 1982 [52]. An image of a backscattered electron is produced by a BES, which can be directly correlated to the inclination of the surface that is being scanned by the electron beam. Thus, by analyzing the intensity of the BES, information about the surface topology can be obtained, leading to a surface roughness measurement. With this technique, a surface map can be obtained by making several scans. For this process to be executed, the sample's material must be conductive or possess a conductive coating, and it usually takes a great time interval for the scan to be concluded.

The stereomicroscopy technique is the third technique based on the electron microscopy approach, and is based on the principle of stereo effects. By capturing two images of the same surface, using slightly different angular views, it is possible to obtain a parallax shift between

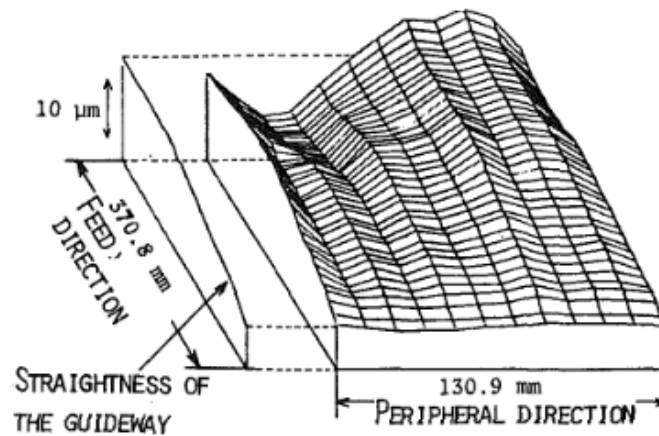


Figure 2.12: Surface map performed by Backscattered Electron Signals [52].

correspondent points in both images. In both images, correspondent points must be found and the shift on the horizontal axis must be measured. From that measurement, information about the position on the vertical axis can be extrapolated. This process must be repeated for all the pixels of interest. Pairing this process with a scanning electron microscope with enough resolution allows the digital processing of images that capture the surface topology, and information from the sample's surface roughness might be obtained, by matching asperities and valleys in the images taken from both perspectives, and obtaining its respective heights or deepnesses. This technique might be the best option in the electron microscopy methods as it presents few disadvantages, and can achieve adequate resolutions, in order of 5 nm in the horizontal, and vertical resolution depending on the horizontal parallax resolution and the angle which is formed by the two perspectives.

Although being quite interesting approaches, and eliminating the shortcomings from the mechanical profilometer, these techniques bring nothing new to surface roughness measurement, and the other presented methods usually outperform these techniques in all the possible applications, as the instruments are quite expensive, the measurements usually take a great time interval, the specimens require special preparations, the sample materials must be conductive (in case of reflection electron microscopy and integration of backscattered signal), and they usually only scan small areas.

2.3.7 Comparison of the Methods

Throughout the brief presentation of the diverse methods, the respective disadvantages were also introduced. There are many perspectives for the comparison of the methods, and there is no singular best method. As it's been pointed out, the mechanical profilometer is more than enough for most applications of surface roughness measurement. With the drawbacks for each technique in mind, an informed choice must be made, with every method in mind.

In general, we can specify a few areas where the option by one particular method might be obvious:

- the mechanical profilometer is chosen for applications in which detailed surface roughness data is necessary, as long as the material isn't easily damaged, and no surface map is required;
- scanning probe microscopy is chosen for the applications in which the mechanical profilometer can't be used, i.e., where detailed surface roughness data is necessary, but the material is susceptible to damage in case of contact, or if a surface map is required;
- electrical methods are chosen for continuous inspection procedures, such as quality control, as long as the material is electrically conductive;
- fluid methods are chosen for the materials in which the electrical methods are impossible to implement, i.e., any material that isn't electrically conductive.

For the optical methods, the focus of this project, the applications where they are clearly superior are in-process inspection procedures, such as those in production lines [14, 17]. Both optical methods and the procedures for which they are picked for will be explored in chapter 3.

Chapter 3

Optical Techniques

As mentioned in Chapter 2, to better understand the optical methods for surface roughness measurement, there are a few concepts that must be introduced first. This section's purpose is precisely the presentation of these concepts, and also the introduction of image processing techniques in order to obtain statistical properties that can be correlated to surface roughness.

As such, this chapter will begin with the introduction of the principles in which optical analysis techniques are based upon, such as Interferometry, proceeding to the introduction of mathematical transformation of images into arrays of information. These information arrays can then be utilized to accurately describe any picture, reducing it into a set of properties that can be used for several different applications, such as surface topology analysis, which is the objective of this project. A set of these properties will also be introduced, as they will be the backbone of correlating the referred information arrays into physical and measurable properties, such as surface roughness. Finally, a brief introduction of the image processing softwares that are used in this project will be made.

Followingly, a short introduction to the required basics of light analysis, optical methods for surface roughness measurement can now be presented. These methods were missing from the list in the previous chapter, as they are to receive a special focus, given that these techniques were the ones studied and used in this project. As it's been briefly referred, these methods are best applied for in-process inspection procedures.

As such, the Optic methods for roughness measurement will be presented, giving a brief explanation of how each method works, based on the concepts of speckle patterns and interferometry, or other concepts that will be introduced in due course. In the end, one of these methods will be chosen, while illustrating the reasoning behind the choice.

From this chapter, the reader should be able to fully comprehend the optical techniques and phenomena that will be referred to, and the basics of optical methods for surface roughness measurements.

3.1 Speckle Patterns

When a light beam is shone on any surface, it is obviously reflected. The reflection is usually both specular and diffuse. According to Snells' law, for a completely specular reflection to occur, the surface must be perfectly smooth, because in this condition the angle of reflection is equal to the angle of incidence. However, due to surface imperfections, such as micro-roughness, a completely specular reflection is impossible [53], Thus, there is always a specular reflection and a diffuse reflection.

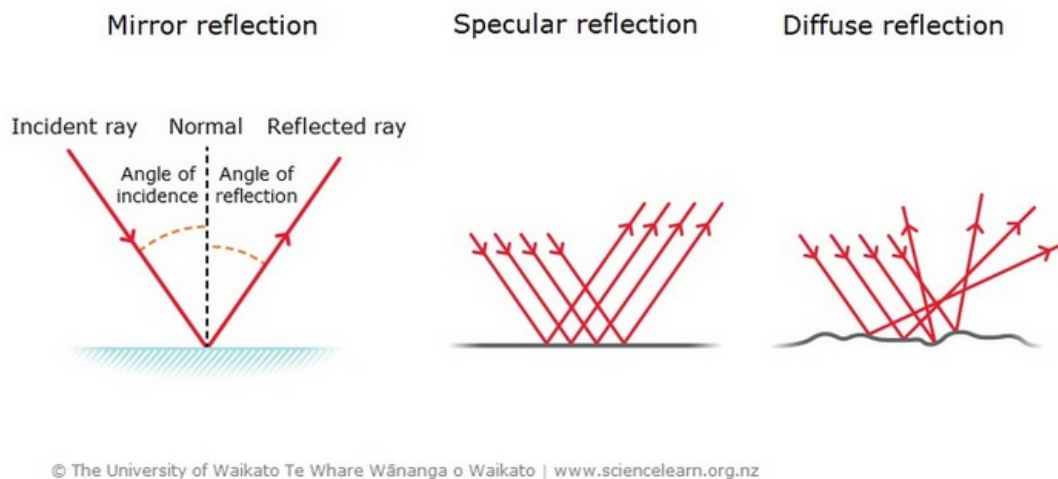


Figure 3.1: Reflection of a light beam, credits given in the image.

The diffuse reflection becomes more intense with the increase of the surface imperfections, i.e., an increase of the surface roughness' value translates into an increase of the diffuse reflection intensity, and a decrease in the specular reflection intensity. As the light field is scattered due to the diffuse reflection, the light rays interfere with each other, resulting in a superimposition, known as speckle pattern, which can be observed in Figure 3.2

As it has been explained, the diffusion of the light beam reflection is increased as with the increase of surface imperfections. As such, the scattering of the light field changes with the surface roughness of the material in which the light beam is incident. It can be expected then for the granular aspect of the speckle pattern to change, with different material surface topography and roughness values. Thus, a relation between the surface roughness and the resulting speckle pattern is initially established [17, 39, 55].

3.2 Interferometry

Interference of light waves is the physical consequence of the superposition principle and results in the observation of bright and dark bands called fringes, when a number of waves coexist in a region in space. These fringes are commonly observed in soap bubbles or on oil films on a

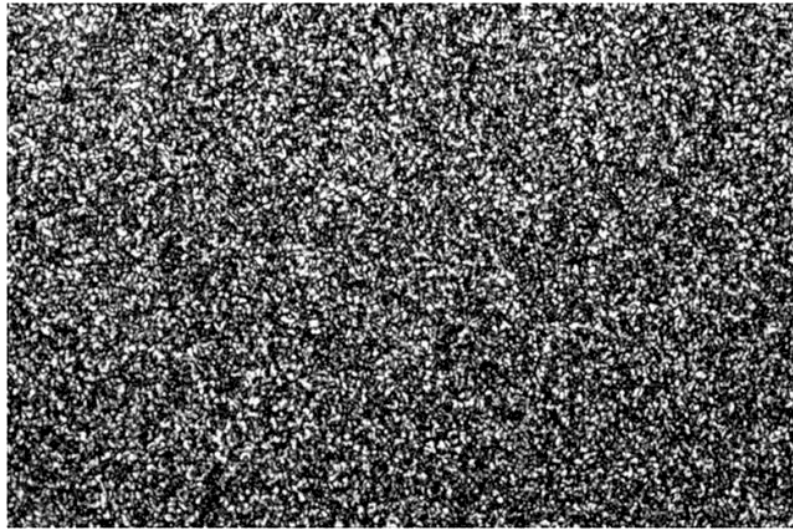


Figure 3.2: Speckle pattern [54].

wet roadway. The bright regions are called constructive interference and occur when a number of waves add together to produce an intensity maximum of the result wave. Destructive interference occurs when the waves add together to produce an intensity minimum. Collectively, the distribution of fringes is called an interference pattern.

The speckle pattern possesses a granular aspect, also the result of the referred superimposition of the scattered light rays. The light spots are actually spots in which the incident light rays were in the same phase, and the dark spots are spots in which the incident light rays were in opposite phases, as demonstrated in Figure 3.3.

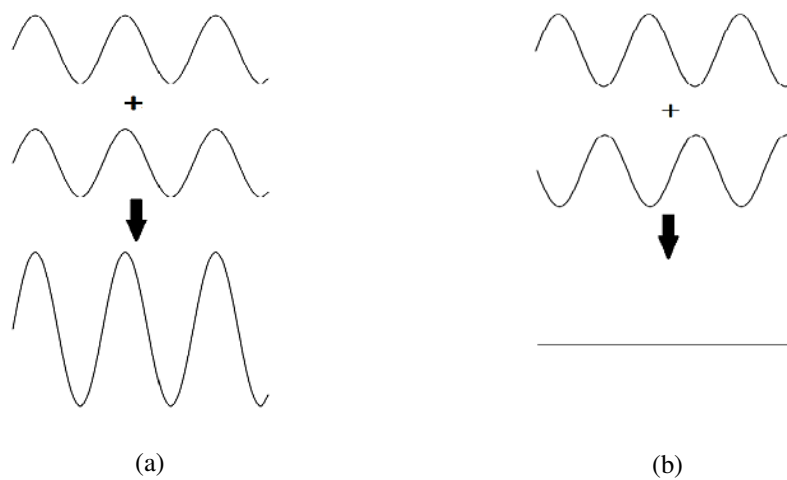


Figure 3.3: Results of wave superimposition in (a) waves with the same phase (b) waves with a phase difference of half a wavelength.

A quick example will provide a good explanation of what optical interferometry is, by introducing the Michelson interferometer, one of the most basic models of interferometry available. An interferometer is a mechanism that is used to for optical interferometry - through beam splitters and mirrors, the original light beam is divided and reflected, originating a fringe pattern. A schematic representation may be observed in Figure 3.4.

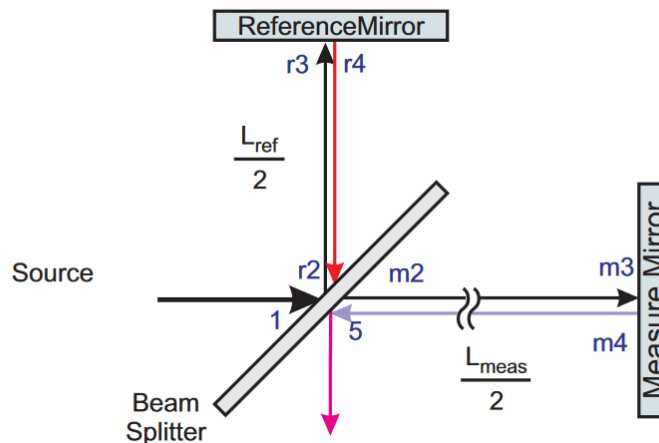


Figure 3.4: Schematic of a Michelson interferometer [56].

A source is shining a light beam on a beam splitter, usually a half-silvered mirror, which divides it. Each of the reflected beams is reflected once again in another mirror, recombining at the beam splitter. The recombined beam possesses now an interference pattern, due to the phase difference in the two reflected beams, that is changed whenever one of the mirrors is moved, due to phase alteration whenever the reflective surface is moved. Thus, if one mirror is fixed, any alterations to the resulting interference pattern will be attributed to the displacement of the moving mirror [56]. For surface topology analysis, one of the mirrors, usually the moving one, is replaced by the material sample. The created interference fringes are demonstrated in Figure 3.5.

From the analysis of these so called interferometry fringes, information about the state of the opaque material's surface can be obtained. As such, there are techniques that involve interferometry for surface roughness analysis [57–59].

The example given is the simplest mechanism that can be used for optical interferometry. Usually, interferometers are more complex than the presented one. Interferometers have several different possible compositions, depending on the technique that is going to be used [60]. More details about their construction will be given in the section dedicated to interferometry as an optical method for surface roughness measurement.

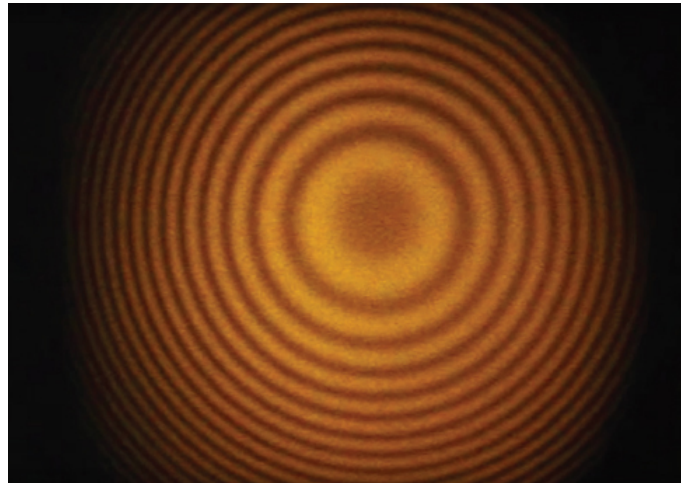


Figure 3.5: Interferometry fringes (credits to openstax CNX).

3.3 Image Analysis

With the basics of light reflection and interferometer mechanisms presented, there is still lacking an introduction to the post-capture image processing methods. This section will be dedicated to these concepts.

3.3.1 Analysis Statistics

The intensity value of an image captured by a monochrome camera represents a quantity related to the surface under observation in a scale defined by the number of bits attributed to each pixel. As an example, an 8-bit representation has 2^8 , or 256, levels of gray. It is then possible to delve deeper into the processing of the captured images. At this point, all that has been achieved is a matrix with grey values of any image. The process of transforming this seemingly random value matrix into something that can be correlated to physical properties is quite a simple process nowadays. However, this hasn't always been the case.

In 1973, Robert M. Haralick and his colleagues K. Shanmugam and Its'Hak Dinstein published what has probably been the most important article in this subject, carving their names in the history of image processing [61]. Their work suggested a process to transform the grayscale matrix into textural features that would allow a further interpretation of any image. By the time this article was published, their focus was on correctly identifying objects of interest in any given image, namely which kind of surface topography of aerial photographs was observed. Whether it was seaside, a forest or an arid desert, for example, or what kind of sandstone was present in the image. The following sections will follow the methodology developed by Haralick.

3.3.1.1 Gray-Tone Spatial-Dependence Matrix

This process begins with the creation of a second matrix, called a Gray-Tone Spatial-Dependence matrix, that established the proximity of grayscale values between neighbouring pixels, in a certain direction. The process will now be explained in a simple manner, by accompanying simple images to better demonstrate the process.

Let us assume an image is described in a grayscale of 0 to 4 (each pixel possesses 2 bits of information), and its matrix is the one presented in Figure 3.6.

$$\begin{bmatrix} 0 & 0 & 1 & 1 \\ 0 & 0 & 1 & 1 \\ 0 & 2 & 2 & 2 \\ 2 & 2 & 3 & 3 \end{bmatrix}$$

Figure 3.6: Grayscale Matrix [61].

This is the basic matrix that describes whatever image was given to the computer. However, in this state, it's not useful at all. The process of transformation of this matrix is an unusual concept: a relation of values between neighbouring pixels is established, leading into another matrix, the Gray-Tone Spatial-Dependence matrix. Depending on the direction (or angle) of analysis, the resulting matrix will be different. Usually, four angles of analysis are presented: 0°. 45°, 90° and 135°, or, respectively, horizontal, right diagonal, vertical, left diagonal.

Beginning with the horizontal direction, or 0°, we first count how many sets of two values where both gray-tone values are 0 exist. In this case, there are 4 sets of values with this condition, the set of two values in the first line, first and second column, which counts twice, as it is a (0-0) relation, and the set of two values in the second line, first and second column, which also counts twice, for the same reason. The first element of the Gray-Tone Spatial-Dependence matrix is now obtained, 4.

This process must be repeated for every combination of two neighbouring gray-tone values (0-1, 1-0, 0-2, 2-0, 1-2, etc.), constituting the Gray-Tone Spatial-Dependence matrix, with a structure similar to the one in Figure 3.7. It may have been noted that this matrix is symmetric, as the value sets for (0-1) are the same for (1-0), with the same rationale for any combination of values; and that in case the value set has the same graytone in both positions, the counting must be doubled as the count from left to right and right to left are treated as different counts.

As such, we can additionally count two value sets for the (0-1) combination, four value sets for the (1-1) combination, one value set for the (0-2) combination, no value sets for the (1-2) combination, three value sets for the (2-2) combination, one value set for the (2-3) combination and one value set for the (3-3) combination.

In the end, a matrix such as the one in Figure 3.8 is obtained for the horizontal direction (0°).

Were the Gray-Tone Spatial-Dependence transformations to occur in the other three different directions, the matrices demonstrated in Figure 3.9 would have been obtained.

		Grey Tone			
		0	1	2	3
Grey Tone	0	#(0,0)	#(0,1)	#(0,2)	#(0,3)
	1	#(1,0)	#(1,1)	#(1,2)	#(1,3)
	2	#(2,0)	#(2,1)	#(2,2)	#(2,3)
	3	#(3,0)	#(3,1)	#(3,2)	#(3,3)

Figure 3.7: Gray-Tone Spatial-Dependence matrix structure, in any given direction [61].

$$\begin{bmatrix} 4 & 2 & 1 & 0 \\ 2 & 4 & 0 & 0 \\ 1 & 0 & 6 & 1 \\ 0 & 0 & 1 & 2 \end{bmatrix}$$

Figure 3.8: Gray-Tone Spatial-Dependence matrix for the horizontal direction [61].

$$\begin{bmatrix} 4 & 1 & 0 & 0 \\ 1 & 2 & 2 & 0 \\ 0 & 2 & 4 & 1 \\ 0 & 0 & 1 & 0 \end{bmatrix}$$

(a)

$$\begin{bmatrix} 6 & 0 & 2 & 0 \\ 0 & 4 & 2 & 0 \\ 2 & 2 & 2 & 2 \\ 0 & 0 & 2 & 0 \end{bmatrix}$$

(b)

$$\begin{bmatrix} 2 & 1 & 3 & 0 \\ 1 & 2 & 1 & 0 \\ 3 & 1 & 0 & 2 \\ 0 & 0 & 2 & 0 \end{bmatrix}$$

(c)

Figure 3.9: Gray-Tone Spatial-Dependence matrix for the (a) 45° direction. (b) 90° direction. (c) 135° direction [61].

The name Gray-Tone Spatial-Dependence matrix eventually fell out of use, and now this type of matrix is called Gray Level Co-occurrence Matrix, or GLCM. The following section will make use of these matrices to calculate a set of properties, also established by Haralick, that will enable the initial obtained information, the matrix with pixel intensity, to be transformed into useful information that can be correlated to physical properties.

3.3.1.2 Textural Features

As it's been just referred, information in the form of a gray level co-occurrence matrix allows the calculation of certain statistical properties that can be correlated to physical properties. These statistical properties are called Textural Features, and were established by Haralick. There is a total of fourteen different properties that can be calculated from any GLCM, and all of them will be presented as they were established in Haralick's work.

Before demonstrating the used equations in order to obtain these properties, an initial notation is established:

- $p(i,j)$ is the (i,j) th entry in the GLCM;
- N_g is the number of distinct gray levels in any given image, that also equals to the dimension of the GLCM matrix (the matrix has as many rows and columns as different graytone values);
- \sum_i and \sum_j is, respectively, the same as $\sum_{i=1}^{N_g}$ and $\sum_{j=1}^{N_g}$;
- $p_x(i)$ is the i th entry in the marginal-probability matrix, that is obtained from the sum of the rows of the GLCM matrix ($= \sum_j p(i,j)$);
- $p_y(j)$ is the j th entry in the marginal-probability matrix, that is obtained from the sum of the columns of the GLCM matrix ($= \sum_i p(i,j)$);
- $p_{x+y}(k) = \sum_i \sum_j p(i,j)$, with $k = 2, 3, \dots, 2 N_g$;
- $p_{x-y}(k) = \sum_i \sum_j p(i,j)$, with $k = 0, 1, \dots, N_g - 1$.

Listing now the different properties:

1. Angular Second Moment

$$f_1 = \sum_i \sum_j p(i,j)^2 \quad (3.1)$$

2. Contrast

$$f_2 = \sum_{n=0}^{N_g-1} n^2 \sum_i \sum_j p(i,j) \quad (3.2)$$

where $n = |i - j|$.

3. Correlation

$$f_3 = \frac{\sum_i \sum_j (i - \mu_x)(j - \mu_y) p(i,j)}{\sigma_x \sigma_y} \quad (3.3)$$

where μ_x , μ_y , σ_x and σ_y are the means and standard deviations of the already presented p_x and p_y .

4. Sum of Squares: Variance

$$f_4 = \sum_i \sum_j (1 - \mu)^2 p(i,j) \quad (3.4)$$

5. Inverse Difference Moment

$$f_5 = \sum_i \sum_j \frac{1}{1 + (i-j)^2} p(i,j) \quad (3.5)$$

6. Sum Average

$$f_6 = \sum_{i=2}^{2N_g} i p_{x+y}(i) \quad (3.6)$$

7. Sum Variance

$$f_7 = \sum_{i=2}^{2N_g} (i-f_8)^2 p_{x+y}(i) \quad (3.7)$$

8. Sum Entropy

$$f_8 = - \sum_{i=2}^{2N_g} p_{x+y}(i) \log[p_{x+y}(i)] \quad (3.8)$$

9. Entropy

$$f_9 = - \sum_i \sum_j p(i,j) \log[p(i,j)] \quad (3.9)$$

10. Difference Variance

$$f_{10} = \text{variance of } p_{x-y} \quad (3.10)$$

11. Difference Entropy

$$f_{11} = - \sum_{i=0}^{N_g-1} p_{x-y}(i) \log[p_{x-y}(i)] \quad (3.11)$$

12. Information Measures of Correlation (1)

$$f_{12} = \frac{HXY - HXY1}{\max[HX, HY]}, \quad (3.12a)$$

where

$$HXY = - \sum_i \sum_j p(i,j) \log[p(i,j)] \quad (3.12b)$$

$$HXY1 = - \sum_i \sum_j p(i,j) \log[p_x(i) p_y(j)] \quad (3.12c)$$

$$HXY2 = - \sum_i \sum_j p_x(i) p_y(j) \log[p_x(i) p_y(j)] \quad (3.12d)$$

and with HX being the entropy of p_x , and HY being the entropy of p_y .

13. Information Measures of Correlation (2)

$$f_{13} = (1 - \exp[-2.0(HXY2 - HXY)])^{1/2} \quad (3.13)$$

with HXY2 and HXY being calculated the same way as in for f_{12} .

14. Maximum Correlation Coefficient

$$f_{14} = (\text{Second largest eigenvalue of } Q)^{1/2} \quad (3.14a)$$

with

$$Q(i,j) = \sum_k \frac{p(i,k) p(j,k)}{p_x(i) p_y(k)} \quad (3.14b)$$

From all these properties, fourteen in total, four different results can be obtained, one for each direction matrix. As such, for a single image analysis, 56 different values would have to be studied, in case every property was included. To simplify the matter, what is usually done is a mean calculation for each property, with the 4 directions, while also obtaining the value range. This way, a full image analysis can be reduced to a total of 28 values, two for each property.

In this project, not every single property will be studied. Most of these are not applicable or needed to obtain the wished end result. A selection of properties and the reasoning behind it will be demonstrated in chapter 4, Methodology.

3.4 Softwares

Throughout the project, two different image processing softwares were used: MATLAB and MVTec Halcon.

MATLAB is widely known and used in the engineering fields, as it possesses many different tools and functionalities, ranging from data analysis in order to explore, model and visualize data, to Simulink, a powerful tool designed to simulate any mechanical system in a virtual system, or deep learning and machine learning tools. For the project, it's main purpose was to run an analysis on a given set of captured images, obtaining a gray co-occurrence matrix, in order to calculate the already referred statistical properties. As the author already possessed some experience with the software, and due to its vast documentation and functionalities, the scripts developed for the project weren't difficult to write at all, as MATLAB already possessed many functions to achieve the required results.

MVTec Halcon is a less-known software that focuses purely on machine vision and its many applications, from detecting shapes in images to controlling robotic arms in an industrial environment. The author had no previous experience with this software but, similarly to MATLAB, due to its vast documentation and intuitive development environment, the scripts were quite straightforward to write, and achieved the required results without much difficulty.

There will be a step-by-step explanation on the scripts written in both these softwares in chapter 4, where the methodology process will be demonstrated.

3.5 Optical Methods

With the basics of light analysis introduced, optical methods for surface roughness measurement can now be presented. These methods were missing from the list in chapter 2, as they are to receive a special focus, given that these techniques were the ones studied and used in this project. As it's been briefly referred, these methods are best applied for in-process inspection procedures.

This section will present most optics method for roughness measurement, giving a brief explanation of how each method works, based on the concepts of speckle patterns and interferometry, or other concepts that will be properly introduced. In the end, one of these methods will be picked, while demonstrating the reasoning behind the choice.

This review ends the introduction of theoretic knowledge, containing the last set of information needed to achieve a better understanding of the developed project.

3.5.1 Taper-Sectioning Method

As the name dictates, this method consists on making a small incision on the surface of the sample at a precise angle, in order to magnify the surface texture by a factor, which is a function of the cutting angle, to then be examined under an optical microscope. This technique was proposed in 1969, by Nelson [62].

The sample must be prepared with a special coating, as not to damage the surface during the sectioning operation. The coating must possess a special set of compatible properties, such as the hardness, which must be approximate to the sample material's hardness; it must also firmly adhere to the sample's surface; and, finally, should not diffuse into the surface. For example, for steel surfaces, a coating of electroplated nickel is recommended, with a thickness of 0.5 mm.

Usually, the cutting angle is around 1° and 6° . The taper section must then go through a special process of surface treatment, as it is lapped, polished, and possible lightly etched, or heat tinted, as to provide a good contrast for observation under the microscope.

After the sectioning is performed, the taper is observed under a microscope, and a complete visualization of the surface topography is enabled.

This method is not widely used as it requires a special preparation and destruction of the specimen, and presents poor accuracy in the results.

3.5.2 Light-Sectioning Method

The first experiment with light-sectioning techniques and surface roughness measurement was proposed in 1967 by David Myles Huddart [63], referring the development of light-sectioning techniques by Gustav Schmaltz in 1936 [64].

A quite simple method, a radiating slit emits a light source that is incident on the surface at an angle, usually 45° , as demonstrated in Figure 3.10. Where the surface is perfectly smooth, its reflection is a straight line. Where the surface contains some degree of roughness, its reflection is be an undulating light. It is possible with some post-measurement analysis to correlate the undulation of the reflection with surface roughness.

The resolution of this system is a function of the incidence angle and, if the surface that is to be measured is mounted onto a moving table, it's possible to do obtain a single line profile measurement across the surface.

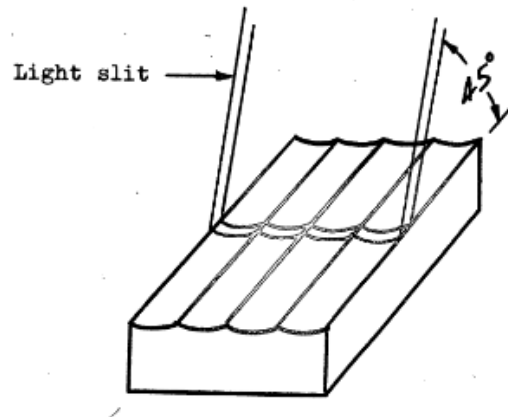


Figure 3.10: Example of a light slit for the light-sectioning method [63].

3.5.3 Specular Reflection Methods

As it's been stated previously, any reflected beam will be part specular and part diffuse, due to the surface topology of any material. As such, it is possible to describe specular reflectance using the roughness of the surface and the refractive index of the material. The inverse is also possible, i.e., estimating the surface roughness by measuring it's specular reflectance.

A mechanism, usually called glossmeter, was built for the purpose of measuring any material's specular reflection. This mechanism measures the gloss of the sample's surface, which is simply the fraction of the incident light reflected from a surface. To the result of the measurement, the specular reflectance quantity, is assigned a gloss number, which directly relates to the degree of the state of the surface's finish. The comparison term is a perfect mirror, a theoretical gloss standard, that has an assigned value of 1000.

Defining λ as the wavelength of light, R_0 as the total reflectance of the rough surface, which is found by measuring the specular reflectance in all the directions, including the specular direction, θ_i as the angle of incidence of the beam, a relation between specular reflectance in the angle of incidence, R , and the surface roughness variance, σ , can be established by [65]

$$\frac{R}{R_0} = \exp\left[-\left(\frac{4\pi\sigma \cos \theta_i}{\lambda}\right)^2\right] \approx 1 - \left(\frac{4\pi\sigma \cos \theta_i}{\lambda}\right)^2 \quad (3.15)$$

This relation remains true as long as $\sigma \geq \frac{\lambda}{10}$. This way, using a gloss meter, the value of R is obtained, and consequently the value of surface roughness variance is obtained.

Glossmeters are simple mechanisms, easy to use and quick. In industries such as paint, varnish and paper-coating industries, they are vastly utilized, as they can be easily inserted in any line of production, obtaining information about the sample's surface while it's still being manufactured, as it's suggested in Gardner-Sward Handbook [66].

This method's biggest shortcoming is the fact that it greatly depends on the refractive index [67]. A slight change in the refractive index, that may happen due to a change in the material's chemical composition will greatly affect its surface refractive index, may it be due to the aging of the surface, a change in the material supply, or other causes. As such, for tight surface roughness tolerances, a glossmeter may not be the ideal method. Nevertheless, it still is a very good method for evaluating general surface appearance in the industries that were previously referred.

3.5.4 Diffuse Reflection (Scattering) Methods

It was previously demonstrated that surface roughness greatly contributes to the scatter of the reflected light [55]. The rougher the surface, the more diffuse the reflected beam will be. In the previous method, the specular reflection was measured and quantified. However, in this method, it's the scattering of the light, resulting in the diffusion of the reflected beam, that is measured.

Scatterometers, also called diffusionmeters, are, as the name suggests, instruments that measure the scattering of a reflected beam of light through a medium such as air. Scatterometers are insensitive to temperature variation and mechanical or acoustical vibrations, as they measure directly the light reflectance and not the physical distance between surface and sensor. As a result, these instruments are extremely robust [68].

With traditional surface roughness measurement methods, the area covered with a singular scan is usually small. If a full surface scan is required, the scans must be repeated until the whole area is covered, a process that can take a huge time gap. Another advantage of scatterometers is that these instruments, in opposition of traditional instruments, are able to inspect the whole surface, in a short amount of time.

The combination of these advantages makes these instruments quite desirable and they are vastly employed in on-line roughness measurement during manufacture, as the measurement "is a continuous, fast, noncontacting, nondestructive, and relatively insensitive to the environment".

A total of three approaches to surface roughness measurement using Scattering methods have been developed, and they will be illustrated in the following sub-sections.

3.5.4.1 Total Integrated Scatter

The first method is a complement to the specular reflectance method. Total Integrated Scatter, or TIS, is a property that quantifies the total intensity of the diffusely scattered light, as opposed to quantifying the intensity of the specularly reflected light. For this purpose, a setup such as the one in Figure 3.11 is constructed.

In this mechanism, a light beam enters a high-reflectance diffuse integrated sphere. The light beam is reflected at the sample's surface, and the specular part of beam leaves the sphere, entering specular detector D2, where it'll be analysed. The diffuse part of the beam gets scattered even further by the sphere, which possesses a diffuse white coating. This way, a uniform glow is obtained inside of the sphere, regardless of the initial diffusion direction. The scattered light waves are then measured by a scatter detector, D1.

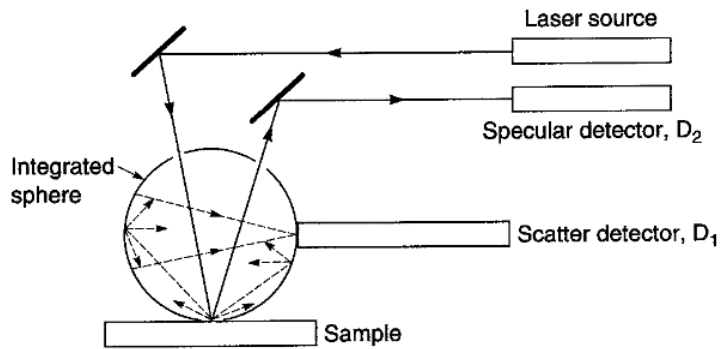


Figure 3.11: High-reflectance diffuse integrated sphere [69].

The property TIS is then obtained as the ratio between the total light scattered inside the sphere and the total intensity of scattered radiation, both specular and diffuse. In the specular reflection methods, an equation to establish the relation between specular reflectance, R , and surface roughness variance, σ was given. As the sum of specular reflectance and light scatter equals to 1, the expression that establishes the relation between TIS and surface roughness variance, σ , is given by [70]

$$\text{TIS} = 1 - \frac{R}{R_0} = 1 - \exp\left[-\left(\frac{4\pi\sigma \cos \theta_i}{\lambda}\right)^2\right] \approx \left(\frac{4\pi\sigma \cos \theta_i}{\lambda}\right)^2 \quad (3.16)$$

This equation also still only stands valid for $\sigma \geq \frac{\lambda}{10}$.

The calibration of this mechanism is made through the use of samples of known specular reflectance. By using these samples, the measured scattered power in scatter detector is adjusted to the theoretical measurements that should be obtained.

3.5.4.2 Diffuseness of Scattered Light

This technique is based on the concept that scattered radiation becomes more diffuse with the increase of surface roughness, as it's been already stated before. As such, a parameter that allows the characterization of surface topology might be found in relation to the scattered light pattern.

Two different reflection intensity measurements are performed: one at the specular angle, and another at a pre-defined angle, other than the specular angle. A ratio is then calculated between the reflection intensity of these two measurements. This ratio decreases with the increase of surface roughness. As such, information about surface roughness may be obtained from the referred ratio.

This technique allows R_a measurements up until $0.3 \mu\text{m}$ [71].

3.5.4.3 Angular Distributions

Returning once again to the idea of surface roughness causing the scatter of the reflected light beam, obtaining the entire angular distribution (or AD) of the scattered radiation could potentially

contribute to the determination of the surface topology state. When referring to the surface topology state, not only surface roughness is included, but parameters such as average wavelength or average slope of the surface might additionally be obtained.

Depending on the type of surface topography of the material that is being examined, the information that can be derived from AD changes. The type of surface state information that is sought is surface roughness, i.e., for roughness variations values until the light wave's wavelength value. This set of values is usually the one with the most difficult AD interpretation. Many surface topology properties, such as roughness' vertical scale or its angular width, determine the intensity of the scattered light. Theoretically, AD is a method should be able to achieve the correlation of the power spectral density function and surface roughness.

Experimental systems using this approach to surface roughness measurements have been developed throughout the years. The most simple one, developed by Clarke and Thomas consisted on a laser beam, reflected from a polygonal mirror, which was rotating at high speeds, onto a surface where it'd be reflected again [72]. A photodetector receiver, masked to a narrow slit, was set up in a way that it'd always be capturing scattered light originating from the single point which happened to be illuminated by the light beam, at any moment of the scan. In post-measurement analysis, a correlation between the captured reflection curves and surface roughness was found.

A more sophisticated approach was developed by Vorburger, in which a beam from a laser would illuminate a sample's surface at a variable angle of incidence, and 87 light sensors mounted into an array that can also rotate by itself capture the scattered light [73]. This way, the capture range corresponds to an entire semi-sphere, a broader capture range than the range in the mechanism developed by Clarke and Thomas. Simulations were run where a similar light beam would be incident on a surface with previously measured roughness. The data obtained from the simulations was then compared to the measurement results and a correlation was established. The mechanism is shown in Figure 3.12.

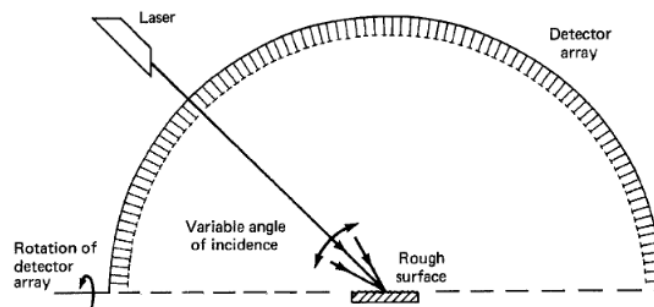


Figure 3.12: Angular distribution mechanism developed by Vorburger [73].

The three Diffuse Reflection methods referred so far are fit for surfaces whose surface roughness value is greatly below the light wave's wavelength. As such, the maximum range of these methods should be around surface roughness values of $0.1 \mu\text{m}$. Therefore, they are viable options

for surface roughness measurement in this range, as they can provide high-speed measurements of any sample's material.

3.5.5 Speckle Pattern Method

The basic concepts of speckle formation have been already introduced in the previous chapter. In sum, speckle pattern is the result of the intensity variation in neighboring spots due to superimposition of the scattered light. The main difference between speckle pattern and angle distribution is that speckle is the intensity noise that is usually removed through the use of filters to obtain a clean angle distribution capture [74, 75].

The usual approach to speckle pattern analysis is to reflect a beam of light on the sample's surface, capture the pattern that is formed, modify the position of the components such that the sample is illuminated with a different angle of incidence or wavelength of light, and capture the pattern again. Both captured patterns are then compared and information about the surface roughness can be obtained. This method is usually associated with the already defined Haralick's statistical properties. [11, 13, 61, 76, 77].

Is its a very fast measurement method, with its resolution usually ranging from 1 to 100 μm .

3.5.6 Optical Interference Method

An introduction to optical interferometry has also been previously given. The usual approaches involve the analysis of interference fringes. With computer processing, information about the state of a materials surface can be obtained from the inclination and space between fringes [59].

Historically, different approaches to optical interference have been developed, with diverse mechanisms being constructed, each with its different shortcomings. The need for the sample surface to be covered in a reflective coating, which is usually a special dust that hinders any specular reflections, and the high sensitivity to vibration, are the most common disadvantages, and some of them even need to be in contact with the surface, possibly damaging it [57].

One of the most used optical approaches for surface roughness assessment is to use a two-beam interferometer, as it's been previously referred. A big advantage of techniques that utilize this approach is that the sample's surface can be assessed without the need to apply a high-reflectivity coating. It's a very flexible method as the magnification can be easily changed, allowing different values of resolution and fields or view. Short-wavelength visible-light interferometry and computerized phase shifting techniques allow measurement resolutions up to one hundredth of the wavelength of light's value, or even better. This area has been greatly explored, as there are multiple techniques available and their respective instruments or contraptions. In this section, the focus will be given to one particular techniques, as it presents the best results, while balancing out its shortcomings.

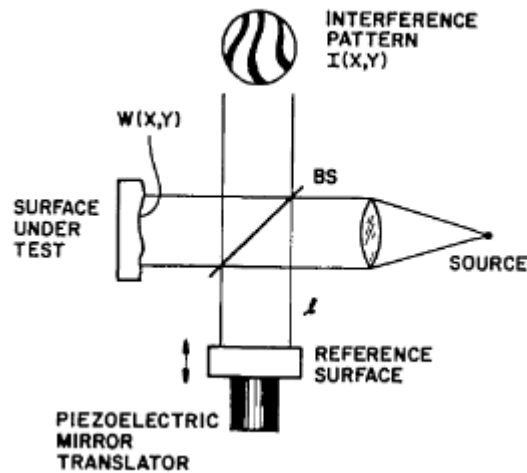


Figure 3.13: Example of an interferometer for fringe creation, the Twyman-Green interferometer [78].

3.5.6.1 Phase Shifting Interferometry

As the name hints, these techniques involve phase variation in order to obtain different interference patterns, making it possible to extrapolate information about the surface topology that other techniques do not allow to [78–80]. At least, three different phase shifted frames are necessary in order to apply this technique, due to the fact that the equation that describes the intensity distribution of an interference pattern (Equation 3.17) containing three variables - ϕ , $I_O(x,y)$ and $I_R(x,y)$ [81] although for frames PSI is much more popular because of the calculation simplicity.

$$I(x,y) = I_O(x,y) + I_R(x,y) + \sqrt{2I_O(x,y)I_R(x,y)} \cos \phi(x,y) \quad (3.17)$$

Using three different frames allows the obtention of ϕ .

In order to obtain these different interference patterns, a known phase shift between the object and reference beams is introduced, in order to generate phase-shifted frames. For this purpose, it is commonly utilized a calibrated PZT to move the object surface a certain distance.

Although the minimum amount of phase shifts is three, it's possible to perform as many phase shifts as wished, altering the algorithm that is used in order to obtain ϕ . The higher the amount of phase shifts, the more complicated the algorithm will be, but the tolerance for errors in calibration will also increase. As such, a balance between required processing power and tolerance for phase shift errors must be evaluated for each application.

After capturing the generated interference patterns, computer processing is required. A common procedure is to first filter the obtained patterns, calculate phase and finally unwrap the phase map, which is bound to $[-\pi, \pi]$ values, and then to unwrap the filtered data. A common filtering method is to divide the original phase map into sine and cosine functions, filtering each of the generated data, and then combining them to reduce the visual noise. For unwrapping, rather large

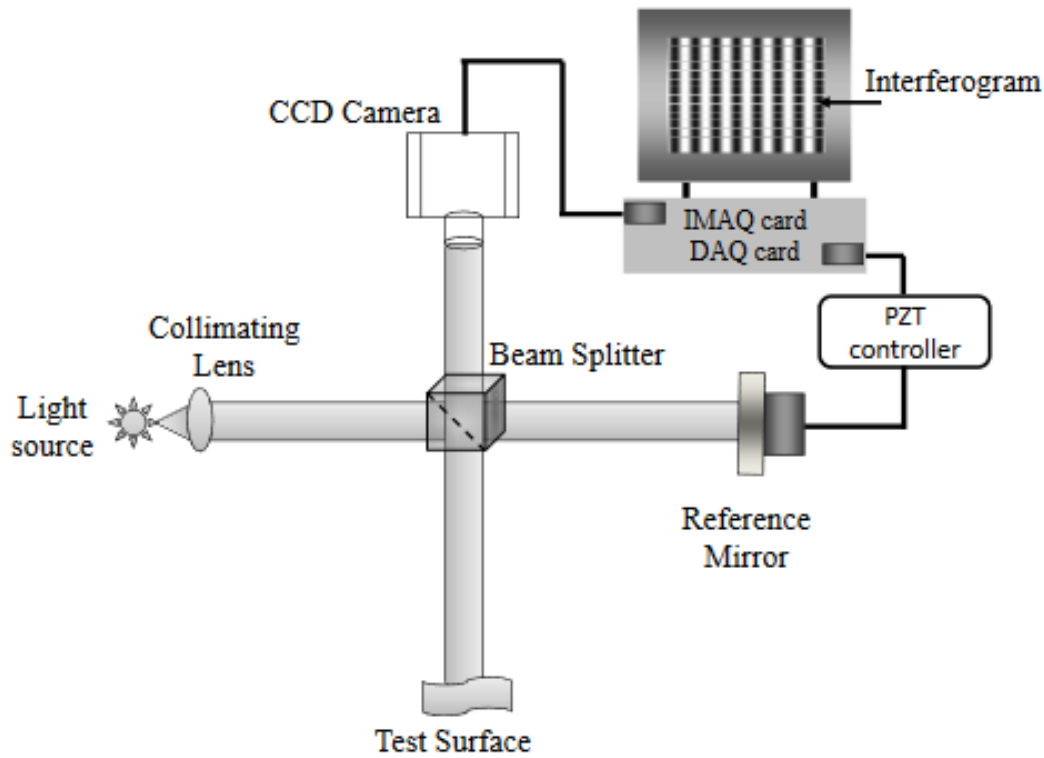


Figure 3.14: Adapted Twyman-Green interferometer for PSI analysis [81].

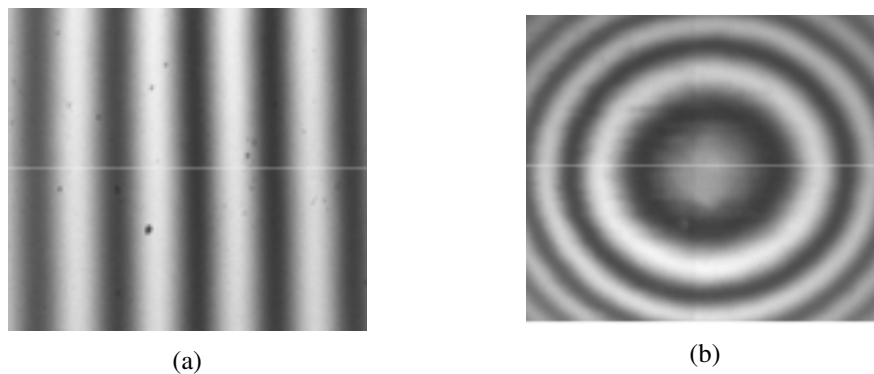


Figure 3.15: Fringe patterns from (a) plane surfaces (b) spherical surfaces [81].

number of algorithms exist that may be split into "path" methods, that calculate phase at one point by counting the number of times phase returns to $-\pi$ through a determined path, and point-wise methods that calculate phase at each image pixel regardless of the phase in the remaining image pixels, is usually performed [82]. The unwrapped phase map can then be transformed into a contour map of the ground specimen, allowing the assessment of the surface topology.

As it's been said, this approach has been greatly explored due to its advantages, the two principal ones being high measurement accuracy at high resolutions, and the elimination of any system

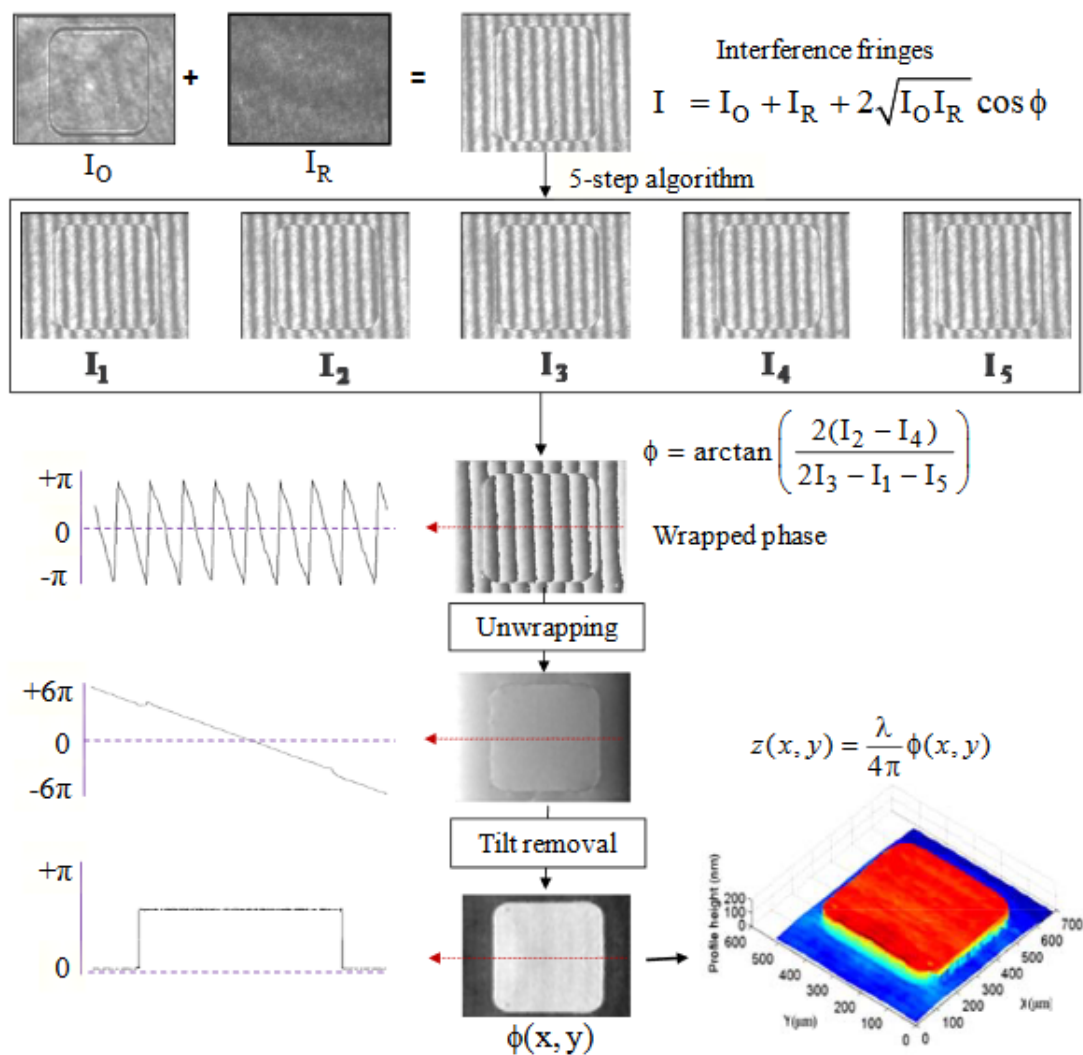


Figure 3.16: Example of an algorithm for PSI analysis [81].

errors, which can be measured and removed from the final results. However, these techniques require expensive hardware and software, the calibration of the PZT phase shifter usually lasts a long time, and is also prone to errors, dynamic measurements aren't possible as there is the need for multiple frame captures (one frame per phase shift), also making this method hugely sensitive to vibration and air turbulence. This technique is also not appropriate for rougher surfaces, as its resolution value range is usually below $1 \mu\text{m}$. As such, for higher values of surface roughness, it's recommended to use other methods.

3.5.6.2 White Light Interferometry

As it's been referred, recent experimentation in the field of optical interferometry all focuses on phase-shifting interferometry. Other technique worth mentioning is Scanning White Light interfer-

ometry, which was a technique that was developed to avoid the huge computing power needed for phase-shifting interferometry [83], and is still used in industrial environments in order to quickly obtain information about the surface topology of any given sample.

There are three main techniques inside the White Light Interferometry field, Coherence Scanning Interferometry (or Coherence Scanning Microscopy), Spectroscopic Analysis Interferometry, and Fourier Transform Spectroscopy of white light interferograms. In this section, focus will be given to coherence scanning interferometry.

The interferometer components' disposition is usually the same as the disposition in other many interferometers. The difference is that white light is used, which has low coherence. This has a positive aspect, which the fact that it is easy to find interference fringes, and a negative aspect, that it may be too easy to find interference fringes, and any reflection can generate its own interference fringes, leading to inaccurate results [84]. The low coherence of white light avoids the ambiguity in determining the fringe order, allowing easier measurements.

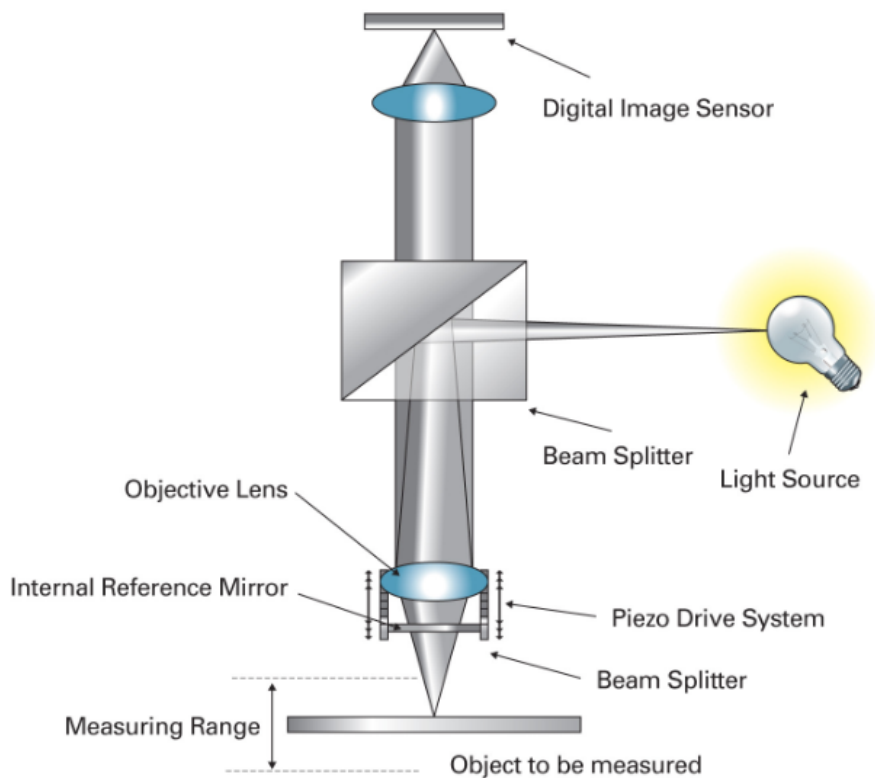


Figure 3.17: Example of a CSI instrument (credits to the NPL - "A National Measurement Good Practice Guide", No.108).

In the CSI instrument, the objective lens is moved, changing the intensity of the interference fringes. The intensity variation is recorded, as the highest points in the surface will be the first to generate an interference fringe, and information about the surface's topology may be obtained with further analysis of the intensity variation.

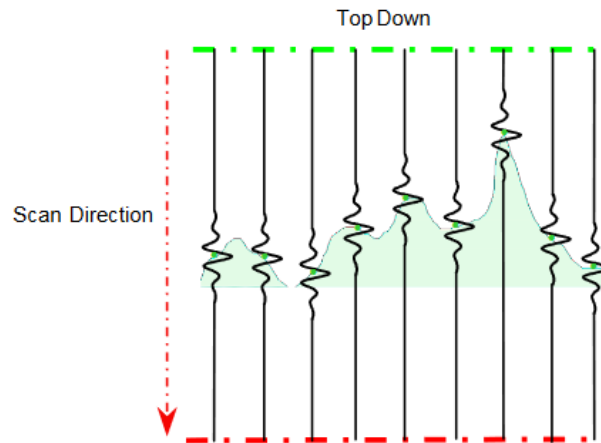


Figure 3.18: Schematic of the obtained information from the CSI process (credits to the NPL - "A National Measurement Good Practice Guide", No.108).

3.5.7 Choosing a Method

A comparison between the presented methods was performed by Bushan [17], focusing on the ability to provide quantitative information or three-dimensional data, the resolution achieved with the technique, spatially and vertically, the capability of performing on-line measurements, and their main limitations. The comparison is shown in Table 3.1.

Table 3.1: Optical methods comparison [17].

Method	Quantitative Information	Three-Dimensional Data	Resolution (nm)		On-line Measurement Capability	Limitations
			Spatial	Vertical		
Taper Sectioning	Yes	No	500	25	No	Destructive, tedious specimen preparation
Light Sectioning	Limited	Yes	500	0.1-1	No	Qualitative measurement
Specular Reflection	No	No	$10^5 - 10^6$	0.1-1	Yes	Semiquantitative measurement
Diffuse Reflection	Limited	Yes	$10^5 - 10^6$	0.1-1	Yes	Restricted to smooth surfaces (<100 nm)
Speckle Pattern	Limited	Yes			Yes	Restricted to smooth surfaces (<100 nm)
Optical Interference	Yes	Yes	500-1000	0.1-1	No	Highly sensitive to vibrations

As it's been referred in the beginning of this project, the developed technique must be capable of fast measurements, must not be too monetarily demanding, and its setup will be in an industrial environment. The surfaces that are to be examined also range its roughness in the dozens of

micrometers.

The most prominent method in actuality is, without a doubt, the phase-shifting interferometry technique. But the shortcomings of this technique fail to make it an obvious choice in terms of accuracy, as its measured values range will not go as high as the required for the application, and the industrial environment is not adequate for this technique as the measurement apparatus will be prone to vibrations.

Taper-sectioning method would be a wasteful choice, as the materials would need special treatment to then be destroyed, making it a quite expensive method while also not being able to be adapted for an on-line measurement.

Scattering methods (diffuse reflection) are also not a good choice as the apparatus needed for the technique might be too expensive for the application, and their counterpart, the specular reflection methods, are also not a good choice as the surface roughness value's tolerance for the analysed surfaces may be too tight for these techniques.

With light-sectioning and speckle analysis methods remaining, both possess the resolution range needed. It is stated that the original light sectioning method isn't able of on-line measurements, but adapting the technique for this purpose is possible. In the end, the speckle pattern analysis techniques were chosen, as they seemed more flexible for possible corrections and adjustments, as light-sectioning methods seemed too rigid due to their nature - any visual noise or vibration would greatly affect the obtained reflection, making the method inaccurate. As it's been said, speckle analysis techniques utilize Haralick's formulations [61], and their manipulation and calibration seemed more accessible. Besides, the method uses one camera and one laser, which are relatively inexpensive, is quite robust, and easily implemented in an industrial setting.

Chapter 4

Methodology

With the basic theoretical concepts for this project established, and its basis technique chosen, it is time for the methodology to be described. As it's been referred to in chapter 3, a speckle pattern approach to surface roughness will be utilized, with the aid of Haralick's statistical properties that were also discussed.

This chapter will be introduced with the exposition of the physical assembly that was developed for this project, including the description of each component, while also introducing the samples whose surface is to be examined. The adjustments made to the established Speckle Pattern methods, in order to obtain better results, will also be presented. An explanation of the thought process presented in the scripts written for the speckle analysis will also be given, in both Matlab and MVTec Halcon.

The purpose of this chapter is to fully establish the procedures that allowed obtaining the results, which will be discussed in chapter 5.

4.1 Physical Assembly

For the purpose of capturing speckle patterns, a physical system was developed, similar to the systems present in the literature. The assembly consisted of a laser, a collimator with a pin hole filter, a biconvex lens, the sample that is to be examined, and finally a monochromatic camera to capture the speckle patterns.

The laser, a MLL-III-532 model with a potency of 200 mW, which can be observed in Figure 4.1, is present obviously as a source of coherent light. As a side note, it is worth mentioning that this laser is quite powerful and should be handled with great care. It is recommended to use protective gear around it, as the smallest time interval while directly exposed to is susceptible to inflict damage such as skin burns, or permanent damage to the cornea, if observed directly. It should be noted, however, that as a precaution, the beam expander, which will be highlighted further ahead, is set up as close as possible to the laser radiation exit, in order to minimize the risk due to the rather high power density of the original beam. Once the laser is expanded and filtered, only a small portion of the input radiation is available for propagation to the object surface under

analysis, with a small power density. More information may be found in norms IEC 60825-1:2014/ISH1:2017 and ANSI Z136.4-2005.

The light beam passes through the collimator, whose function is to expand the light beam, and through the inserted pinhole, which filters the high spatial frequencies, which result from dust or beam deficiencies, in a similar way as a low-pass filter does in electronics. As a result, after going through the collimator, the light beam should propagate without diverging, and without any visual noise. The collimator and pinhole system can be seen in Figure 4.2.

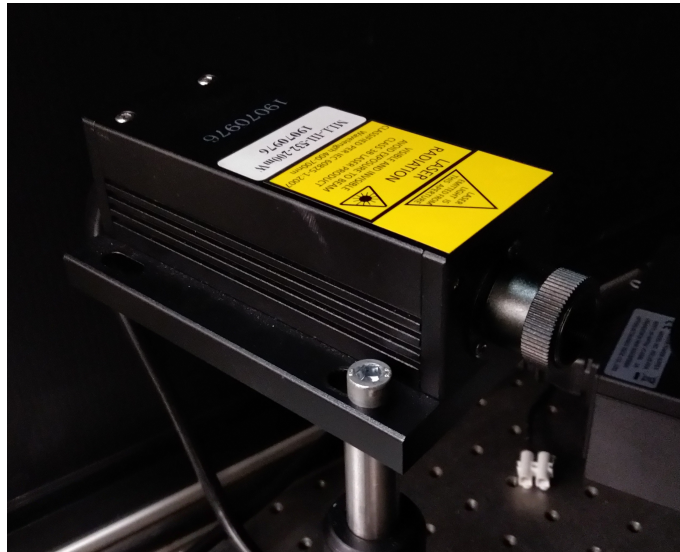


Figure 4.1: Source of coherent light, the laser.

Effects of the collimator and pinhole setup filtering in the light beam is demonstrated in Figure 4.3. In the unfiltered light beam, a reflection resembling an interferometry fringe may be observed, due to the referred high spatial frequencies. In the filtered light beam, visual noise is completely absent, due to the elimination of the high spatial frequencies, and the intensity is higher, as the light rays are parallel to each other.

The bi-convex lens, designated KBX043 with a focal length of 19.0 mm, focuses the beam that comes out of the collimator and pinhole system. With this component, it is possible to focus the light intensity on the sample surface, and the diameter of the high intensity spot can be manipulated by changing the distance from the lens to the sample. Lower diameters of the spot usually mean that the intensity is higher, and vice-versa. The lens' focal length is an important parameter as it indicates the distance at which the diameter is the lowest, or the light intensity is the highest. In this project, the distance between the lens and the sample was set at 10 cm. The lens can be observed in Figure 4.4.

The final component of the system is a camera, a Basler ace acA2000-165 um, for image capture, has a lens was attached, a LFF-8012C-D75 model. This lens possesses manual configurable aperture, or iris range, and zoom, or focus control, through the means of rotating rings. It possessed a focal length of 75mm. The iris range varied between F1.8 and F22, even though the lens

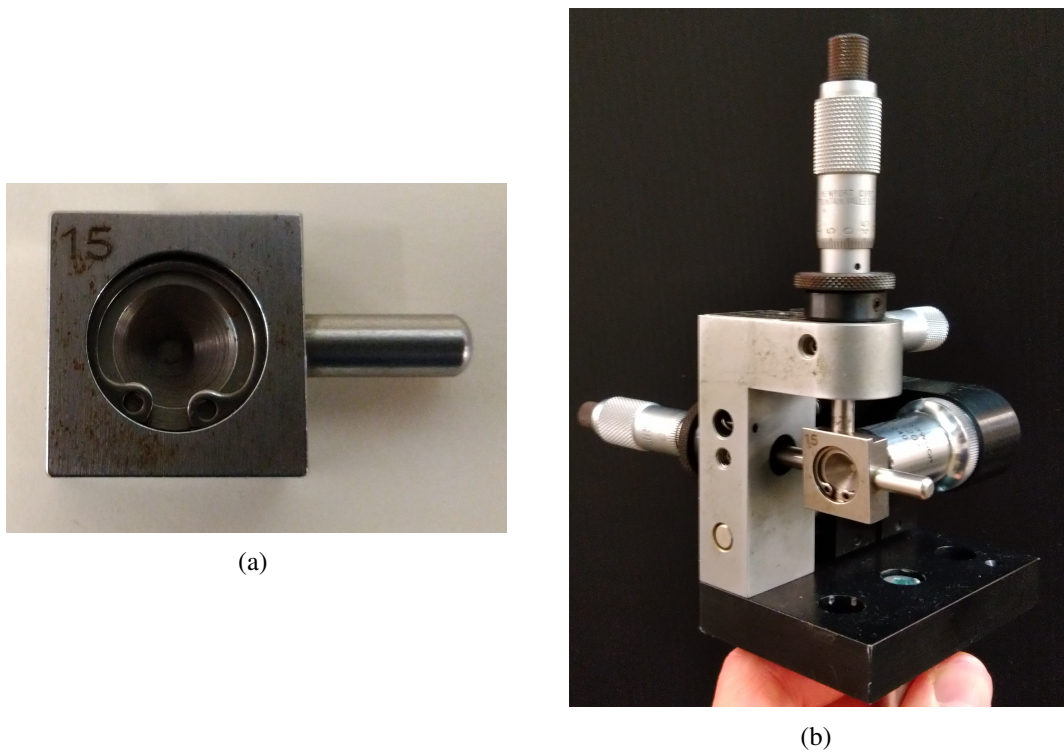


Figure 4.2: The Collimator + Pinhole component (a) Pinhole (b) Mounted component

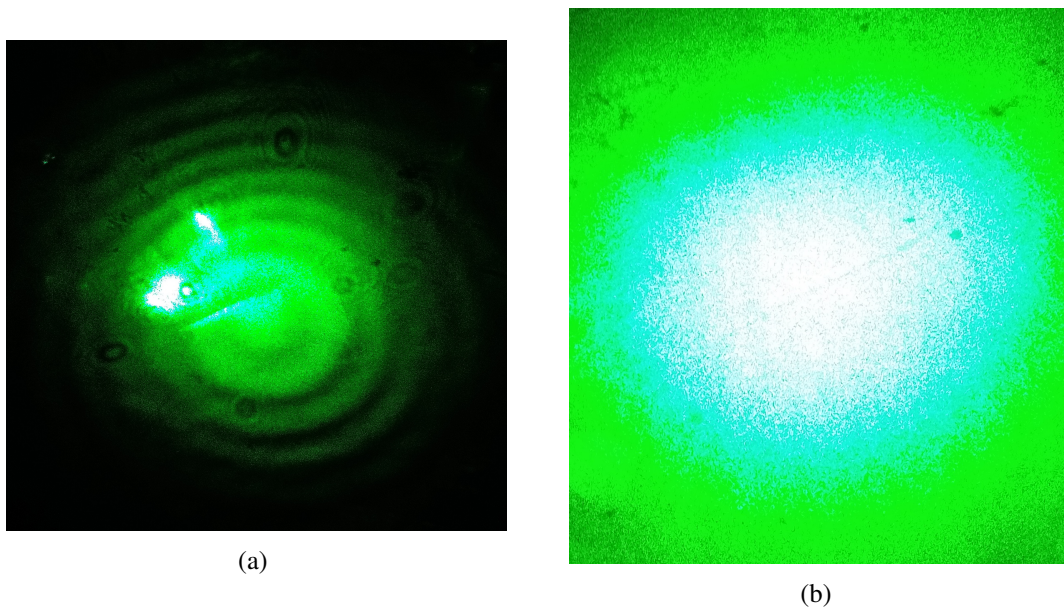


Figure 4.3: The light beam (a) Unfiltered (b) Filtered with the collimator and pinhole setup.

could be closed a bit more than the closure at F22. The component can be observed in Figure 4.5.

The entire assembly may be seen in Figure 4.6.

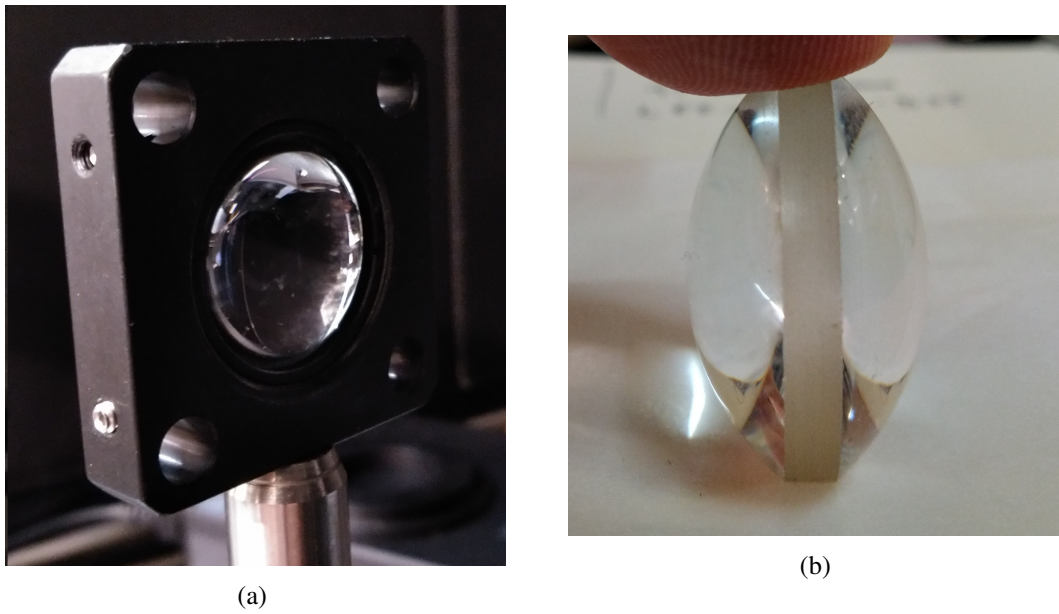


Figure 4.4: Biconvex lens (a) Mounted in the assembly (b) Unmounted

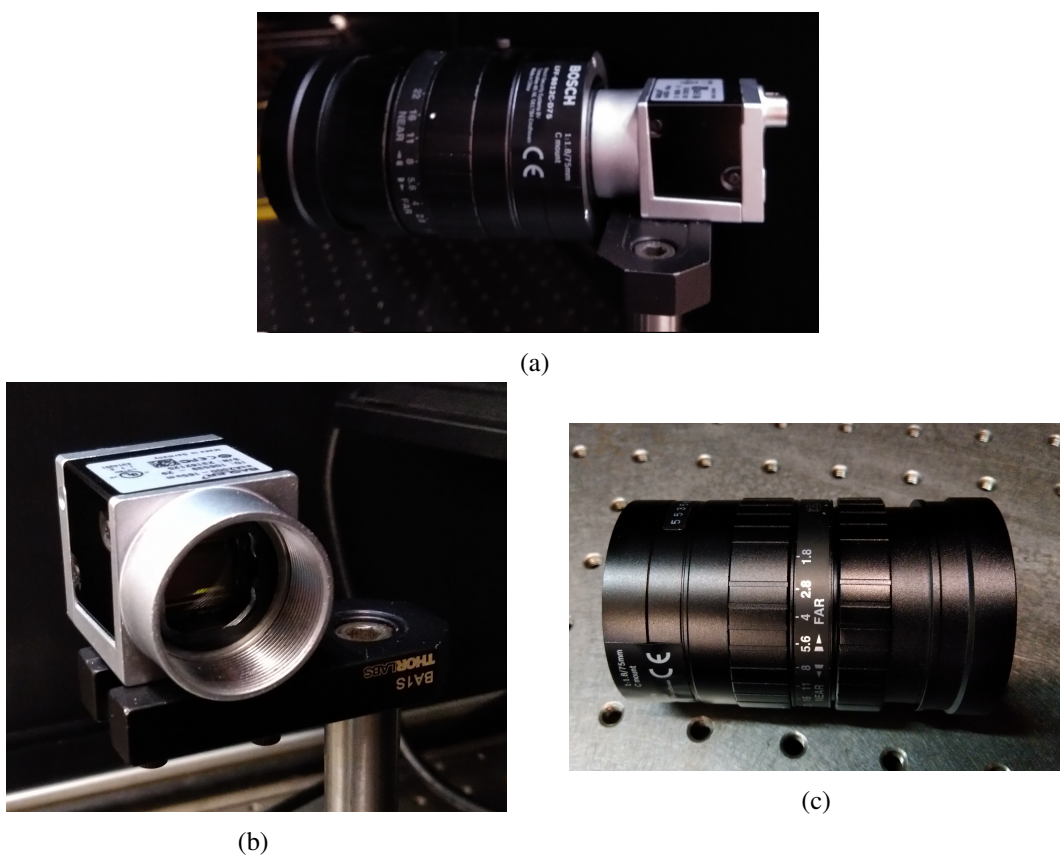


Figure 4.5: Camera and lens setup (a) Mounted in the assembly (b) Camera (c) Lens

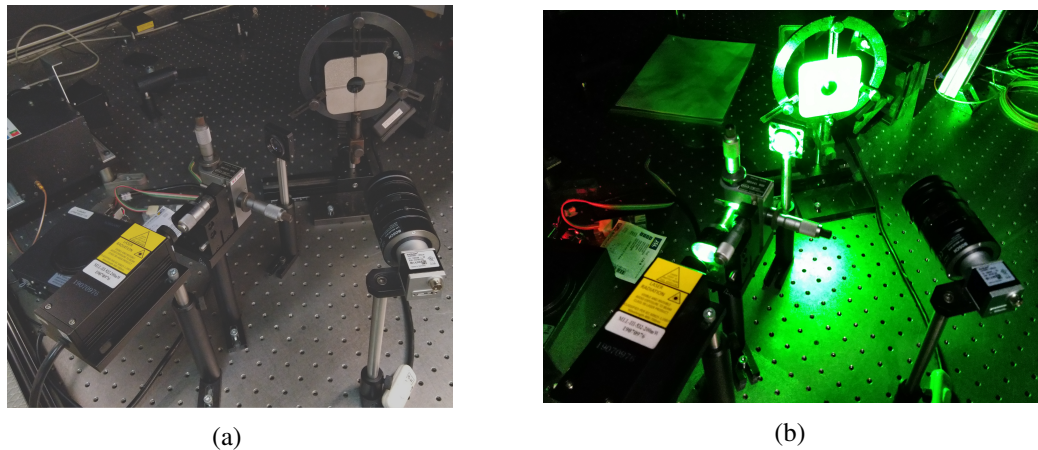


Figure 4.6: System disposition (a) Laser turned off (b) Laser turned on

4.2 Samples

One component that was left out from the previous section were the samples that are to be examined. The samples consisted of calibrated metal sheets with known surface roughness sections. Two different pieces were available, with different roughness ranges. One is designated Rugotest No. 3, acquired from Senze Instruments, and the other is a simple Surface Roughness Comparator, acquired from Paint Test Equipment . These two instruments will be reviewed next, and the technical datasheets of both samples is included in the appendix sections.

4.2.1 Rugotest No. 3

This comparator (Figure 4.7) is made of high-nickel test plate, and complies with standards NF/E05-051, ASTM D 4417/A, ISO 2632 / I 1975, ISO 2632/II 1977. It possesses 18 different sections, 9 of them were treated with shot-blasting (column A), the other 9 with grit blasting (column B). Depending on the possessed surface topology, each section of the sheet was assigned a designation. The designations are, from bottom to top, 6, 7, 8, 9b, 9a, 10b, 10a, 11b, 11a. To each surface roughness value is assigned a different number (6, 7, 8, 9, 10, 11). The "a" and "b" part, present on the numbers 9 upwards, depends on if the grain is designed as coarse or fine: "a" for coarse grain, "b" for fine grain.

The roughness parameter chosen to describe the surface was R_a , and the values for each section are:

- $N6 = 0.8 \mu\text{m}$;
- $N7 = 1.6 \mu\text{m}$;
- $N8 = 3.3 \mu\text{m}$;
- $N9 = 6.3 \mu\text{m}$;

- N10 = 12.5 μm ;
- N11 = 25 μm .

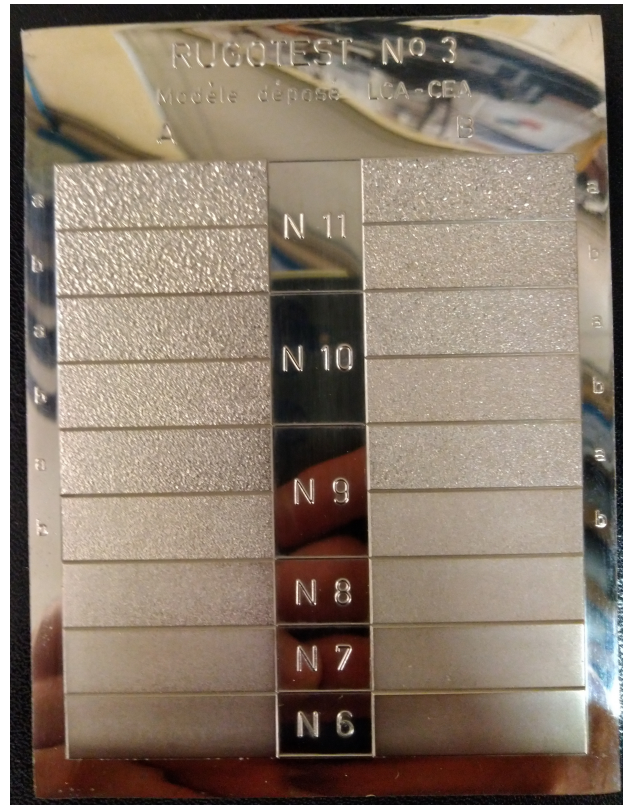


Figure 4.7: Rugotest No. 3.

Even though the type of grain is different between 9a and 9b, 10a and 10b, and 11a and 11b, their R_a values are still equal.

4.2.2 Paint Comparator

Similarly to the Rugotest no.3, the Paint Comparator (Figure 4.8) is also made of nickel, complying with the standards ISO 8503-1, ISO 8503-2 and ASTM D4417. It is divided in 4 different sections, numbered 1 through 4, each one with a different surface roughness value. Its surface suffered shot-blasting treatment.

The chosen roughness parameter was also R_a , and the values for each section are:

- N1 = 25 μm ;
- N2 = 40 μm ;
- N3 = 70 μm ;
- N4 = 100 μm .



Figure 4.8: Paint Comparator.

With the Paint Comparator's surface being shot-blasted, only the Rugotest's column A, with the shot-blasted surfaces, will be considered in the project. In the next chapters, the surfaces will be referred to as their respective number, with surfaces N1, N2, N3 and N4 belonging to the Paint Comparator, while surfaces N6, N7, N8, N9a, N9b, N10a, N10b, N11a and N11b belong to the Rugotest No. 3. Surfaces N4 and N6 possess the same roughness value, which will be useful to see the discontinuity between surfaces.

4.3 Captured Images

Before explaining the technique which was utilized in order to correlate the speckle pattern to surface roughness, a quick exposition of the captured images is important. By visually showing the results of the physical assembly, the task of explaining the adjustments made to the speckle pattern approach will be made easier. As such, an example of the speckle pattern that will be the focus of analysis is given (Figure 4.9).

As it's been explained in a previous chapter, the different spots result from the interference of the reflected light waves on the innumerable surface disturbances. The intensity percentage varies between 0 and 1, 0 being the algebraic sum of waves with a phase difference of half a wavelength, originating dark spots, and 1 being the algebraic sum of waves with the same phase, originating bright spots.

It must be added that the overall "brightness" of the surface greatly depends on the lens aperture and the distance between the camera and the samples, a fact well known from Speckle Metrology

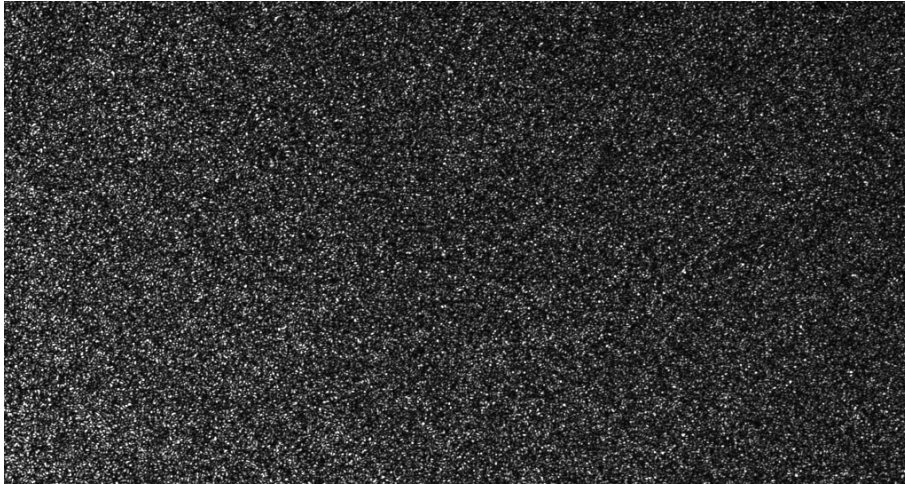


Figure 4.9: Speckle pattern example, with a distance of 4 cm and maximum iris range.

- subjective speckle which is what observed by the imaging system, changes size according to the lens aperture. Adjusting these two factors will severely affect the aspect of the reflection's result. The above speckle pattern example (Figure 4.9) was captured with a distance between the lens and camera of 4 cm, and the maximum iris range, while the example below (Figure 4.10) was captured with the same distance, but with an iris range of F16. Although the angle of incidence remained the same, and the distance was also not altered, the lens aperture (or iris range) affected the overall visual result of the captures.

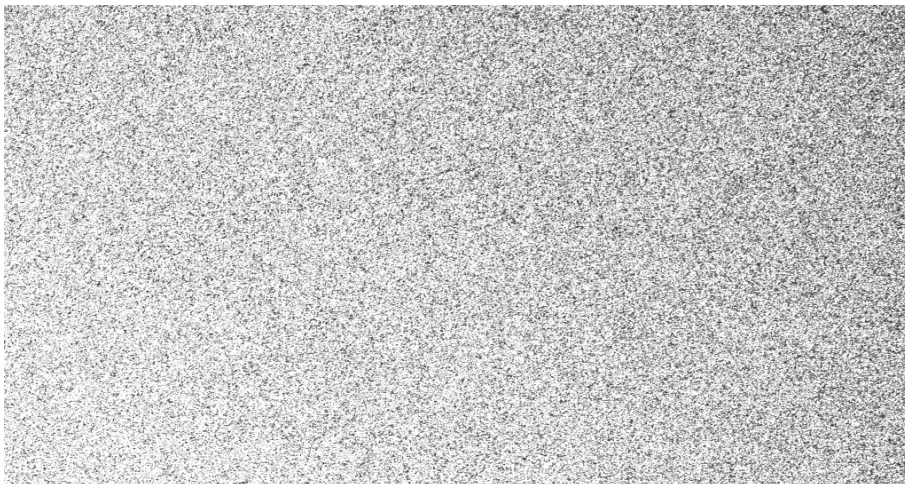


Figure 4.10: Speckle pattern example, with a distance of 4 cm and an iris range of F16.

With these additional principles introduced, the explanation of the final approach utilized in speckle pattern analysis will be better understood.

4.4 Adjustments to Speckle Pattern Techniques

In chapter 3, it has been established a common approach to the analysis of Speckle Pattern, that consisted in capturing the reflection of a coherent light beam on the sample's surface, to then rotate the sample, and capturing the reflection again. The change in the incidence angle would alter the reflection of the light, by changing the light's scattering, resulting in a different speckle pattern.

The absence of a mechanism that would ensure the rotation of the sample that was being examined greatly affected the initial results, as the rotation would have to be done manually, providing a low rotation accuracy. As such, the angle wouldn't be the same for each rotation, resulting in low precision results.

As the manual rotation process was rendered unreliable, instead of building a mechanism that would ensure an accurate rotation for each examination of the sample, a different approach was devised and implemented. Instead of making an examination based on a single surface, making it an absolute measurement, a relative measurement methodology was considered. This means that the results of the developed method would greatly depend on the calibration and environmental circumstances of the system, and not on pre-established empirical evidence.

Before establishing the procedures that were experimented, it is important to introduce the means that were used in order to quantify speckle pattern's properties. The Haralicks' procedures [61], referred to in chapter 3, were the perfect fit for the necessity to translate visual patterns into physical quantities. These statistical parameters described perfectly the information that can be obtained from the speckle pattern, and there was an attempt to achieve a correlation between them and surface roughness. That is why, as suggested above, the visual result of the lens aperture and camera distance was so important, as the statistical parameters were altered in function of the referred adjustable settings.

Describing then the procedures, a number of system geometries was tried out, and any possible correlations between surface roughness and the camera distance to the sample, and/or lens aperture settings, were studied. The procedure consisted in capturing all of the surfaces with the camera without changing either the camera distance to the sample or the lens aperture. After all the surfaces were photographed, the lens aperture would be changed, capturing again all of the surfaces. Once the surfaces were captured with every lens aperture setting, the distance would be changed, repeating once again the photographs with all the lens aperture settings. The objective was to find an optimal spot for surface roughness correlation.

It is worth nothing that the captured images were all off-set to the left instead of centered, for reasons that will be explained in a future section.

Once the speckle patterns were captured, each set of photographs of each section taken with the same distance and lens aperture were introduced into a software that would analyse them and find if the statistical parameters calculated for each image would form any kind of correlation or not. This analysis would put in numerical terms how optimal the combination of distance and lens aperture for that particular set of captures would be.

As it's also been referred to in a previous chapter, not all of the Haralick's statistical parameters would be utilized. After several trial and error analysis, only two of the statistical parameters would be conclusive in finding some kind of correlation between image information and surface roughness. These were the Contrast (Equation 3.2) and Energy, or Angular Second Moment (Equation 3.1). To these two parameters, a third was added: Intensity. This third parameter is quite simple, and doesn't need the gray level co-occurrence matrix; it is simply the average of the pixel intensity value for each pixel on a certain image.

For each set of 13 images, a total of 5 analysis in each software were carried out:

- A Paint Comparator analysis with sections N1, N2, N3 and N4, which will be named surface group 1;
- A Rugotest No. 3 analysis with common and coarse grain sections N6, N7, N8, N9a, N10a and N11a, which will be named surface group 2;
- A Rugotest No. 3 analysis with common and fine grain sections N6, N7, N8, N9b, N10b and N11b, which will be named surface group 3;
- A Paint Comparator + Rugotest No. 3 (coarse grain) with sections N1, N2, N3, N4, N6, N7, N8, N9a, N10a and N11a, which will be named surface group 4;
- A Paint Comparator + Rugotest No. 3 (fine grain) with sections N1, N2, N3, N4, N6, N7, N8, N9b, N10b and N11b, which will be named surface group 5.

The analysis groups are visually arranged in Table 4.1:

Table 4.1: Analysis Groups

	Group 1	Group 2	Group 3	Group 4	Group 5
N1	X			X	X
N2	X			X	X
N3	X			X	X
N4	X			X	X
N6		X	X	X	X
N7		X	X	X	X
N8		X	X	X	X
N9a		X		X	
N9b			X		X
N10a		X		X	
N10b			X		X
N11a		X		X	
N11b			X		X

The objective of the 5 analysis was to find out the influence of the surface roughness value range in the accuracy of the measurements.

The computer analysis will be thoroughly explained in the following section.

4.5 Image processing

As it's been referred to, a great part of this project is computer processing of the captured image. For this analysis, the procedure can be separated in several steps, as to help the comprehension of this process.

Step 1

The first step was storing the captured images in a pre-defined folder and their introduction in the software. As such, for each distance and lens aperture setting, a different folder was created, that contained a total of 13 pictures, one for each section (sections N1, N2, N3, N4, N6, N7, N8, N9a, N9b, N10a, N10b, N11a, N11b). The act of introducing them in the software depends on the program used.

Step 2

After the introduction in the software, a cropping of these images was done. As the sections from Rugotest No. 3 dimensions' were small, it was necessary to crop each image to correctly describe only the correct section. This is the reason that the intensity peak was off-set to the left, it was easier to capture and crop each section proceeding as stated.

As the distance from the camera to the sample increases, the dimension of the section of the area being analysed decreases. As such, the dimensions for the cropping of the images that were taken with a distance between camera and sample of 4 cm will not be the same dimensions for the cropping of the images for a distance of 24 cm. Thus, each set of captures must be evaluated and the dimensions for the cropping manually inserted.

Step 3

As the images are ready to be analysed, Intensity can now be calculated, as it does not depend on the gray level co-occurrence matrix. Thus, the mean intensity of every image in the software is calculated and concatenated into a vector. This way, intensity is ready to be analysed.

Step 4

The gray level co-occurrence matrix is now calculated for every direction (0°, 45°, 90° and 135°).

Step 5

Haralick's parameters, Contrast and Energy, are calculated for every direction, from the gray level co-occurrence matrix, for each image.

Step 6

For each image, the average value of the 4 different directions of the parameters Contrast and Energy is calculated. The obtained average values are then concatenated into two vectors, one for Contrast and one for Energy. Both statistical parameters are now ready to be utilized.

Step 7

Vectors for each group of sections are created, as defined above for each analysis, concatenating the adequate section's parameters values to the vectors. A total of 5 different vectors, one for each surface section group, is then created for the three parameters (Intensity, Contrast and Energy), totalling 15 vectors.

Step 8

A linear regression is performed with the values of the vectors on the y axis, and the surface roughness values respective each parameter on the x axis. The linear regression is performed for every vector concatenated in Step 7, also totalling 15 linear regressions.

Step 9

The linear regression error is evaluated for every performed linear regression. This error is what informs us of how appropriate the approximation to a linear function is. As each linear regression error is calculated for every performed linear regression, a total of 15 different values of error will be output.

Step 10

The different error values are then saved in an Excel file, that will allow the visualization of the optimal measurement settings combination.

A demonstration of the software scripts will be given followingly, carefully exhibiting and explaining each used function for each of the steps described above. As the full script is quite repetitive for each of the images and vectors concatenated, only cutouts from it will be shown, exemplifying only one case (the treatment of of one image, the calculations involving one vector, etc.). The full scripts are available in the Appendices section.

4.5.1 Matlab

In this section, the script written for Matlab will be demonstrated, while following the just established steps. As it's been said, only one example for each function will be exhibited, as the code is quite repetitive and this section would just become too cluttered.

In the beginning of the code, the dimension of the GLCM matrix and the roughness vectors which will be used in the drawing of the graphics were initialised. It is worth noting that a special notation was used for each surface section group:

- The notation Comp is used for the Paint Comparator Analysis (sections N1, N2, N3 and N4);
- The notation RugF is used for the Rugotest No. 3 fine grain analysis (sections N6, N7, N8, N9b, N10b and N11b);
- The notation RugC is used for the Rugotest No. 3 coarse grain analysis (sections N6, N7, N8, N9a, N10a and N11a);
- The notation Comp_RugF is used for the Paint Comparator + Rugotest No. 3 fine grain analysis (sections N1, N2, N3, N4, N6, N7, N8, N9b, N10b and N11b);
- The notation Comp_RugC is used for the Paint Comparator + Rugotest No. 3 coarse grain analysis (sections N1, N2, N3, N4, N6, N7, N8, N9a, N10a and N11a);

```

1 %% Variable declaration
2 M = 256; %Matrix dimension
3 Roughness = [0.8; 1.6; 3.2; 6.3; 12.5; 25; 25; 40; 70; 100];
   %For Comparator + Rugotest (Fine/Coarse)
4 Roughness_Comp = Roughness(7:10); %For Comparator
5 Roughness_RugF = Roughness(1:6); %For Rugotest (Fine)
6 Roughness_RugC = Roughness(1:6); %For Rugotest (Coarse)

```

Algorithm 4.1: Matlab analysis - General variable initialisation

Step1

Introducing the images in Matlab is quite an easy task. As the images are stored in the .bmp format, it is not necessary to convert them to binary. If they were stored as any other image format (.png, .jpg or .jpeg, per example), an additional function would be necessary to convert them to binary. The function *imread*, whose only parameter is the name of the image, stores the image in the Matlab memory by assigning it to a variable, which will be named *I1r*.

```

1 %% Image Introduction
2 I1r = imread('1.bmp');

```

Algorithm 4.2: Matlab analysis - Storing the images in Matlab's memory

Step 2

For the cropping of the images, the function *imcrop* was used, whose parameters are the variable in which the image was stored, and the dimensions of the crop. A separate variable was created to store the dimensions of the crop, named *targetsize*. For the *imcrop* function, the dimensions must be in the form of a 1x4 vector, whit the first two values being the horizontal and vertical offsets, and the last two being the horizontal and vertical cropping dimensions.

```

1 %% Image Cropping
2 targetsize = [0 0 825 1050];
3 I1 = imcrop(I1r, targetsize);

```

Algorithm 4.3: Matlab analysis - Cropping of the introduced images

As such, in this example, the image resulting from the cropping will have the resolution 825x1050. This image is stored in the variable *I1*.

Step 3

The Intensity value for each cropped image is then calculated, using the function *mean2*. The only parameter for this function is the variable in which image was stored, whose Intensity value will be calculated.

```

1 %% Intensity Calculation
2 Intensity1 = mean2(I1);

```

Algorithm 4.4: Matlab analysis - Calculation of the Intensity for each image

Step 4

Using the cropped images obtained in **Step 2**, the GLCM for each image is calculated. For this purpose, the function *graycomatrix* is used. The parameters for this function are the variable in which the image whose GLCM is being calculated was stored, the gray levels range that will be utilized (GrayLimits), the dimension of the matrix (NumLevels) and finally the direction in which the GLCM will be calculated (Offset).

As it is necessary to calculate the GLCM in all four directions, a vector is created to specify the directions, *offsets*. This vector, declared in the code below, has a special kind of input ([0 1] is the equivalent to 0°, [-1 1] is the equivalent to 45°, [-1 0] is the equivalent to 90° and [-1 -1] is the equivalent to 135°).

```

1 %% GLCM Creation
2 offsets = [0 1; -1 1; -1 0; -1 -1];
3 glcm1 = graycomatrix(I1, 'GrayLimits', [0 255], 'NumLevels', M,
  'Offset', offsets);
4 \label{alg:glcmcreation}

```

Algorithm 4.5: Matlab analysis - Creation of the Gray Level Co-occurrence Matrices for each image

Step 5 and Step 6

Both **step 5** and **step 6** are done in one line of code, so they were joined in this example.

The calculation for both Contrast and Energy is done in a similar way. The result of Algorithm 4.5 is the creation of 4 matrices for each image, one for each direction. As such, it is necessary to transform the GLCM into the properties Contrast and Energy for every matrix, and averaging the values of the four directions. Thus, the function *graycoprops* is used. This function returns the value for four different parameters, Contrast, Energy, Homogeneity and Correlation. As only Contrast and Energy are needed, the last two will be ignored.

The commands that allow the calculation of the average value from the four dimension's matrices for both parameters will then be showcased, using basic algebraic manipulation.

```

1 %% Contrast Calculation
2 Contrast1 = (graycoprops(glcm1(:, :, 1)).Contrast +
  graycoprops(glcm1(:, :, 2)).Contrast +
  graycoprops(glcm1(:, :, 3)).Contrast +
  graycoprops(glcm1(:, :, 4)).Contrast) ./ 4;
3 %% Energy Calculation
4 Energy1 = (graycoprops(glcm1(:, :, 1)).Energy +
  graycoprops(glcm1(:, :, 2)).Energy +
  graycoprops(glcm1(:, :, 3)).Energy +
  graycoprops(glcm1(:, :, 4)).Energy) ./ 4;

```

Algorithm 4.6: Matlab analysis - Calculation of Contrast and Energy for each image

Step 7

With the three established statistical parameters obtained for each image, the vector concatenation for further analysis is now performed. Referring to the notation established in the beginning of the Matlab section, the vectors are created with the respective values for the already established surface sections.

```

1 %% Intensity Vector Concatenation
2 Intensity_Comp = [Intensity1; Intensity2; Intensity3;
   Intensity4 ];
3 Intensity_RugC = [Intensity6; Intensity7; Intensity8;
   Intensity9a; Intensity10a; Intensity11a ];
4 Intensity_RugF = [Intensity6; Intensity7; Intensity8;
   Intensity9b; Intensity10b; Intensity11b ];
5 Intensity_Comp_RugF = [Intensity_RugF; Intensity_Comp ];
6 Intensity_Comp_RugC = [Intensity_RugC; Intensity_Comp ];
7 %% Contrast Vector Concatenation
8 Contrast_Comp = [Contrast1; Contrast2; Contrast3; Contrast4 ];
9 Contrast_RugC = [Contrast6; Contrast7; Contrast8; Contrast9a;
   Contrast10a; Contrast11a ];
10 Contrast_RugF = [Contrast6; Contrast7; Contrast8; Contrast9b;
   Contrast10b; Contrast11b ];
11 Contrast_Comp_RugF = [Contrast_RugF; Contrast_Comp ];
12 Contrast_Comp_RugC = [Contrast_RugC; Contrast_Comp ];
13 %% Energy Vector Concatenation
14 Energy_Comp = [Energy1; Energy2; Energy3; Energy4 ];
15 Energy_RugC = [Energy6; Energy7; Energy8; Energy9a; Energy10a;
   Energy11a ];
16 Energy_RugF = [Energy6; Energy7; Energy8; Energy9b; Energy10b;
   Energy11b ];
17 Energy_Comp_RugF = [Energy_RugF; Energy_Comp ];
18 Energy_Comp_RugC = [Energy_RugC; Energy_Comp ];

```

Algorithm 4.7: Matlab analysis - Vector concatenation for each statistical parameter, for each surface section's group analysis

As such, the previously referred 15 vectors are present.

Additionally, as a control measure, different graphics were plotted as to gain the ability to visualize each of these analysis individually, if necessary. An example of the written instructions is given below, for the analysis of the Intensity values for the Paint Comparator.

```

1 %% Roughness - Intensity Graph Plot
2 figure (1)
3 plot(Roughness_Comp , Intensity_Comp );

```

```

4 xlabel('Roughness');
5 ylabel('Intensity');
6 title('Comparator: Roughness - Intensity');

```

Algorithm 4.8: Matlab analysis - Plotting of the graphics for individual group analysis control

Step 8 and Step 9

As the last step, the linear regression is performed and the error is calculated. An example will be given, for the Paint Comparator analysis, performing the linear regression on the Contrast parameter. The variable R_Comp1 at the end is the linear regression error for the parameter Contrast.

```

1 %% Linear Regression Analysis for Comparator
2 % Contrast
3 X_Comp1 = [ones(length(Roughness_Comp),1) Roughness_Comp];
4 b_Comp1 = X_Comp1 \ Contrast_Comp;
5 yCalc_Comp1 = X_Comp1 * b_Comp1;
6 figure(15)
7 scatter(Roughness_Comp, Contrast_Comp);
8 hold on
9 plot(Roughness_Comp, yCalc_Comp1);
10 xlabel('Roughness');
11 ylabel('Contrast');
12 title('Roughness-Contrast');
13 grid on
14 R_Comp1 = 1 - sum((Contrast_Comp - yCalc_Comp1).^2) /
    sum((Contrast_Comp - mean(Contrast_Comp)).^2);

```

Algorithm 4.9: Matlab analysis - Linear regression for each parameter for the Comparator

At the end of the linear regressions for the three parameters, the error values for each one are concatenated into a vector.

```

1 R_Comp = [R_Comp1, R_Comp2, R_Comp3];

```

Algorithm 4.10: Matlab analysis - Concatenation of each parameter's linear regression errors for the Comparator

Finalizing the script, all the linear regressions associated errors for each of the statistical parameter, for the five analysis' group, are concatenated into one matrix.

```

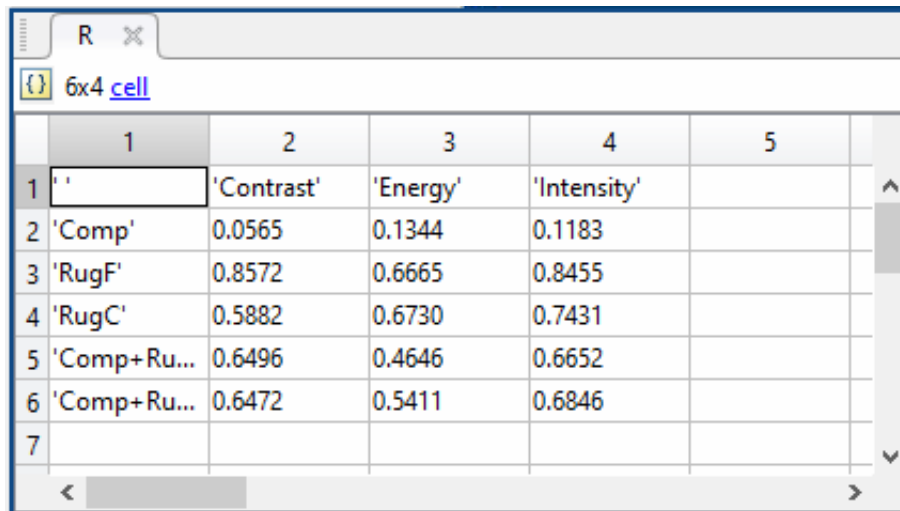
1 R1 = [R_Comp; R_RugF; R_RugC; R_Comp_RugF; R_Comp_RugC];
2 header1 = {'Comp'; 'RugF'; 'RugC'; 'Comp+RugF'; 'Comp+RugC'};
3 header2 = {' ', 'Contrast', 'Energy', 'Intensity'};
4 R = [header2; header1, num2cell(R1)];

```

Algorithm 4.11: Matlab analysis - Matrix creation for all linear regression analysis' error

As described, the script performs a complete analysis of the images. The input is the set of images captured from the different surface sections, and the output is the set of the linear regression errors, indicators of the adequacy of each performed approximation.

The output can be visualized in Figure 4.11, the values being meaningless to the current show-case.



	1	2	3	4	5
1	'	'Contrast'	'Energy'	'Intensity'	
2	'Comp'	0.0565	0.1344	0.1183	
3	'RugF'	0.8572	0.6665	0.8455	
4	'RugC'	0.5882	0.6730	0.7431	
5	'Comp+Ru...	0.6496	0.4646	0.6652	
6	'Comp+Ru...	0.6472	0.5411	0.6846	
7					

Figure 4.11: Output of the Matlab script for speckle pattern analysis.

4.5.2 MVTec Halcon

In a similar way, a script for the software MVTec Halcon was also written. The commands and instructions are quite different, and, as it is not a mathematical software, so the concatenation of the vectors for each surface section's group and further linear regression analysis were also performed in Matlab. Thus, MVTec Halcon was only utilized to acquire the statistical parameters (Intensity, Energy and Contrast). A thorough walkthrough of the script, following the established steps, will be given.

Step 1

The introduction of the images to Halcon's memory is executed with the function `read_image`, whose parameters are the variable in which the image will be stored and the name of the file on the computer.

```
1 read_image ( Image1 , ' 1 . bmp ' )
```

Algorithm 4.12: MVTec's Halcon analysis - Storing the images in Halcon's memory

Step 2

The cropping is performed in a different manner, in comparison to Matlab. In Halcon, the final dimensions of the image after the crop are defined, by creating a region with those dimensions. For the same distance from camera to sample as the one given to Matlab, the final region must

have a resolution of 800x1050. As such, a rectangle with the dimensions 800x1050 is created, and then applied over the images, cutting whatever is left out of the region.

For the region generation, the function *gen_rectangle* is used, whose parameters are the name of the variable in which the region will be stored, the next two values are the offset from the origin, and the last two are the dimensions of the region.

Each of the future functions that will be utilized in the remaining steps include a parameter for the region in which they will operate. As such, the next two functions are only to generate visual feedback on the cropping, in order to verify if the cropping was done correctly or not. For the actual cropping, the function *reduce_domain* is used, whose parameters are the variable in which the image that will be cropped is stored, the variable in which the region is stored, and finally the name of the variable in which the cropped image will be stored.

Finally, the function *emphasize* is present only to provide the referred visual feedback from the cropping.

```
1 gen_rectangle1 (Rectangle , 0.0 , 0.0 , 1050 , 800)
2 reduce_domain (Image1 , Rectangle , Mask1)
3 emphasize (Mask1 , Emphasize1 , 9 , 9 , 1.0)
```

Algorithm 4.13: MVTec's Halcon analysis - Cropping of the introduced images

Step 3

After the generation of the region in which the parameters will be evaluated, Intensity can be calculated. For this purpose, the function *intensity* is used, whose parameters are the region in which the parameter will be calculated, the image that will be evaluated, the variable in which the mean intensity will be stored, and the variable in which the value deviation will be stored.

```
1 intensity (Rectangle , Image1 , Mean1 , Deviation1)
```

Algorithm 4.14: MVTec's Halcon analysis - Calculation of the Intensity for each image

Step 4 and Step 5

With the intensity values for each image calculated, the focus will now be on the remaining parameters. First, the gray level co-occurrence matrices are created. In Halcon, as opposed to Matlab, it is impossible to calculate the matrices of the four direction in one command. As such, it is needed to repeat the command four times for each image, specifying the direction.

The function that allowed the creation of the GLCMs was *gen_cooc_matrix*, whose parameters were the region that would be analysed, the original image, the variable in which the generated matrix would be stored, the gray level range values (0 for minimum, 8 for maximum), and finally, the direction of the analysis.

The calculation of the parameters was performed along the creation of the multiple GLCMs. The function for the parameter calculation returned values for the Energy, Correlation, Homogeneity and Contrast, similarly as the function *graycoprops* in Matlab. Again, as only Energy and Contrast are needed, the other two are ignored.

The function utilized for the calculation of these statistical parameters was *cooc_feature_matrix*, whose parameters were the name of the matrix from which the calculations would be made, followed by the variables in which each parameter's value would be stored.

The example below is solely for the calculation of the parameters of one image.

```

1 gen_cooc_matrix(Rectangle , Image1 , Matrix01 , 8 , 0)
2 cooc_feature_matrix(Matrix01 , Energy01 , Correlation01 ,
   Homogeneity01 , Contrast01)
3
4 gen_cooc_matrix(Rectangle , Image1 , Matrix451 , 8 , 45)
5 cooc_feature_matrix(Matrix451 , Energy451 , Correlation451 ,
   Homogeneity451 , Contrast451)
6
7 gen_cooc_matrix(Rectangle , Image1 , Matrix901 , 8 , 90)
8 cooc_feature_matrix(Matrix901 , Energy901 , Correlation901 ,
   Homogeneity901 , Contrast901)
9
10 gen_cooc_matrix(Rectangle , Image1 , Matrix1351 , 8 , 135)
11 cooc_feature_matrix(Matrix1351 , Energy1351 , Correlation1351 ,
   Homogeneity1351 , Contrast1351)

```

Algorithm 4.15: MVTec's Halcon analysis - Creation of the Gray Level Co-occurrence Matrices in all four directions and calculation of Contrast and Energy for each direction

Step 6

The calculation of the average from the four direction's values for each parameter is now easily performed.

```

1 Energy1 := (Energy01 + Energy451 + Energy901 + Energy1351)/4
2 Contrast1 := (Contrast01 + Contrast451 + Contrast901 +
   Contrast1351)/4

```

Algorithm 4.16: MVTec's Halcon analysis - Calculation of the average Energy and Contrast with values from the four established directions

Step 7

The concatenation of the vectors is now made possible. Nevertheless, as already mentioned, Halcon is not a mathematical software. As such, the "jump" to Matlab was considered adequate at this moment. Thus, there were three vectors that were concatenated in Halcon, containing all the parameter's values from each image. Along the concatenation of these vectors, three text file (.txt) were generated, each containing information about one of the parameters. These text files were promptly named "Energy", "Contrast" and "Intensity".

```

1 Energy := [Energy1 , Energy2 , Energy3 , Energy4 , Energy6 ,
            Energy7 , Energy8 , Energy9a , Energy9b , Energy10a , Energy10b ,
            Energy11a , Energy11b ]
2 write_tuple (Energy , 'Energy')
3
4 Contrast := [Contrast1 , Contrast2 , Contrast3 , Contrast4 ,
             Contrast6 , Contrast7 , Contrast8 , Contrast9a , Contrast9b ,
             Contrast10a , Contrast10b , Contrast11a , Contrast11b ]
5 write_tuple (Contrast , 'Contrast')
6
7 Intensity := [Mean1 , Mean2 , Mean3 , Mean4 , Mean6 , Mean7 , Mean8 ,
              Mean9a , Mean9b , Mean10a , Mean10b , Mean11a , Mean11b ]
8 write_tuple (Intensity , 'Intensity')

```

Algorithm 4.17: MVTec's Halcon analysis - Concatenation of the vectors containing information about each image, and generation of the text file containing them

This way, the operation in MVTec Halcon has been finalized.

Returning now to Matlab, the text file must be opened in the software's area and the parameter's values information contained in it must be stored. The way Halcon generates these files is quite peculiar, as every line that is wrote contains a "2" in the beginning of it, meaning that the writing of the value was successful. Additionally, a number is wrote in the first line. An example might be observed in Figure 4.12.

This characteristic of the generated files made it quite hard for a rapid storage in Matlab, as only the second column is needed, and the first line is unnecessary. First, the problem of opening the text files and the consequent storage of the information contained in them was solved.

```

1 %% Copy of the Halcon generated files
2 formatSpec = '%f';
3 fileID1 = fopen('Contrast', 'r');
4 sizeContrast_1 = [2 Inf];
5 Contrast_1 = fscanf(fileID1, formatSpec, sizeContrast_1);
6 Contrast_1 = Contrast_1';
7 fclose(fileID1);

```

Algorithm 4.18: MVTec's Halcon analysis - Opening the text files generated by Halcon in Matlab's environment

By now, the information that was contained in the Halcon generated files is inserted in Matlab. Only the problem of the column of "2"s and the removal of the first line remains. This was solved by accessing into the created matrix, and extracting the lines below the first, and the second column, creating a single column vector, in which the information was organized by the section's number, by the following order: N1 - N2 - N3 - N4 - N6 - N7 - N8 - N9a - N9b - N10a - N10b - N11a - N11b.

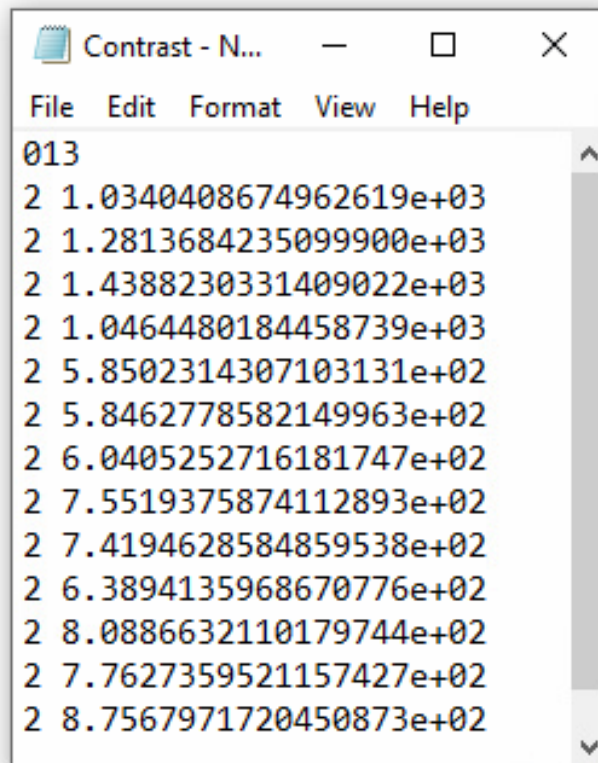


Figure 4.12: Text file generated in MVTec Halcon.

```
1 %% Parameter's values extraction
2 Contrast = Contrast_1(2:14,1);
```

Algorithm 4.19: MVTec's Halcon analysis - Obtaining the surface information from the text file

Now, the information on each parameter's values is inside Matlab, neatly organized. At the same time, the vectors for the Surface Roughness values were created, similarly to the variable initialisation in the Matlab section.

```
1 Roughness = [0.8; 1.6; 3.2; 6.3; 12.5; 25; 25; 40; 70; 100];
2 Roughness_Comp = Roughness(6:9);
3 Roughness_RugF = Roughness(1:6);
4 Roughness_RugC = Roughness(1:6);
```

Algorithm 4.20: MVTec's Halcon analysis - Vectors containing surface roughness values for each section group were created

The concatenation of the vectors for each parameter and each analysis group was also performed.

```
1 %% Concatenating Parameter Vectors
2 % Contrast
```

```

3 Contrast_Comp = Contrast(1:4, :); % Comparator
4 Contrast_RugC = [Contrast(5); Contrast(6); Contrast(7);
    Contrast(8); Contrast(10); Contrast(12)]; % Rugotest Coarse
5 Contrast_RugF = [Contrast(5); Contrast(6); Contrast(7);
    Contrast(9); Contrast(11); Contrast(13)]; % Rugotest Fine
6 Contrast_Comp_RugC = [Contrast_RugC; Contrast_Comp]; %
    Comparator + Rugotest Coarse
7 Contrast_Comp_RugF = [Contrast_RugF; Contrast_Comp]; %
    Comparator + Rugotest Fine

```

Algorithm 4.21: MVTec's Halcon analysis - Concatenation of the parameters values for each image into vectors

Similarly to what had been done in the Matlab section, the plotting of the graphics for each property were also programmed, as a control measure.

```

1 %% Roughness - Intensity Graph Plot
2 figure(1)
3 plot(Roughness_Comp, Intensity_Comp);
4 xlabel('Roughness');
5 ylabel('Intensity');
6 title('Comparator: Roughness - Intensity');

```

Algorithm 4.22: MVTec's Halcon analysis - Plotting of the graphics for individual group analysis control

Step 8 and Step 9

Finally, the exact same instructions given in the Matlab section were repeated here, allowing the performing of the linear regressions, and calculating the error associated to them.

```

1 %% Linear Regression Analysis - Comparator
2 %Contrast
3 X_Comp1 = [ones(length(Roughness_Comp), 1) Roughness_Comp];
4 b_Comp1 = X_Comp1 \ Contrast_Comp;
5 yCalc_Comp1 = X_Comp1 * b_Comp1;
6 figure(15)
7 scatter(Roughness_Comp, Contrast_Comp);
8 hold on
9 plot(Roughness_Comp, yCalc_Comp1);
10 xlabel('Roughness');
11 ylabel('Contrast');
12 title('Roughness-Contrast');
13 grid on

```

```

14 R_Comp1 = 1 - sum((Contrast_Comp - yCalc_Comp1).^2) /
    sum((Contrast_Comp - mean(Contrast_Comp)).^2);

```

Algorithm 4.23: MVTec's Halcon analysis - Linear regression for each parameter for the Comparator

After calculating the linear regression error for each parameter, they are concatenated into a single vector.

```

1 R_Comp = [R_Comp1, R_Comp2, R_Comp3];

```

Algorithm 4.24: MVTec's Halcon analysis - Concatenation of each parameter's linear regression errors for the Comparator

And at the end of all the group's analysis, all the errors associated with the multiple linear regressions are concatenated into a matrix.

```

1 header1 = { 'Comp'; 'RugF'; 'RugC'; 'Comp+RugF'; 'Comp+RugC' };
2 header2 = { ' ', 'Contrast', 'Energy', 'Intensity' };
3 R = [header2; header1, num2cell(R1)];

```

Algorithm 4.25: MVTec's Halcon analysis - Matrix creation for all linear regression analysis' error

The output values are visually similar to the ones obtained in the Matlab analysis, and an example is demonstrated in Figure 4.11.

The MVTec Halcon analysis is now finished.

4.5.3 Excel

In both software packages, Matlab and MVTec Halcon, the final outputs were the linear regression errors. As mentioned before, the values of these errors are good indicators of how adequate the linear regression was to the set of values that were given. As such, to find the optimal combination of lens aperture and distance from camera to sample, the errors must be analysed.

For this purpose, the values were inserted in Excel, and graphs were plotted that would be able to indicate the optimal combination of the referred settings.

The author studied the possibility of Matlab automatically pasting the error values in an Excel spreadsheet, that would then be inserted into the referred graphs. The elaboration of this script seemed far too complex, as there would be the need either of creating a verification on which cells any type of value would already be present and paste the values in the cells under those, or then the cells in which the values should be pasted would need to be specified individually for each script, for each set of images (there were roughly 33 sets of images, and every time a change was made to the script, the cells would need to be redefined). As such, the author had to resort to manually copying and pasting, a quite inelegant solution.

4.6 Conclusion

The methodology for the experimentation is then finalized. The whole process has been explained, and there only remains the showcase of the results and their associated discussion. The objective of these procedures were estimating the surface roughness of any sample's surface, but for that objective, the surface roughness value range must be established by measuring surfaces whose roughness had previously been established, as limits of the value range, and the technique must also be experimented in its real environment.

It must be added that the proposed methodology is quite boring and inefficient, and it would require an operator to switch the camera distances and manipulate the surfaces, while also inputting the values in the Excel spreadsheets and clicking on an additional software to capture the images. As such, an automated solution must also be explored, as it would be a vital requirement for a possible industrial implementation.

Chapter 5

Results and Discussion

A method that allowed the measurement of surface roughness through optical means has been proposed. The technique is based on the principles of speckle pattern analysis, and resorts to the Haralick's statistical parameters in order to quantify image properties, thereby being based on relative measurements, without the need for pre-established empirical correlations.

The objective of the proposed methodology is to devise a flexible way to address the range of surface roughness values, and was so considered due to the volatility of the results from the initial experimentation with speckle analysis methods. Thus, for this technique to work, a precise and careful calibration needs to be executed in order to obtain adequate results.

The procedures for this optical method's calibration have been established in a previous chapter. However, there still exists a lack of any results' exhibition, or even validation. As such, this chapter will review the obtained results, and discuss their adequacy to the method.

A showcase of the various software intermediary outputs, such as the graphics that were referred in the Methodology chapter, will be exhibited, as well as the framework for evaluation. By the end of the chapter, a full system validation should be achieved, and an optimal combination of measurement distance from camera to sample and iris range should be defined, as well as the optimal Haralick's parameter's choice.

5.1 Evaluation Framework

Right from the start, it is important to review what is considered to be a "good result", or a "bad result", generally. As mentioned above, the calibration for this system is the key for its effectiveness. As such, a monotonous relation between whichever parameter is being evaluated and the surface roughness is required.

The indicator to how good the calibration result is would be the linear regression associated error, the parameter R-squared. This parameter is a statistical measure to how close the data is to the fitted regression line. Higher values of R-squared mean the primary data is closer to the fitted

regression. Thus, a good result would be a high R-squared value. But how does a good and bad R-square value look like in terms of raw data from the measurements?

First, it is important to establish the measurement conditions. As referred in a previous chapter, both the distance from the sample to the camera and the iris range were changed to study the influence of these properties in the obtained results. As such, distances between 4 cm and 24 cm, were evaluated, in intervals of 2 cm. Three different iris ranges were also studied, the ones corresponding to the camera's data sheet F16, F22 and the one above F22, which will be designated maximum iris range. Distances beyond 24 cm weren't considered due to the results degradation with the increase of the distance, as it'll be concluded ahead, and iris ranges below F16 would make the captured image too bright and no useful information can be obtained.

Returning to the quality of the measurement results, two different examples will be demonstrated. The first example is corresponds to the measurement done with 12 cm between the camera and the sample, and the iris range set at F22, and was analysed utilizing the Matlab alternative. Looking at the contrast measurements from the Comparator analysis, the graphic obtained is the one in Figure 5.1.

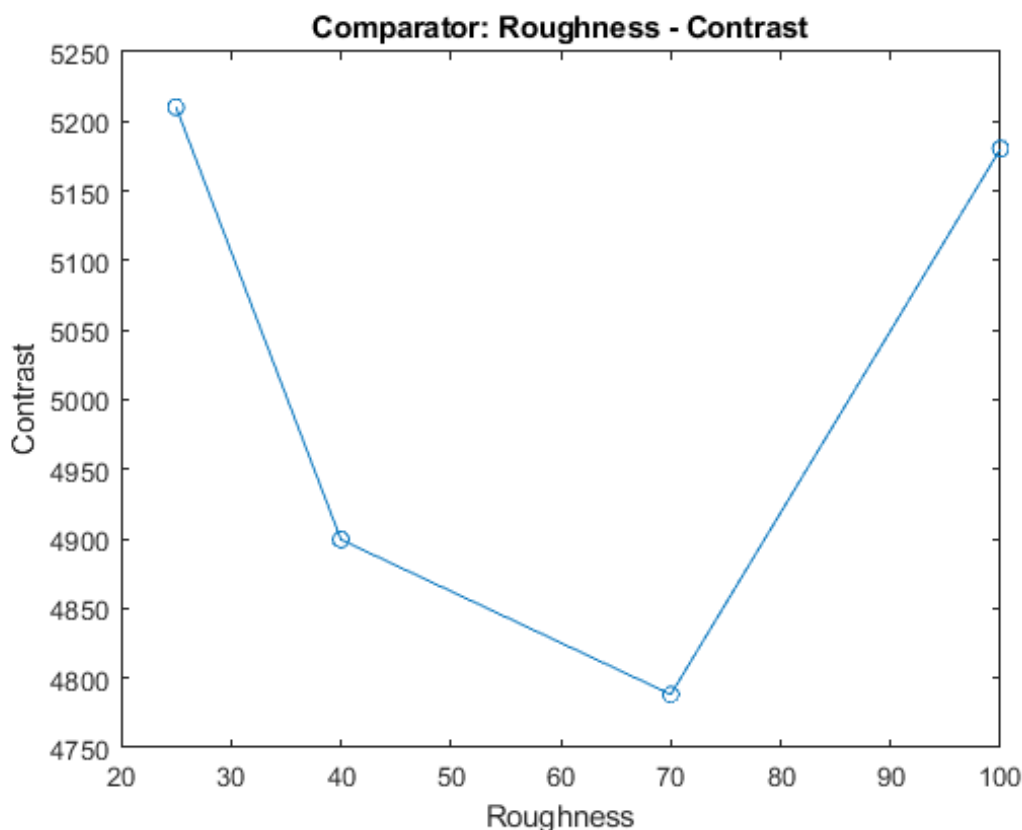


Figure 5.1: Contrast measurements obtained from the Comparator surfaces' analysis, at a distance of 12cm and iris range F22.

The graphic, obtained in Matlab, shows a descent between values of Contrast property of

surfaces N1, N2 and N3, and an abrupt increase for surface N4. Merely by looking at the points, it is expected a bad linear approximation due to the non-monotonous curve that can be observed in the plotted graphic.

By performing the linear regression on this set of data, the graphic that can be observed in Figure 5.2 is obtained.

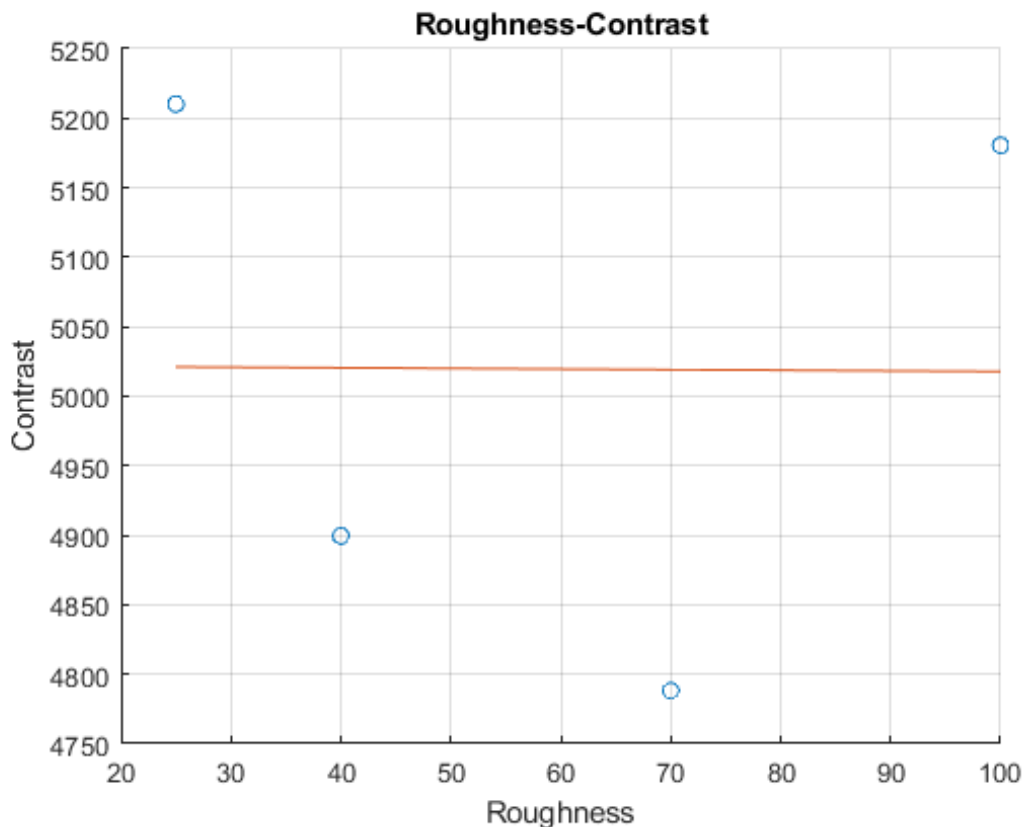


Figure 5.2: Linear regression performed on the data set from Contrast measurements obtained from the Comparator surfaces' analysis, at a distance of 12cm and iris range F22.

As expected, the linear function that was obtained from the data set is nowhere near close to the data points, correspondent to the circles in the graphic. As such, the calculated R-squared value is one of the lowest obtained, and it's equal to 4.87×10^{-5} .

A second measurement, this one was done with a distance of 8cm, and the maximum iris range. Once again, it is the parameter Contrast that will be evaluated, and the surface analysis group was the one for for Rugotest Fine, N6, N7, N8, N9b, N10b and N11b, through the Matlab alternative. The initial rough data is shown in Figure 5.3.

For this data set, there are no changes in the monotony of the data, as the contrast increases with the increase of surface roughness, and the curves from one point to the other possess approximate slopes.

After the linear regression is performed, the approximation shown in Figure 5.4 is obtained.

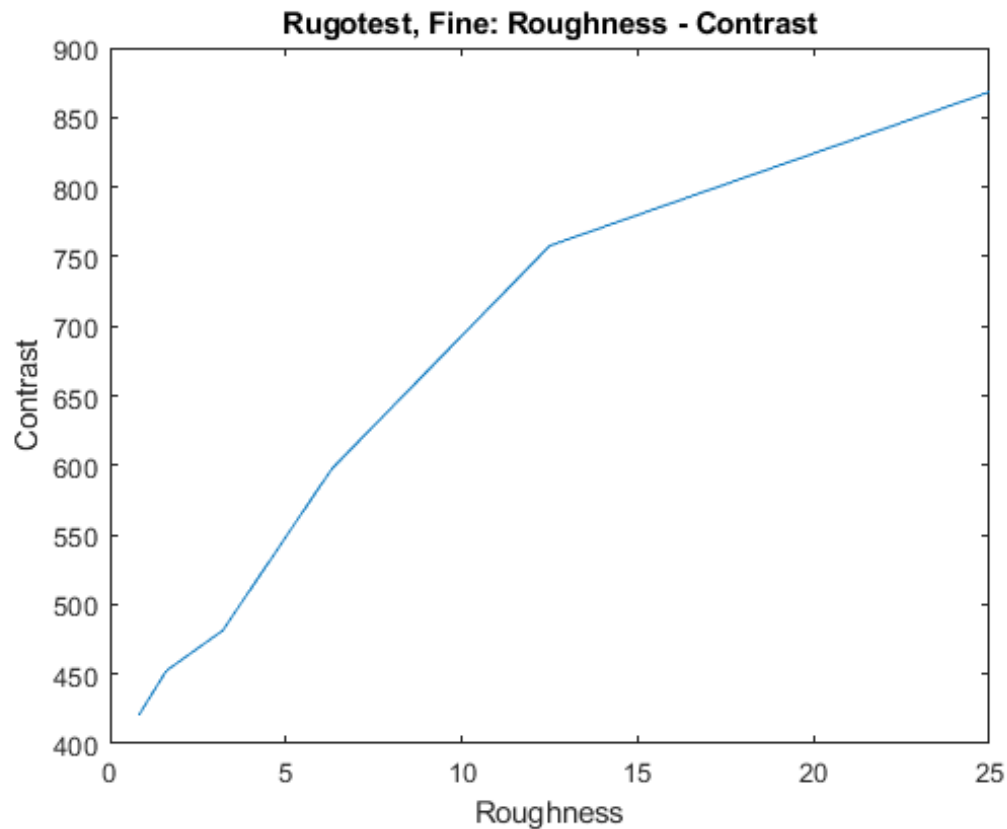


Figure 5.3: Contrast measurements obtained from the Comparator surfaces' analysis, at a distance of 8cm and maximum iris range.

The linear function is much closer to the data points, in comparison with the previous example. Thus, it is expected a good R-squared value to be attained. An R-squared value of 0.93 was obtained in this case.

Thus, any surface roughness measurement performed at the distance 8cm, with the maximum iris range set, would be a good measurement, will result in a low error, for roughness values between 0.8 and 25 μm .

5.2 Possible influence on the result's quality

The quality of the measurement's outcome can be affected by many factors. Simple details such as the system not being properly isolated from light sources can greatly alter results. This section will try to enumerate the various factors that may result in measurement's quality fluctuation.

The first factor is the influence of external illumination. As this is an optical technique that relies on intensity measures, any outside light may greatly affect the results. If the captured images aren't analysed with only the laser beam light as the incident light, the calculation of Haralick's parameters will be affected, and the parameter values won't be the same as the ones that would be

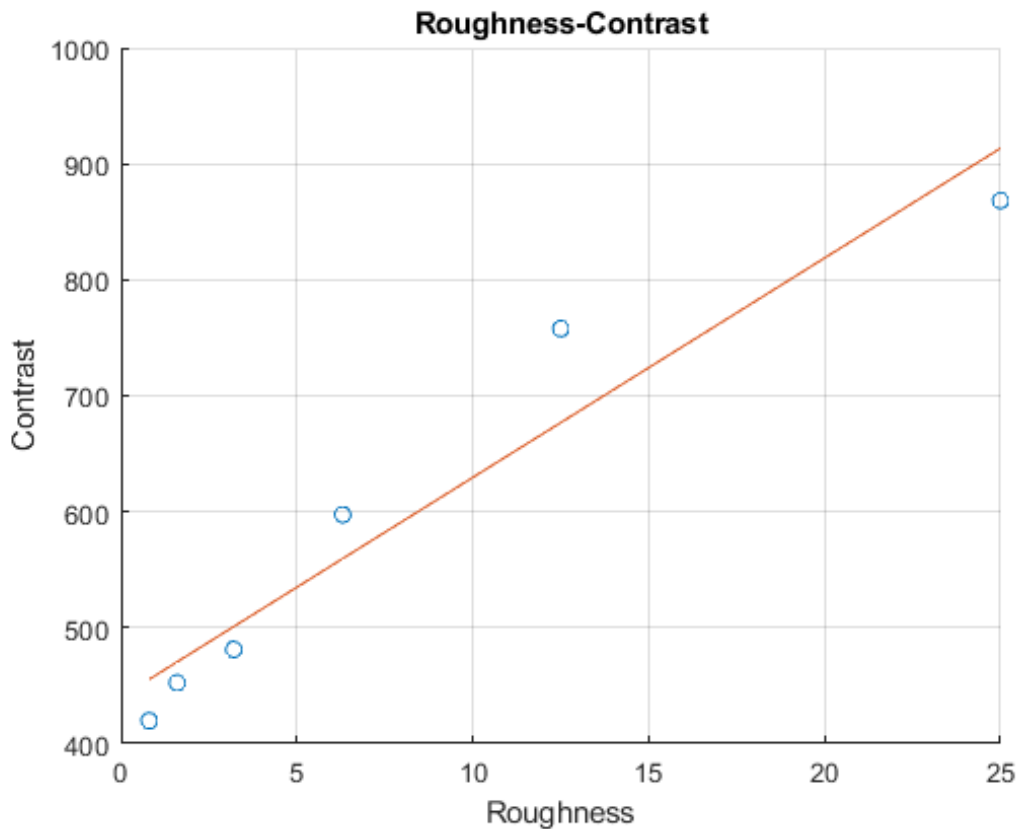


Figure 5.4: Linear regression performed on the data set from Contrast measurements obtained from the Comparator surfaces' analysis, at a distance of 8cm and maximum iris range.

obtained without the outside light sources. Luckily, in the experimentation area, the optical table where the system was mounted on had a black case encivering the table's surface area, and it was possible for the experimentation area to be shut off from outside light sources.

Another factor that must be accounted for is the sample's positioning. Even slight position changes may result in parameter errors. Slip-ups in distance from sample to camera or angle of incidence from the laser will influence the parameter's values. This was one of the reasons that ruled out the suggested rotation method speckle pattern analysis techniques.

The range of measurement of this method is usually considered between $0.1 \mu\text{m}$ and $100 \mu\text{m}$. As such, any surface roughness value outside this range won't be correctly measured, and even with surfaces whose roughness values are close to the limits, another technique might be considered. The experimented samples possessed surfaces whose values were close to the range limit: the surfaces N6, whose roughness value was $0.8 \mu\text{m}$, and N4, whose roughness value was $100 \mu\text{m}$. In many of the performed measurements, these values were the ones that restrained the result's quality, as it may be noticed in the previous example, for the combination of distance from sample to camera of 12 and iris range F22 (Figure 5.2).

The surface quality is another factor. In this project, two samples with diverse surface roughness sections were analysed. As the analysis surface groups isolated both sample's surfaces, the results were fairly better for the surfaces in the sample Rugotest No. 3 than the ones in the sample Paint Comparator. This can be explained by the surface roughness values being higher in the Paint Comparator, as they approached the surface range limit, but it's also worth considering that the sample Rugotest No. 3 was recently acquired. Even though the Paint Comparator was stored with care and following the storage precautions, its surface degradation might also explain why the method produced better results for Rugotest No. 3.

The granularity of the surface might also impact the measurements. As it'll be seen in the further sections, the analysis that included fine grain had an overall better result than the analysis that included coarse grain.

With these factors in mind, the measurement results for each of the analysis surface groups, with both the software alternative routes, will now be shown.

5.3 Measurement Results

In the following sections, each surface group analysis' results will be carefully examined. There will be a separate section for each surface group, exhibiting the results and their R-squared distribution, with both software packages. In the end, an optimal combination of both distance from sample to camera and iris range should be clear.

These analysis will all follow the same steps, starting with a showcase of the R-squared values obtained for each distance and iris range combination. The distance values that were analysed were 4cm to 24cm, with 2 cm intervals between each other. The iris range settings were F16, F22 and the maximum allowed.

An analysis based on the provided information will be performed, with a table containing all the data acquired, and a graphic containing pertinent information.

5.3.1 Surface group 1 - Paint Comparator

The Surface Group 1 included surfaces N1, N2, N3 and N4, whose surface roughness values correspond to 25 μm , 40 μm , 70 μm and 100 μm , respectively.

5.3.1.1 Matlab analysis

The complete list of the obtained R-squared values can be observed in Table 5.2.

The higher R-squared values for each of the parameters were:

- 0.9409 for Contrast, with a distance between sample and camera of 8cm, and F16 iris range;
- 0.9737 for Energy, with a distance between sample and camera of 4cm, and F22 iris range;
- 0.9242 for Intensity, with a distance between sample and camera of 8cm, and F16 iris range.

Thus, it can be concluded that, for the most accurate measurements for this surface roughness value range, the distance between sample and camera should be set at 4cm, and the iris range set at F22, with Energy being the analysed parameter, as it corresponds to the higher R-squared value.

Table 5.1 demonstrates the consistency of the R-squared values for each parameter, exhibiting the quality of the linear regressions.

Table 5.1: Evaluation of the quality of the obtained R-squared values for the Matlab analysis of surface group 1.

R-squared	Contrast	Energy	Intensity
≥ 80	2	4	5
≥ 90	1	1	1
≥ 95	0	1	0

It might also be noticed that, for all three parameters, the highest R-squared values are in the distances between sample and camera range of 4cm to 10cm, for all iris range settings, and then they sharply decrease, with occasional peaks in distances 16cm and 24cm, as it can be observed in Figure 5.5.

Table 5.2: R-squared values obtained from Matlab analysis of surface group 1.

Distance [cm]	Iris Range	Contrast	Energy	Intensity
4	Max.	0.0565	0.1344	0.1183
	F22	0.1056	0.9737	0.6394
	F16	0.3005	0.259	0.1831
6	Max.	0.6672	0.5767	0.7174
	F22	0.422	0.7803	0.7018
	F16	0.5208	0.768	0.6605
8	Max.	0.773607	0.55568	0.84768725
	F22	0.67913	0.78378	0.88690232
	F16	0.940905	0.87092	0.92415805
10	Max.	0.748437	0.27569	0.81393619
	F22	0.575657	0.80889	0.87074185
	F16	0.095569	0.80135	0.77377703
12	Max.	0.097215	0.26258	0.15698354
	F22	4.87E-05	0.14776	0.09853895
	F16	0.268746	0.21384	0.17826722
14	Max.	0.017364	0.15515	0.1019913
	F22	0.344161	0.05805	0.03871365
	F16	0.184848	0.15416	0.12176637
16	Max.	0.31212	0.495	0.43268771
	F22	0.110691	0.28223	0.22754764
	F16	0.319442	0.31978	0.27346142
18	Max.	0.010272	0.07512	0.00524848
	F22	0.160972	0.05602	0.02748286
	F16	0.171676	0.1618	0.11515558
20	Max.	0.010329	0.0206	0.00303463
	F22	0.333256	0.02512	0.03802586
	F16	0.000188	0.01634	0.00371351
22	Max.	0.026165	0.04862	0.01751288
	F22	9.37E-06	0.02162	0.01034325
	F16	0.016712	0.00759	0.00484325
24	Max.	0.392112	0.23991	0.28043626
	F22	0.813422	0.32905	0.35370732
	F16	0.185838	0.18442	0.20148452

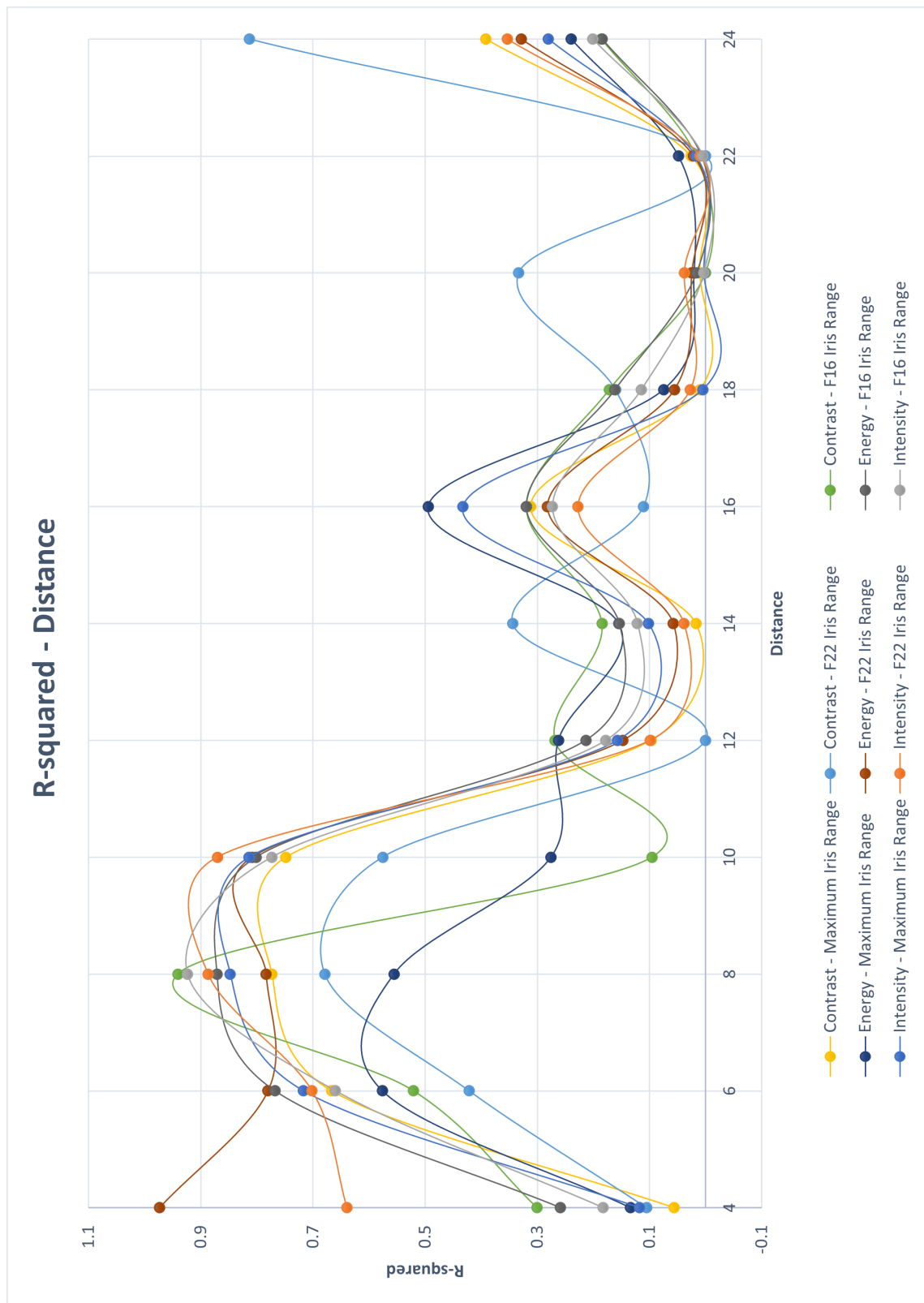


Figure 5.5: Evolution of the different Haralick's parameters with distance, for all iris ranges, for the Matlab analysis of surface group 1.

5.3.1.2 MvTec's Halcon analysis

The complete list of the obtained R-squared values can be observed in Table 5.4.

The higher R-squared values for each of the parameters were:

- 0.8212 for Contrast, with a distance between sample and camera of 8cm, and the maximum iris range;
- 0.9726 for Energy, with a distance between sample and camera of 8cm, and F16 iris range;
- 0.9972 for Intensity, with a distance between sample and camera of 8cm, the maximum F16 iris range.

Thus, it can be concluded that, for the most accurate measurements for this surface roughness value range, the distance between sample and camera should be set at 8cm, and the iris range set at F16, with Intensity being the analysed parameter, as it corresponds to the higher R-squared value.

Table 5.3 demonstrates the consistency of the R-squared values for each parameter, exhibiting the quality of the linear regressions.

Table 5.3: Evaluation of the quality of the obtained R-squared values for the MVTEC's Halcon analysis of surface group 1.

R-squared	Contrast	Energy	Intensity
≥ 80	1	4	6
≥ 90	0	4	6
≥ 95	0	4	4

It might also be noticed that, for all three parameters, the highest R-squared values are in the distances between sample and camera range of 8cm to 10cm, for all iris range settings, and then they sharply decrease, with occasional peaks in distances 16cm, and 20cm, as it can be observed in Figure 5.6.

5.3.1.3 Conclusion

The Matlab analysis of this surface group produced some average results, with only one R-squared value higher than 0.95 in the measurement set.

The MvTec Halcon analysis, on the contrary, produced good results, with a total of eight R-squared values higher than 0.95, one of them even reaching roughly approximately 1.

In its entirety, Contrast was the worse rated parameter, with only one value higher than 0.9.

The fluctuation of values was something expected, and in its generality, the highest R-squared values all focused in the distance between sample and camera of 8cm. The iris range wasn't something constant, as all the different parameters obtained their optimal results with all three settings.

Overall, a good approximation of surface roughness in this value range is definitely possible, as demonstrated.

Table 5.4: R-squared values obtained from Halcon analysis of surface group 1.

Distance [cm]	Iris Range	Contrast	Energy	Intensity
4	Max.	0.071896	0.0738	0.005367
	F22	0.227746	0.5074	0.39813387
	F16	0.312794	0.53797	0.44889473
6	Max.	0.080112	0.46331	0.64731253
	F22	0.107595	0.77546	0.59761558
	F16	0.077758	0.65406	0.48864501
8	Max.	0.821155	0.32028	0.97405186
	F22	0.572233	0.95934	0.99727055
	F16	0.006161	0.97136	0.946629
10	Max.	0.68322	0.50153	0.97703059
	F22	0.164118	0.95273	0.94769224
	F16	0.296258	0.97258	0.95795824
12	Max.	0.169914	0.54836	0.41686977
	F22	0.098831	0.4055	0.33252908
	F16	0.238703	0.49144	0.44603249
14	Max.	0.182026	0.4133	0.32818721
	F22	0.059225	0.25212	0.20444782
	F16	0.283653	0.39765	0.34625765
16	Max.	0.309318	0.77074	0.71951514
	F22	0.069574	0.57069	0.50479768
	F16	0.263627	0.60984	0.55945074
18	Max.	0.094582	0.29592	0.12962442
	F22	0.001675	0.257	0.1930027
	F16	0.201695	0.42602	0.35752042
20	Max.	0.542942	0.56454	0.54372832
	F22	0.098525	0.01572	0.00757997
	F16	0.087707	0.17095	0.12212806
22	Max.	0.110699	0.00447	0.02608399
	F22	0.08188	0.02059	0.03673504
	F16	0.122738	0.04132	0.04918193
24	Max.	0.076858	0.05529	0.07601733
	F22	0.024895	0.11782	0.14628718
	F16	9.68E-02	0.02689	0.03221099

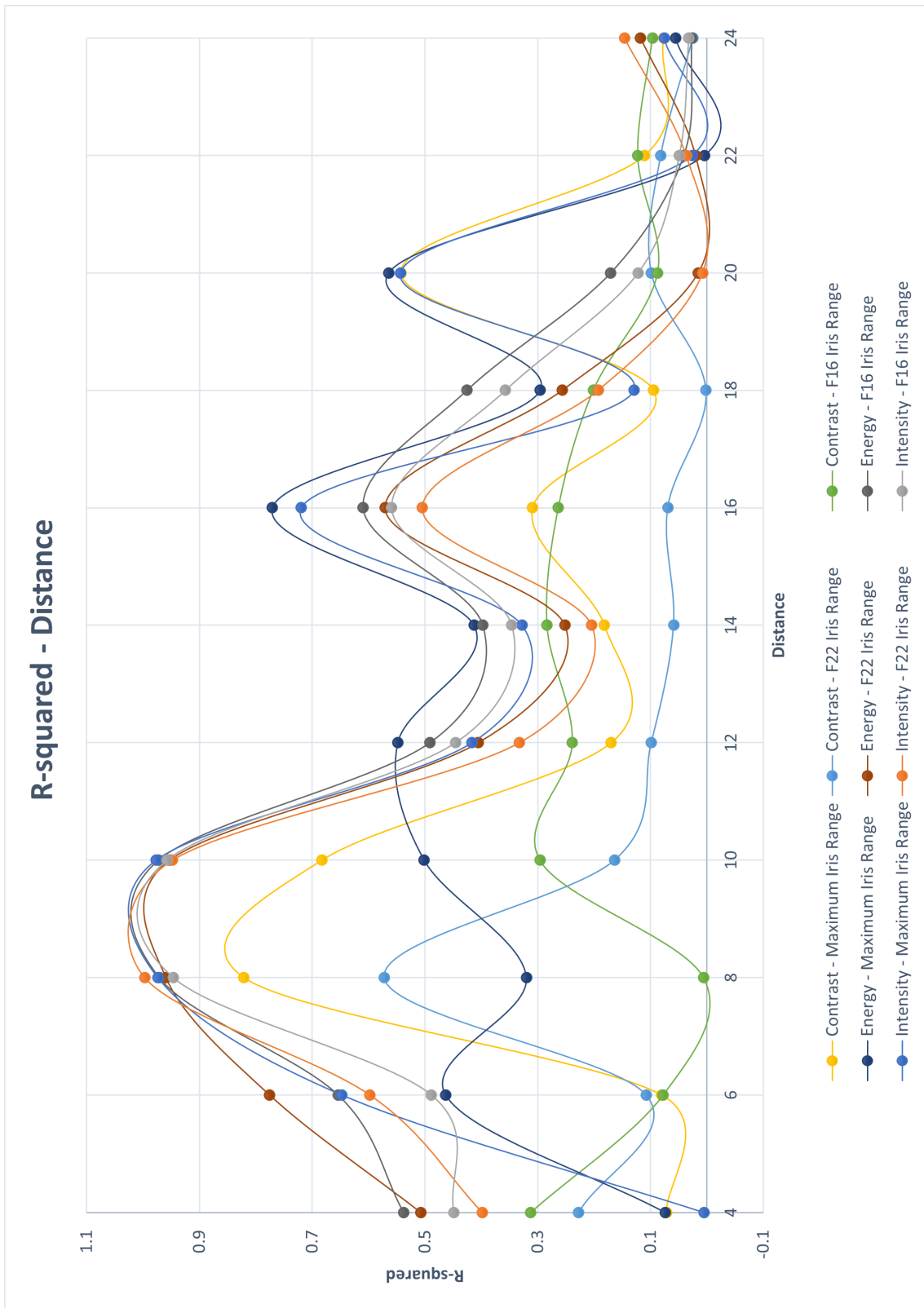


Figure 5.6: Evolution of the different Haralick's parameters with distance, for all iris ranges, for the MVTec's Halcon analysis of surface group 1.

5.3.2 Surface group 2 - Rugotest No. 3 (coarse grain)

The Surface Group 2 included surfaces N6, N7, N8, N9a, N10a, and N11a, whose surface roughness values correspond to 0.8 μm , 1.6 μm , 3.2 μm , 6.3 μm , 12.5 μm , and 25 μm respectively.

5.3.2.1 Matlab analysis

The complete list of the obtained R-squared values can be observed in Table 5.6.

The higher R-squared values for each of the parameters were:

- 0.9429 for Contrast, with a distance between sample and camera of 8cm, and the maximum iris range;
- 0.98202 for Energy, with a distance between sample and camera of 8cm, and F16 iris range;
- 0.9350 for Intensity, with a distance between sample and camera of 8cm, and the maximum iris range.

Thus, it can be concluded that, for the most accurate measurements for this surface roughness value range, the distance between sample and camera should be set at 8cm, and the iris range set at F16, with Energy being the analysed parameter, as it corresponds to the higher R-squared value.

Table 5.5 demonstrates the consistency of the R-squared values for each parameter, exhibiting the quality of the linear regressions.

Table 5.5: Evaluation of the quality of the obtained R-squared values for the Matlab analysis of surface group 2.

R-squared	Contrast	Energy	Intensity
≥ 80	6	4	4
≥ 90	2	2	2
≥ 95	0	2	0

It might also be noticed that, for all three parameters, the highest R-squared values are in the distance between sample and camera range of 8cm, for all iris range settings, and then they decrease, with occasional peaks in distances 12cm, and between 20cm and 22cm, as it can be observed in Figure 5.7.

Table 5.6: R-squared values obtained from Matlab analysis of surface group 2.

Distance [cm]	Iris Range	Contrast	Energy	Intensity
4	Max.	0.5882	0.673	0.7431
	F22	0.6377	0.7244	0.772
	F16	0.8582	0.8349	0.8028
6	Max.	0.4596	0.4676	0.565
	F22	0.6952	0.702	0.7526
	F16	0.8135	0.7688	0.7081
8	Max.	0.942914	0.751078	0.935012
	F22	0.900899	0.963645	0.9303
	F16	0.898475	0.98202	0.89121
10	Max.	0.225018	0.130208	0.283983
	F22	0.05072	0.264444	0.291655
	F16	0.294973	0.30514	0.296212
12	Max.	0.532103	0.024897	0.635623
	F22	0.468523	0.718595	0.703168
	F16	0.808693	0.776871	0.722808
14	Max.	0.104383	0.298001	0.354049
	F22	0.048455	0.345777	0.359345
	F16	0.538783	0.447228	0.438078
16	Max.	0.117176	0.00468	0.003265
	F22	0.144733	0.007363	0.003467
	F16	3.79E-05	0.004099	0.002077
18	Max.	0.247058	0.678552	0.442037
	F22	4.42E-05	0.340064	0.350364
	F16	0.446834	0.312723	0.368018
20	Max.	0.204172	0.263669	0.406565
	F22	0.236833	0.519977	0.524854
	F16	0.681198	0.620298	0.552863
22	Max.	0.4419	0.899872	0.569182
	F22	0.008019	0.411732	0.346709
	F16	0.506723	0.433781	0.400585
24	Max.	0.036719	0.448227	0.219065
	F22	0.012236	0.305595	0.298548
	F16	0.426123	0.30478	0.320093

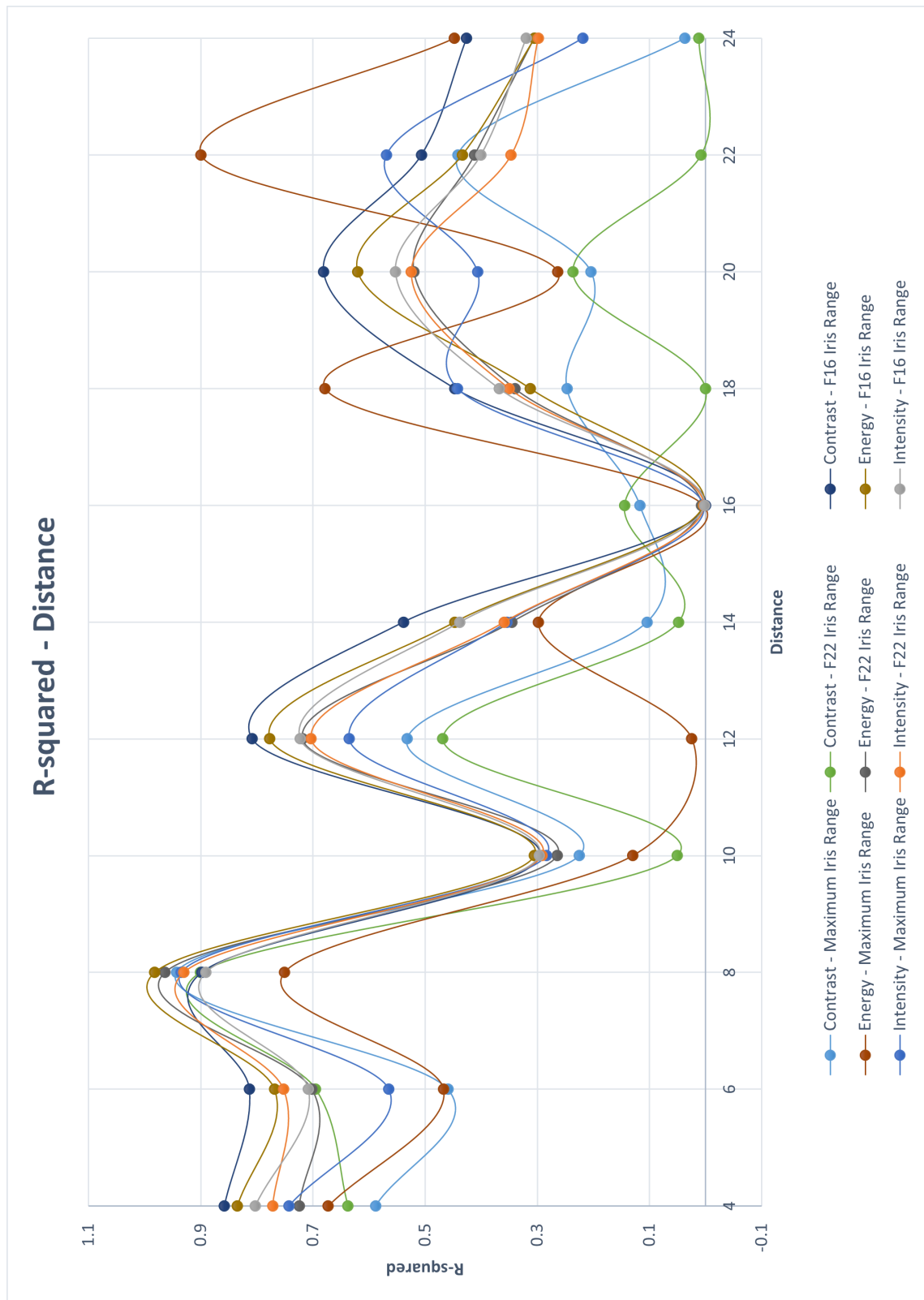


Figure 5.7: Evolution of the different Haralick's parameters with distance, for all iris ranges, for the Matlab analysis of surface group 2.

5.3.2.2 MvTec's Halcon analysis

The complete list of the obtained R-squared values can be observed in Table 5.8.

The higher R-squared values for each of the parameters were:

- 0.9425 for Contrast, with a distance between sample and camera of 8cm, and the maximum iris range;
- 0.9819 for Energy, with a distance between sample and camera of 8cm, and F16 iris range;
- 0.9347 for Intensity, with a distance between sample and camera of 8cm, the maximum iris range.

Thus, it can be concluded that, for the most accurate measurements for this surface roughness value range, the distance between sample and camera should be set at 8cm, and the iris range set at F16, with Energy being the analysed parameter, as it corresponds to the higher R-squared value.

Table 5.7 demonstrates the consistency of the R-squared values for each parameter, exhibiting the quality of the linear regressions.

Table 5.7: Evaluation of the quality of the obtained R-squared values for the MVTEC's Halcon analysis of surface group 2.

R-squared	Contrast	Energy	Intensity
≥ 80	5	4	4
≥ 90	2	2	2
≥ 95	0	2	0

It might also be noticed that, for all three parameters, the highest R-squared values are in the distance between sample and camera range of 8cm, for all iris range settings, and then they decrease, peaking again in distances 12cm, and 18cm to 22cm, as it can be observed in Figure 5.8.

5.3.2.3 Conclusion

The Matlab analysis of this surface group produced good results, with six R-squared values higher than 0.90, although containing only two higher than 0.95 in the measurement set.

The MvTec Halcon analysis, produced exactly the same results' quality as the ones obtained in Matlab, containing exactly the same values in the given intervals.

In its entirety, Energy was clearly the best parameter, possessing the two values higher than 0.95 in both softwares analysis.

The fluctuation of values was, once again, something expected, and in its generality, the highest R-squared values all focused in the distance between sample and camera of 8cm. In this surface group, the iris range that didn't stand out was the F22 setting.

Overall, a good approximation of surface roughness in this value range is also definitely possible, as demonstrated.

Table 5.8: R-squared values obtained from Halcon analysis of surface group 2.

Distance [cm]	Iris Range	Contrast	Energy	Intensity
4	Max.	0.567932	0.680656	0.736153
	F22	0.627449	0.715671	0.773291
	F16	0.850846	0.83075	0.805709
6	Max.	0.447737	0.48359	0.56827
	F22	0.694308	0.702966	0.752407
	F16	0.794779	0.765956	0.721337
8	Max.	0.942477	0.749752	0.934672
	F22	0.90035	0.963741	0.929911
	F16	0.895289	0.981945	0.890808
10	Max.	0.226402	0.131016	0.285487
	F22	0.051494	0.267922	0.292714
	F16	0.295192	0.306339	0.296371
12	Max.	0.531821	0.025334	0.635511
	F22	0.465611	0.719435	0.702956
	F16	0.809091	0.777687	0.722572
14	Max.	0.10434	0.295901	0.353128
	F22	0.049781	0.343101	0.358188
	F16	0.538685	0.445959	0.437179
16	Max.	0.116419	0.004325	0.003385
	F22	0.141693	0.007294	0.003539
	F16	7.35E-05	0.003856	0.002222
18	Max.	0.248542	0.677384	0.44139
	F22	7.29E-06	0.341843	0.35144
	F16	0.446261	0.314635	0.369137
20	Max.	0.204899	0.26481	0.408065
	F22	0.236707	0.522326	0.524974
	F16	0.682752	0.621422	0.552117
22	Max.	0.441965	0.899377	0.569282
	F22	0.008189	0.411602	0.346153
	F16	0.506372	0.433722	0.400138
24	Max.	0.035907	0.449185	0.21769
	F22	0.012961	0.304958	0.297611
	F16	0.426805	0.30624	0.320108

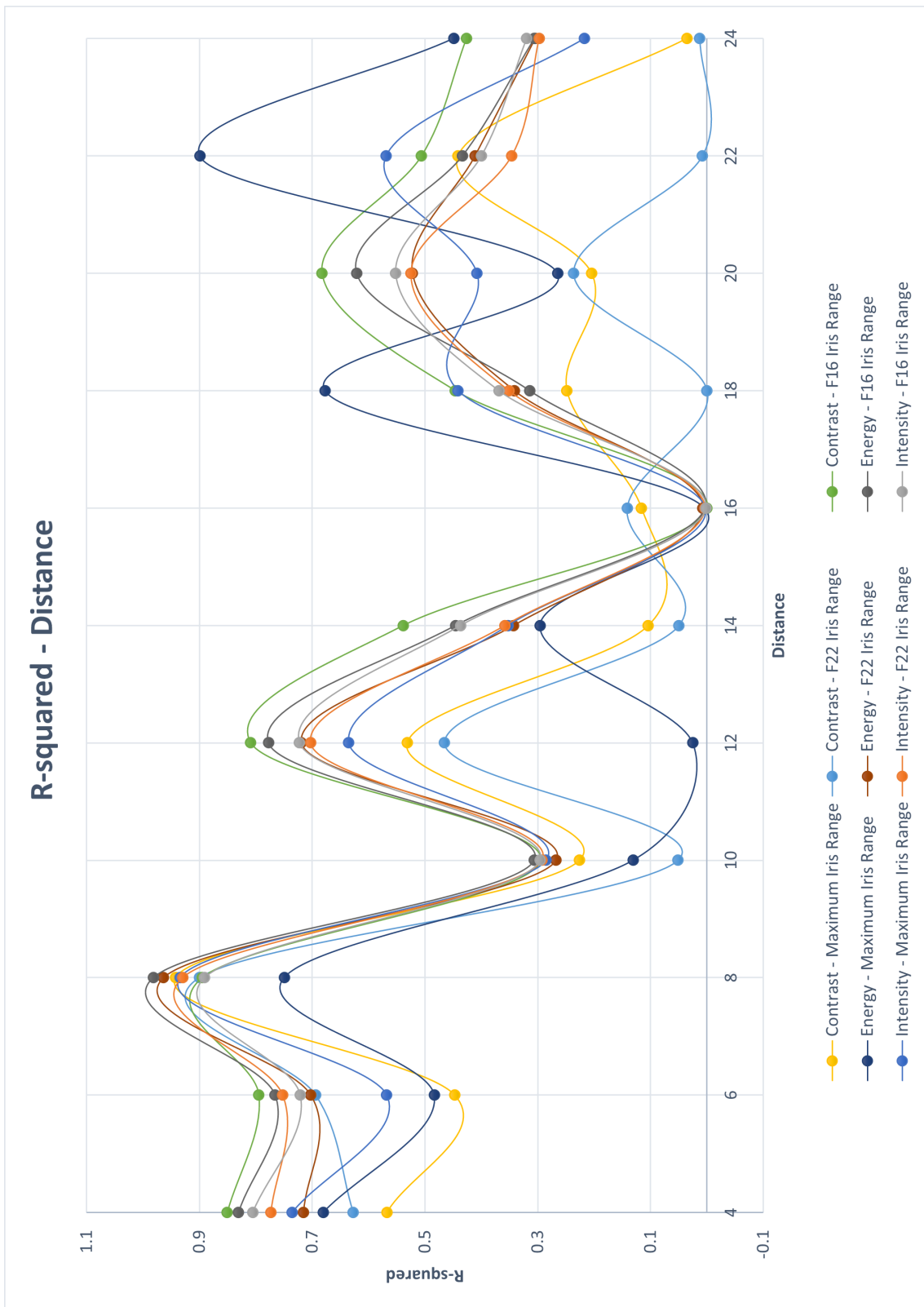


Figure 5.8: Evolution of the different Haralick's parameters with distance, for all iris ranges, for the MVTec's Halcon analysis of surface group 2.

5.3.3 Surface group 3 - Rugotest No. 3 (fine grain)

The Surface Group 2 included surfaces N6, N7, N8, N9b, N10b, and N11b, whose surface roughness values corresponds to 0.8 μm , 1.6 μm , 3.2 μm , 6.3 μm , 12.5 μm , and 25 μm respectively.

5.3.3.1 Matlab analysis

The complete list of the obtained R-squared values can be observed in Table 5.10.

The higher R-squared values for each of the parameters were:

- 0.9525 for Contrast, with a distance between sample and camera of 4cm, and F16 iris range;
- 0.9882 for Energy, with a distance between sample and camera of 8cm, and F22 iris range;
- 0.9195 for Intensity, with a distance between sample and camera of 8cm, and the maximum iris range.

Thus, it can be concluded that, for the most accurate measurements for this surface roughness value range, the distance between sample and camera should be set at 8cm, and the iris range set at F22, with Energy being the analysed parameter, as it corresponds to the higher R-squared value.

Table 5.9 demonstrates the consistency of the R-squared values for each parameter, exhibiting the quality of the linear regressions.

Table 5.9: Evaluation of the quality of the obtained R-squared values for the Matlab analysis of surface group 3.

R-squared	Contrast	Energy	Intensity
≥ 80	6	6	6
≥ 90	2	5	1
≥ 95	1	3	0

It might also be noticed that, for all three parameters, the highest R-squared values are in the distances between sample and camera range between 4 and 8cm, for all iris range settings, and then they decrease, with occasional peaks in distances 12cm, and between 20cm and 24cm, as it can be observed in Figure 5.9.

Table 5.10: R-squared values obtained from Matlab analysis of surface group 3.

Distance [cm]	Iris Range	Contrast	Energy	Intensity
4	Max.	0.8572	0.6665	0.8455
	F22	0.7793	0.9737	0.8435
	F16	0.9525	0.9296	0.8223
6	Max.	0.6686	0.4841	0.6917
	F22	0.534	0.7718	0.6573
	F16	0.8354	0.7928	0.6925
8	Max.	0.92728	0.72865	0.919467
	F22	0.861871	0.988171	0.895433
	F16	0.891444	0.960381	0.872163
10	Max.	0.286312	0.152582	0.329277
	F22	0.108255	0.309645	0.315379
	F16	0.343456	0.352539	0.340162
12	Max.	0.506057	0.359659	0.598298
	F22	0.452413	0.725989	0.651831
	F16	0.740896	0.714311	0.658834
14	Max.	0.063927	0.205875	0.266078
	F22	0.000682	0.325321	0.384276
	F16	0.497818	0.390469	0.407349
16	Max.	0.264889	0.183481	0.014932
	F22	0.172249	0.026274	0.010672
	F16	0.064001	0.000747	0.058977
18	Max.	0.077399	0.167413	0.322153
	F22	0.024789	0.162037	0.288948
	F16	0.398903	0.282467	0.367726
20	Max.	0.435623	0.59275	0.577894
	F22	0.369812	0.728493	0.654947
	F16	0.702098	0.653425	0.593294
22	Max.	0.3249	0.927372	0.528076
	F22	0.092047	0.585064	0.499671
	F16	0.658412	0.574145	0.545445
24	Max.	0.3704	0.865702	0.590665
	F22	0.196986	0.614392	0.570131
	F16	0.633569	0.561373	0.537218

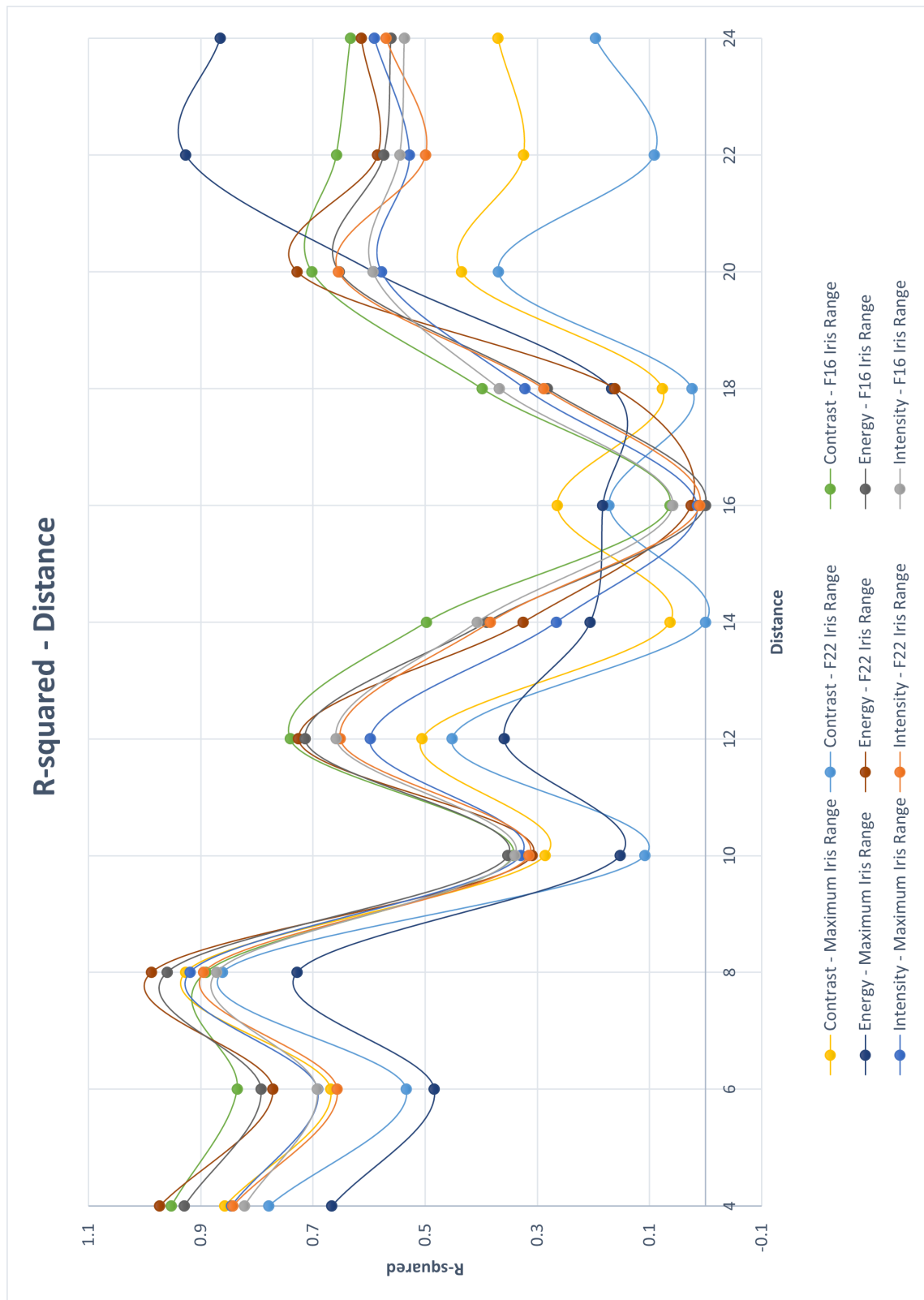


Figure 5.9: Evolution of the different Haralick's parameters with distance, for all iris ranges, for the Matlab analysis of surface group 3.

5.3.3.2 MvTec's Halcon analysis

The complete list of the obtained R-squared values can be observed in Table 5.12.

The higher R-squared values for each of the parameters were:

- 0.9515 for Contrast, with a distance between sample and camera of 4cm, and F16 iris range;
- 0.9881 for Energy, with a distance between sample and camera of 8cm, and F22 iris range;
- 0.9193 for Intensity, with a distance between sample and camera of 8cm, the maximum iris range.

Thus, it can be concluded that, for the most accurate measurements for this surface roughness value range, the distance between sample and camera should be set at 8cm, and the iris range set at F22, with Energy being the analysed parameter, as it corresponds to the higher R-squared value.

Table 5.11 demonstrates the consistency of the R-squared values for each parameter, exhibiting the quality of the linear regressions.

Table 5.11: Evaluation of the quality of the obtained R-squared values for the MVTEC's Halcon analysis of surface group 3.

R-squared	Contrast	Energy	Intensity
≥ 80	6	6	6
≥ 90	2	5	1
≥ 95	1	3	0

It might also be noticed that, for all three parameters, the highest R-squared values are in the distances between sample and camera range between 4cm and 8cm, for all iris range settings, and then they decrease, peaking again in distances 12cm, and 20cm to 24cm, as it can be observed in Figure 5.10.

5.3.3.3 Conclusion

The Matlab analysis of this surface group produced the best results so far, with eight R-squared values higher than 0.90, and four higher than 0.95 in the measurement set.

The MvTec Halcon analysis, produced exactly the same results' quality as the ones obtained in Matlab, once again containing exactly the same values in the given intervals.

In its entirety, Energy was clearly the best parameter, possessing the three values higher than 0.95 in both software analysis, followed by Contrast, with one value higher than 0.95 in also both software analysis.

The fluctuation of values was, once again, something expected, and in its generality, the highest R-squared values all focused in the distances between sample and camera of 4cm to 8cm. In this surface group, all three iris range settings produced good results.

Overall, a good approximation of surface roughness in this value range is also definitely possible, as demonstrated.

Table 5.12: R-squared values obtained from Halcon analysis of surface group 3.

Distance [cm]	Iris Range	Contrast	Energy	Intensity
4	Max.	0.860144	0.670931	0.848221
	F22	0.781357	0.973901	0.849503
	F16	0.951505	0.931592	0.830334
6	Max.	0.675939	0.495742	0.702231
	F22	0.533682	0.772771	0.657818
	F16	0.822753	0.784912	0.698491
8	Max.	0.927101	0.727851	0.91926
	F22	0.861933	0.988183	0.895289
	F16	0.888806	0.96042	0.871917
10	Max.	0.286546	0.151344	0.330064
	F22	0.109366	0.311328	0.316066
	F16	0.343922	0.353313	0.340087
12	Max.	0.507379	0.347132	0.598695
	F22	0.453942	0.726225	0.65163
	F16	0.740219	0.714329	0.658574
14	Max.	0.06349	0.200305	0.264878
	F22	0.001021	0.324306	0.384362
	F16	0.497654	0.390846	0.407068
16	Max.	0.261706	0.179349	0.014219
	F22	0.164588	0.024801	0.01148
	F16	0.064304	0.000932	0.05979
18	Max.	0.07823	0.170361	0.321894
	F22	0.024073	0.163016	0.289904
	F16	0.398185	0.283486	0.367589
20	Max.	0.437523	0.587872	0.579108
	F22	0.371797	0.730314	0.65537
	F16	0.701997	0.654691	0.592572
22	Max.	0.326605	0.92702	0.529599
	F22	0.092624	0.585963	0.499409
	F16	0.659426	0.575725	0.545275
24	Max.	0.371479	0.863682	0.590259
	F22	0.199909	0.614166	0.569346
	F16	0.633434	0.561239	0.53664

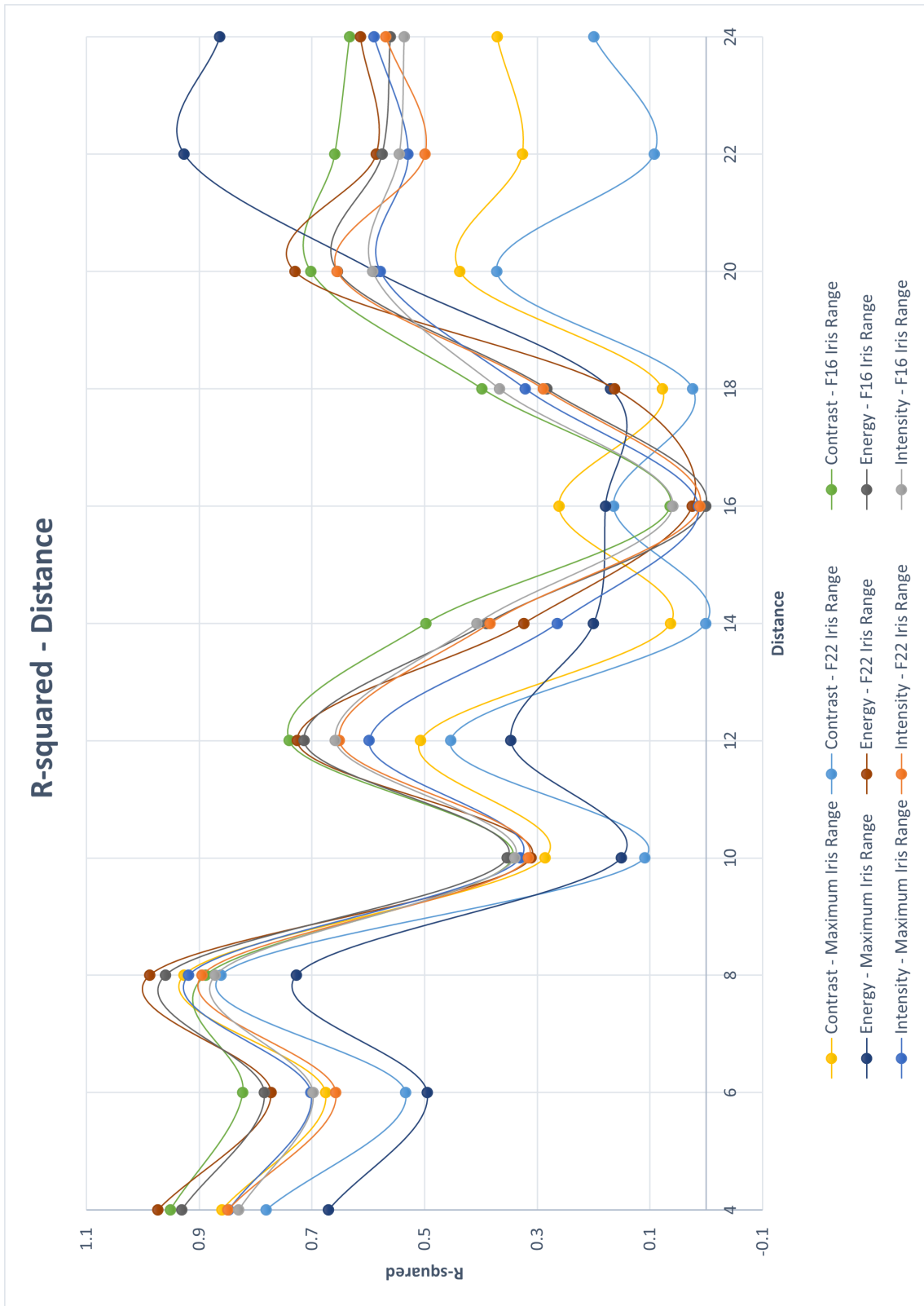


Figure 5.10: Evolution of the different Haralick's parameters with distance, for all iris ranges, for the MVTec's Halcon analysis of surface group 3.

5.3.4 Surface group 4 - Paint Comparator and Rugotest No. 3 (coarse grain)

The Surface Group 2 included surfaces N6, N7, N8, N9a, N10a, N11a, N1, N2, N3, and N4, whose surface roughness values corresponds to 0.8 μm , 1.6 μm , 3.2 μm , 6.3 μm , 12.5 μm , 25 μm , 25 μm , 40 μm , 70 μm , and 100 μm respectively.

5.3.4.1 Matlab analysis

The complete list of the obtained R-squared values can be observed in Table 5.14.

The higher R-squared values for each of the parameters were:

- 0.8967 for Contrast, with a distance between sample and camera of 8cm, and F16 iris range;
- 0.9226 for Energy, with a distance between sample and camera of 8cm, and F16 iris range;
- 0.8352 for Intensity, with a distance between sample and camera of 8cm, and the maximum iris range.

Thus, it can be concluded that, for the most accurate measurements for this surface roughness value range, the distance between sample and camera should be set at 8cm, and the iris range set at F16, with Energy being the analysed parameter, as it corresponds to the higher R-squared value.

Table 5.13 demonstrates the consistency of the R-squared values for each parameter, exhibiting the quality of the linear regressions.

Table 5.13: Evaluation of the quality of the obtained R-squared values for the Matlab analysis of surface group 4.

R-squared	Contrast	Energy	Intensity
≥ 80	3	4	2
≥ 90	0	2	0
≥ 95	0	0	0

It might also be noticed that, for all three parameters, the highest R-squared values are in the distances between sample and camera range between 4cm and 8cm, for all iris range settings, and then they decrease, with occasional peaks in distances 12cm, and between 18cm and 24cm, as it can be observed in Figure 5.11.

Table 5.14: R-squared values obtained from Matlab analysis of surface group 4.

Distance [cm]	Iris Range	Contrast	Energy	Intensity
4	Max.	0.6472	0.5411	0.6846
	F22	0.6721	0.8549	0.7419
	F16	0.7467	0.7412	0.6932
6	Max.	0.4363	0.4651	0.639
	F22	0.1356	0.7597	0.7452
	F16	0.8132	0.8227	0.7076
8	Max.	0.859576	0.572757	0.835162
	F22	0.784955	0.919301	0.819151
	F16	0.89674	0.922573	0.769194
10	Max.	0.08931	0.123583	0.225697
	F22	0.168956	0.217707	0.307407
	F16	0.436308	0.408879	0.339874
12	Max.	0.632349	0.539813	0.668974
	F22	0.536555	0.636607	0.649904
	F16	0.718241	0.71215	0.658988
14	Max.	0.291641	0.361152	0.397038
	F22	0.019163	0.327246	0.316285
	F16	0.43956	0.456682	0.407106
16	Max.	0.015306	0.028966	0.067765
	F22	0.61528	0.014231	0.044469
	F16	0.438534	0.200606	0.244648
18	Max.	0.244887	0.183541	0.347462
	F22	0.029361	0.347113	0.384379
	F16	0.611036	0.563319	0.543378
20	Max.	0.558223	0.527021	0.585447
	F22	0.535179	0.451182	0.504502
	F16	0.557465	0.611364	0.5765
22	Max.	0.389939	0.177167	0.404405
	F22	0.521858	0.323607	0.449382
	F16	0.420406	0.411176	0.475911
24	Max.	0.377133	0.163013	0.423075
	F22	0.437144	0.272448	0.399076
	F16	0.413629	0.410857	0.473294

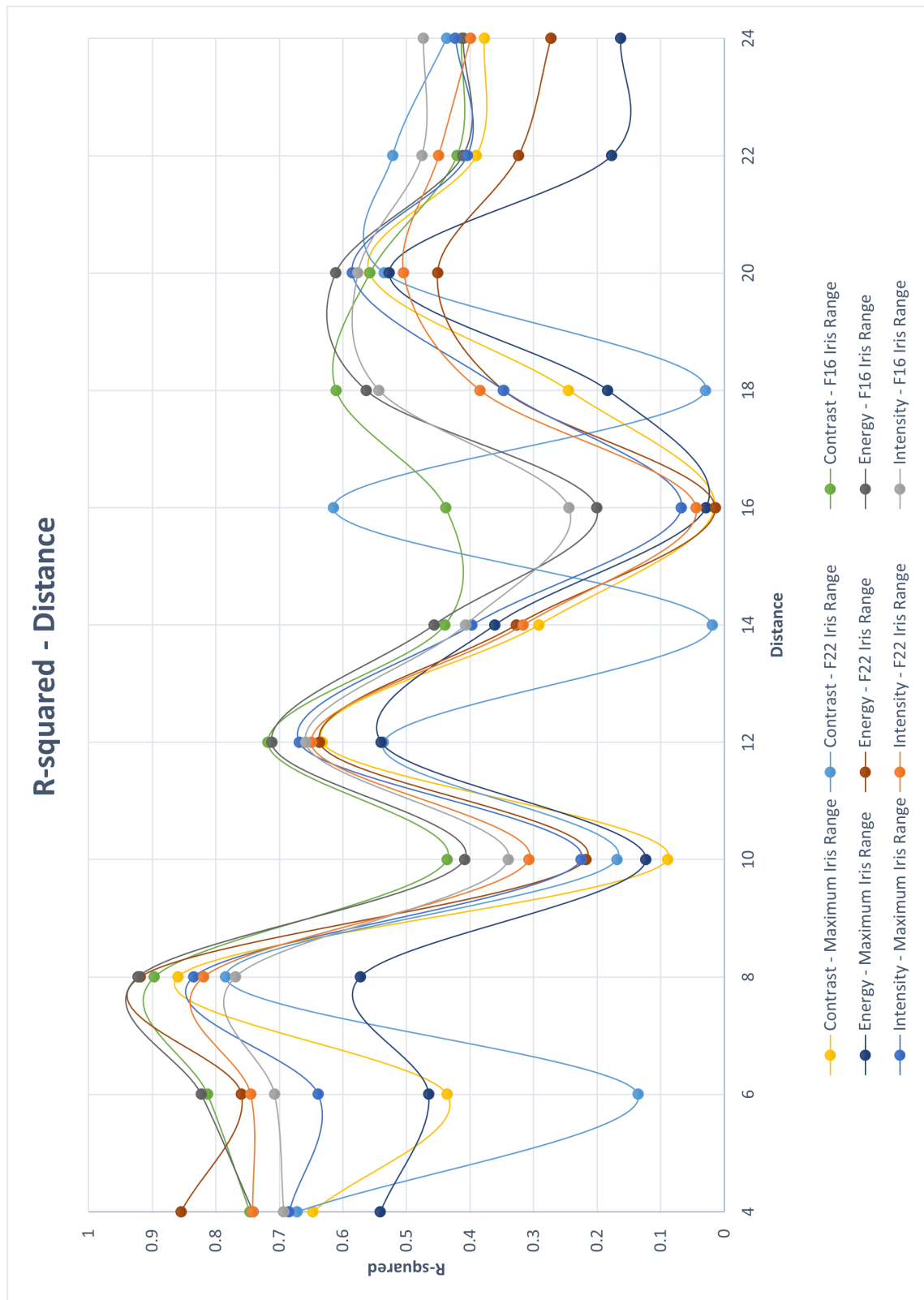


Figure 5.11: Evolution of the different Haralick's parameters with distance, for all iris ranges, for the Matlab analysis of surface group 4.

5.3.4.2 MvTec's Halcon analysis

The complete list of the obtained R-squared values can be observed in Table 5.16.

The higher R-squared values for each of the parameters were:

- 0.7016 for Contrast, with a distance between sample and camera of 8cm, and the maximum iris range;
- 0.9224 for Energy, with a distance between sample and camera of 8cm, and F16 iris range;
- 0.8351 for Intensity, with a distance between sample and camera of 8cm, the maximum iris range.

Thus, it can be concluded that, for the most accurate measurements for this surface roughness value range, the distance between sample and camera should be set at 8cm, and the iris range set at F16, with Energy being the analysed parameter, as it corresponds to the higher R-squared value.

Table 5.15 demonstrates the consistency of the R-squared values for each parameter, exhibiting the quality of the linear regressions.

Table 5.15: Evaluation of the quality of the obtained R-squared values for the MVTEC's Halcon analysis of surface group 4.

R-squared	Contrast	Energy	Intensity
≥ 80	0	4	2
≥ 90	0	2	0
≥ 95	0	0	0

It might also be noticed that, for all three parameters, the highest R-squared values are in the distances between sample and camera range between 4cm and 8cm, for all iris range settings, and then they decrease, peaking again in distances 12cm, and between 18cm and 24cm, as it can be observed in Figure 5.12.

5.3.4.3 Conclusion

The Matlab analysis of this surface group produced average results, with only two R-squared values higher than 0.90, and none higher than 0.95 in the measurement set. Only the Energy parameter should be considered for this surface group in Matlab analysis, as it's the only one whose R-squared value went above 0.90.

The MVTec Halcon analysis, produced bad results, with only two R-squared values higher than 0.90, and none higher than 0.95 in the measurement set. The results are worse than Matlab as the highest R-squared associated to the parameter Contrast was 0.7016, and to the parameter Intensity was 0.8351. Only the Energy parameter should also be considered for this surface group, in Halcon analysis.

In its entirety, Energy is clearly the only viable option for this surface group, as it's the one who possessed values above 0.90 in both software analysis.

The fluctuation of values was, once again, something expected, and in its generality, the highest R-squared values all focused in the distances between sample and camera between 4 and 8cm. In this surface group, for all iris range settings.

As it was referred, there was an expected drop in the results quality, to the point where it might not actually be viable to use a speckle pattern technique in this particular surface group.

With only one surface group remaining, the obtained results should be similar to the ones presented for this surface group.

Table 5.16: R-squared values obtained from Halcon analysis of surface group 4.

Distance [cm]	Iris Range	Contrast	Energy	Intensity
4	Max.	0.565396	0.53998	0.688625
	F22	0.594504	0.856168	0.743492
	F16	0.685358	0.739591	0.693712
6	Max.	0.037655	0.484492	0.646024
	F22	0.016149	0.759711	0.744994
	F16	0.495312	0.826205	0.718926
8	Max.	0.701628	0.572284	0.83505
	F22	0.669978	0.919308	0.81878
	F16	0.670067	0.922402	0.76881
10	Max.	2.53E-05	0.121715	0.226358
	F22	4.21E-01	0.218473	0.307787
	F16	0.434718	0.410363	0.340364
12	Max.	0.578784	0.539543	0.668799
	F22	0.543821	0.636738	0.649991
	F16	0.643529	0.712504	0.658991
14	Max.	0.305727	0.36243	0.398362
	F22	0.165454	0.329623	0.317506
	F16	0.38371	0.458599	0.407793
16	Max.	0.026326	0.025958	0.06815
	F22	0.516979	0.014179	0.044755
	F16	0.274492	0.201373	0.245069
18	Max.	0.287015	0.182986	0.346934
	F22	0.065431	0.348446	0.38506
	F16	0.542942	0.564543	0.543728
20	Max.	0.567303	0.527105	0.585407
	F22	0.59485	0.451872	0.504493
	F16	0.56211	0.612254	0.576335
22	Max.	0.464674	0.179247	0.405278
	F22	0.519737	0.324854	0.450073
	F16	0.487307	0.412585	0.476278
24	Max.	0.538959	0.163985	0.423291
	F22	0.549974	0.273263	0.39941
	F16	0.53938	0.411559	0.473272

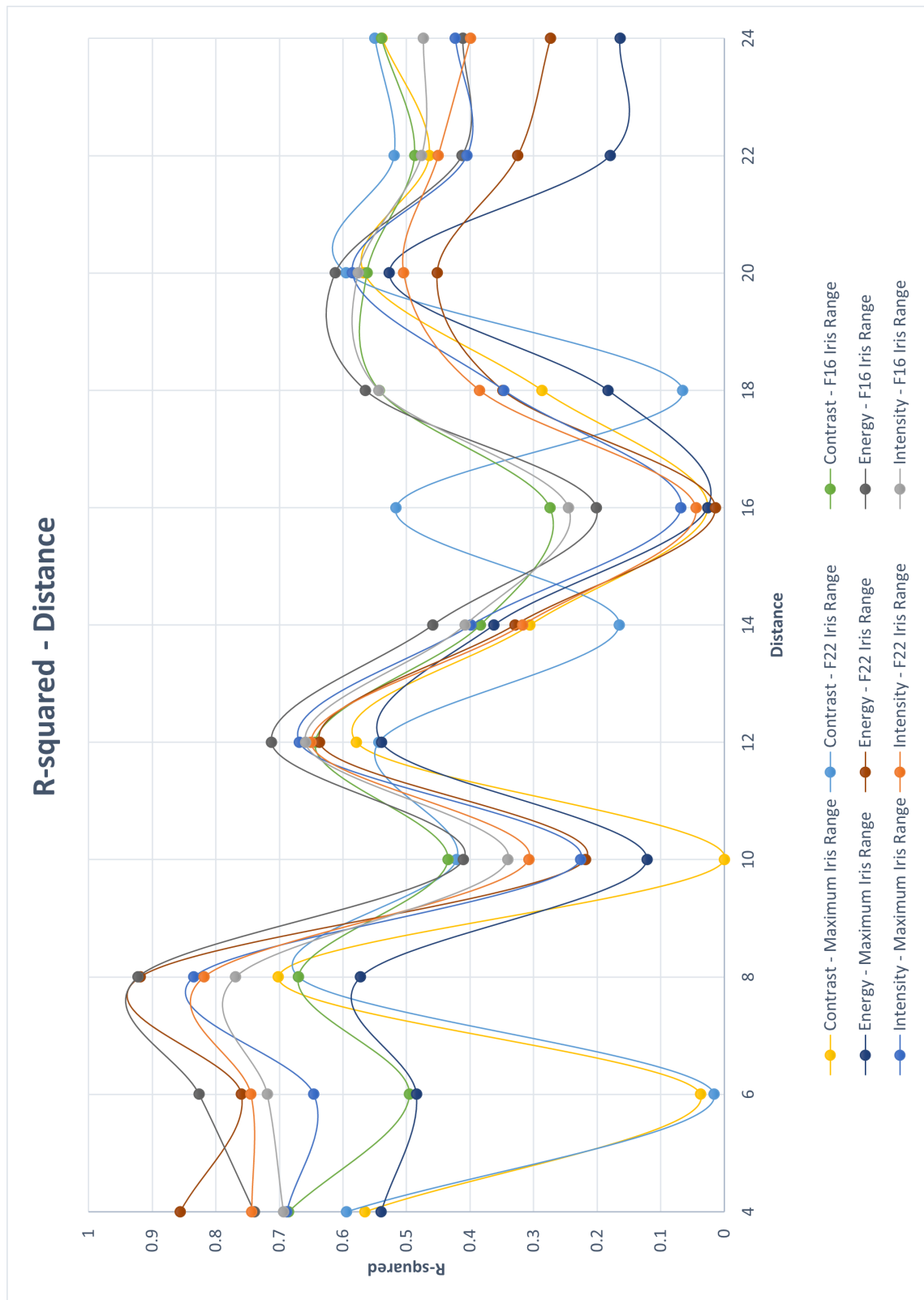


Figure 5.12: Evolution of the different Haralick's parameters with distance, for all iris ranges, for the MVTec's Halcon analysis of surface group 4.

5.3.5 Surface group 5 - Paint Comparator and Rugotest No. 3 (fine grain)

The Surface Group 5 includes surfaces N6, N7, N8, N9b, N10b, N11b, N1, N2, N3, and N4, whose surface roughness values correspond to 0.8 μm , 1.6 μm , 3.2 μm , 6.3 μm , 12.5 μm , 25 μm , 40 μm , 70 μm , and 100 μm , respectively.

5.3.5.1 Matlab analysis

The complete list of the obtained R-squared values can be observed in Table 5.18.

The higher R-squared values for each of the parameters were:

- 0.8837 for Contrast, with a distance between sample and camera of 8cm, and F16 iris range;
- 0.9187 for Energy, with a distance between sample and camera of 8cm, and F22 iris range;
- 0.7736 for Intensity, with a distance between sample and camera of 8cm, and the maximum iris range.

Thus, it can be concluded that, for the most accurate measurements for this surface roughness value range, the distance between sample and camera should be set at 8cm, and the iris range set at F22, with Energy being the analysed parameter, as it corresponds to the higher R-squared value.

Table 5.17 demonstrates the consistency of the R-squared values for each parameter, exhibiting the quality of the linear regressions.

Table 5.17: Evaluation of the quality of the obtained R-squared values for the Matlab analysis of surface group 5.

R-squared	Contrast	Energy	Intensity
≥ 80	2	3	0
≥ 90	0	2	0
≥ 95	0	0	0

It might also be noticed that, for all three parameters, the highest R-squared values are in the distances between sample and camera range between 4cm and 8cm, for all iris range settings, and then they decrease, with occasional peaks in distances 12cm, and between 16cm and 24cm, as it can be observed in Figure 5.13.

Table 5.18: R-squared values obtained from Matlab analysis of surface group 5.

Distance [cm]	Iris Range	Contrast	Energy	Intensity
4	Max.	0.6496	0.4646	0.6652
	F22	0.6557	0.8645	0.6984
	F16	0.7452	0.7455	0.6696
6	Max.	0.2201	0.3348	0.4409
	F22	0.0036	0.5232	0.5667
	F16	0.7368	0.6245	0.5545
8	Max.	0.805332	0.479441	0.773571
	F22	0.703065	0.918693	0.753914
	F16	0.883673	0.913047	0.705896
10	Max.	0.047589	0.164028	0.149194
	F22	0.172485	0.116692	0.208815
	F16	0.398787	0.307309	0.28323
12	Max.	0.618559	0.546232	0.653015
	F22	0.51178	0.631795	0.62775
	F16	0.693487	0.698462	0.626492
14	Max.	0.297836	0.405963	0.405861
	F22	0.011896	0.336038	0.312015
	F16	0.477649	0.484613	0.429593
16	Max.	0.005589	0.104603	0.12354
	F22	0.615852	0.036497	0.070796
	F16	0.513757	0.260255	0.298694
18	Max.	0.285374	0.396126	0.407422
	F22	0.025068	0.419506	0.420259
	F16	0.600481	0.573279	0.523139
20	Max.	0.568246	0.534962	0.588332
	F22	0.555746	0.459937	0.516165
	F16	0.538471	0.601956	0.55465
22	Max.	0.379565	0.1755	0.398007
	F22	0.550409	0.323534	0.45052
	F16	0.412552	0.410361	0.473329
24	Max.	0.381996	0.16685	0.426367
	F22	0.453674	0.273275	0.396823
	F16	0.405779	0.411217	0.463945

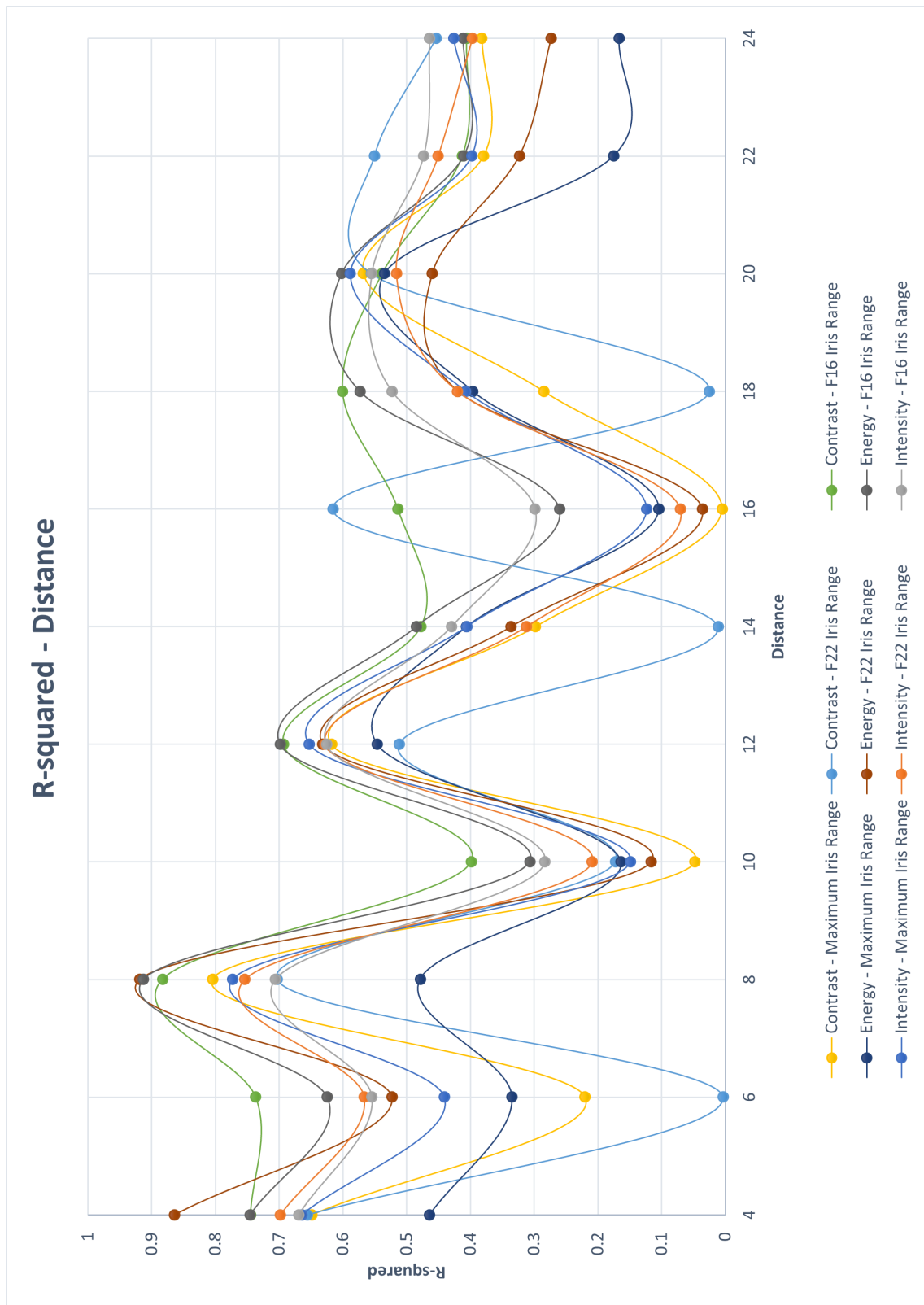


Figure 5.13: Evolution of the different Haralick's parameters with distance, for all iris ranges, for the Matlab analysis of surface group 5.

5.3.5.2 MvTec's Halcon analysis

The complete list of the obtained R-squared values can be observed in Table 5.20.

The higher R-squared values for each of the parameters were:

- 0.6797 for Contrast, with a distance between sample and camera of 4cm, and F16 iris range;
- 0.9188 for Energy, with a distance between sample and camera of 8cm, and F22 iris range;
- 0.7735 for Intensity, with a distance between sample and camera of 8cm, the maximum F16 iris range.

Thus, it can be concluded that, for the most accurate measurements for this surface roughness value range, the distance between sample and camera should be set at 8cm, and the iris range set at F2, with Energy being the analysed parameter, as it corresponds to the higher R-squared value.

Table 5.19 demonstrates the consistency of the R-squared values for each parameter, exhibiting the quality of the linear regressions.

Table 5.19: Evaluation of the quality of the obtained R-squared values for the MVTEC's Halcon analysis of surface group 5.

R-squared	Contrast	Energy	Intensity
≥ 80	0	3	0
≥ 90	0	2	0
≥ 95	0	0	0

It might also be noticed that, for all three parameters, the highest R-squared values are in the distance between sample and camera range of 8cm, for all iris range settings, and then they decrease, peaking again in distances 12cm, and 16cm to 24cm, as it can be observed in Figure 5.14.

5.3.5.3 Conclusion

The Matlab analysis of this surface group produced bad results, with two R-squared values higher than 0.90, and none higher than 0.95 in the measurement set. Once again, only the parameter Energy should be considered in Matlab analysis, as it's the only one with R-squared values above 0.90.

The MvTec Halcon analysis, produced even worse results compared to the Matlab ones, with worse values on both Contrast and Intensity parameters. The only two R-squared values above 0.90 are associated to Energy, and none are higher than 0.95. In this software analysis too, only should the parameter Energy be considered.

In its entirety, Energy was the only viable option for this group too, as it's the only one with associated R-squared values above 0.90.

The fluctuation of values was, once again, something expected, and in its generality, the highest R-squared values all focused in the distances between sample and camera between 4cm and 8cm. In this surface group, all iris ranges performed the same.

The expected results' quality drop is also present in this surface group, and only a speckle pattern technique associated to the Energy parameter should be considered.

Table 5.20: R-squared values obtained from Halcon analysis of surface group 5.

Distance [cm]	Iris Range	Contrast	Energy	Intensity
4	Max.	0.563244	0.460753	0.669645
	F22	0.571352	0.865288	0.69884
	F16	0.679708	0.743948	0.669849
6	Max.	0.0032	0.343536	0.440403
	F22	0.04318	0.523467	0.566846
	F16	0.40481	0.624093	0.561389
8	Max.	0.622543	0.479138	0.773518
	F22	0.574977	0.918783	0.753634
	F16	0.644052	0.912924	0.705584
10	Max.	0.00249	0.161197	0.149537
	F22	0.402361	0.11721	0.209208
	F16	0.397193	0.308684	0.283686
12	Max.	0.563228	0.545833	0.652807
	F22	0.51973	0.631919	0.627692
	F16	0.61496	0.698733	0.626403
14	Max.	0.310901	0.405802	0.406786
	F22	0.157523	0.337995	0.31305
	F16	0.421527	0.486094	0.43009
16	Max.	0.10471	0.10547	0.12382
	F22	0.515949	0.036587	0.071181
	F16	0.350039	0.261079	0.299029
18	Max.	0.328162	0.398936	0.40798
	F22	0.054965	0.421276	0.421167
	F16	0.532014	0.574091	0.523162
20	Max.	0.594721	0.538252	0.588187
	F22	0.615199	0.460606	0.516203
	F16	0.543221	0.602884	0.554531
22	Max.	0.454742	0.177502	0.398895
	F22	0.548408	0.324747	0.451135
	F16	0.480879	0.411742	0.473694
24	Max.	0.553357	0.167852	0.426549
	F22	0.57246	0.274105	0.397189
	F16	0.535608	0.411918	0.463936

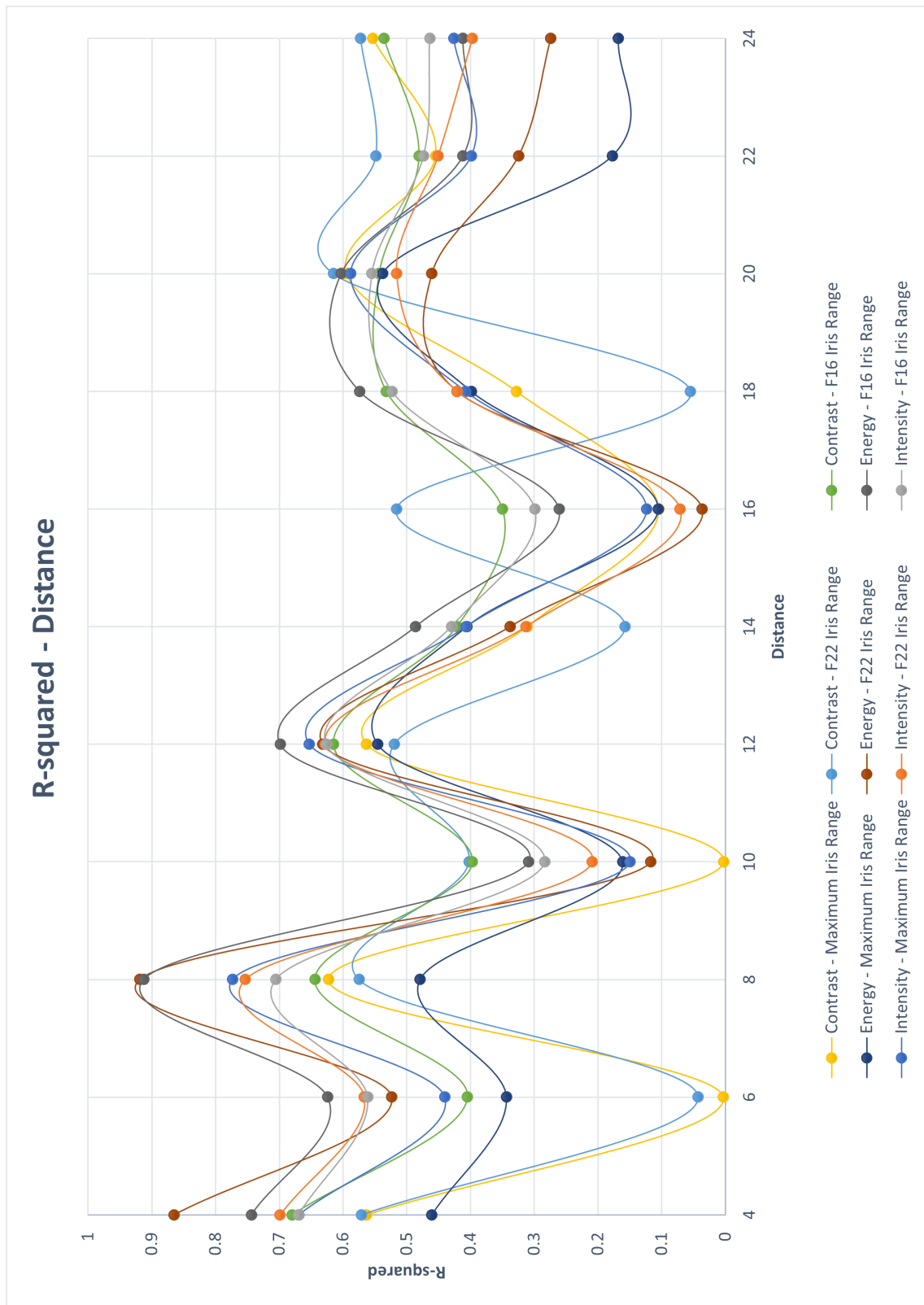


Figure 5.14: Evolution of the different Haralick's parameters with distance, for all iris ranges, for the MVTec's Halcon analysis of surface group 5.

5.4 Results Discussion

As the results' showcase is finished, it is now appropriate to discuss their quality in its generality.

As demonstrated, the results were good for the first three surface groups, correspondent to the individual material's analysis. When the two samples were put together for a broad surface roughness measurement, the results' quality immediately dropped.

This might result from the previously referred factors, such as the difference in the state of degradation of the surface of both materials.

It is also worth noting that the results were of better quality for the Rugotest No. 3 analysis (surface groups 2 and 3). This is probably the influence of the surface N4, that had a surface roughness value of $100\ \mu\text{m}$, approaching the stated technique value range, whose limit was at around $100\ \mu\text{m}$. Between the two surface groups, surface group 3, which corresponds to the fine grain sections, obtained slightly better results than surface group 2, which corresponds to the coarse grain sections. As mentioned before, the granularity of the surface might also affect the results.

Between the two softwares, there isn't much of a difference. Matlab obtained slightly better results in general, but for surface groups 4 and 5, MVTec's Halcon's analysis originated quite mediocre results in the parameters Contrast and Intensity. As MVTec's Halcon isn't transparent on how it calculates these parameters, no further conclusions can be drawn.

Overall, the so called "good" results all fluctuated around the distance of 8cm, with different iris range settings. As such, it might be the appropriate distance for this method, requiring further confirmation from several more experiments, with a distance between sample and camera ranging from 6cm to 10cm, with shorter intervals.

As the results' quality severely dropped with distance increase, there were no further analysis of higher distances between sample and camera, as the cropped pictures were getting smaller with each distance interval increase.

Independently of the software, Energy was the parameter that behaved better. It also seems to be the most constant one, as there was not a single surface group in which it didn't possess at least one R-squared value higher than 0.90. As such, the method should be a viable option for optical surface roughness measurement if the distance between camera and sample is 8cm, and the chosen analysis parameter is Energy.

For a more in-depth measurement, the calibration is absolutely crucial, following the steps demonstrated in this paper, to obtain at least the degree of certainty associated to the surface roughness measurement using the proposed technique.

Chapter 6

Conclusions and Future Work

The present thesis focused on developing a capable and relevant procedure for optical surface roughness measurement, by utilizing or adapting previously developed techniques, in order to obtain a quick and reliable method, that would also be affordable, fit to be employed in an industrial environment, as to verify the state of the products while still in production.

In the first place, to better evaluate each of the methods in the diverse panoply of optical measurement techniques, an extensive literature review was done. By introducing the basic concepts of surface roughness, and the classical techniques for its measurement, it was less difficult to understand why it's so important to measure it, and the shortcomings of the classical techniques. For example, the most renowned method, the mechanical profilometer, has a list of disadvantages to its utilization. As such, it is vital to comprehend why the need for other alternatives is so important.

Light reflection and dispersion mechanisms were also studied, as to understand the fundamentals of the optical techniques. Interferometry is an extensive subject area, that is to this day studied and employed in diverse subjects across the fields of science and engineering. In this project, its applicability to the fields of surface roughness measurement has been reviewed. The basics of speckle patterns were also introduced, as a result of light interference at surface disturbances. This last introduction proved to be quite useful, as the developed technique was based on speckle pattern analysis. Associated to the subjects of light analysis, an important work was also introduced, containing the parameters which were named Haralick's parameters, that would translate any image's light information into statistical properties.

The introduction of optical techniques was chosen as a method that would better fit the problem description. Weighing all the pros and cons for each technique, speckle pattern analysis was chosen, as it seemed a not too complex method, that didn't require a sizable quantity of expensive hardware, and would swiftly provide a full surface roughness analysis.

Starting by applying the previously described methodology to obtain surface roughness measurements, a physical system was mounted on top of an optical table, with a black coverage to the whole experiment area, which proved very useful in view of environment light influence. The

components, a laser, included as the source of light, a collimator and its integrated pin hole, that filtered high frequency components from the light beam, eliminating any noise due to dust or disperse rays of light, and a lens, focusing the filtered light beam in a given distance, produced, as referred, a filtered and focused light beam, which was then directed at a sample, whose surface would reflect the light beam. The resultant reflection was then captured by a camera. The sample would then rotate on an vertical axis, changing the light beam's angle of incidence. The reflection would once again be captured by a camera.

The analysis and comparison of the obtained reflections, through the use of Haralick's parameters, provided important information about the surface topology. However, due to several factors, no useful conclusions were drawn. As such, the technique was adapted and, instead of rotating the surface, in order to obtain information based only on two measurements of the same surface, the measurements were broadened to a number of surfaces, whose surface roughness is known, and analysed through the same methodology. Then, a linear regression was performed with the Haralick's parameters obtained from the referred analysis. Performing these procedures defined a method that works in a variable range, depending on the roughness values of the surfaces under test. That is, if the measured surfaces have surface roughness values between, for example, $10\ \mu\text{m}$ and $80\mu\text{m}$, the method is able to provide accurate information about their roughness.

To validate the experiments, two different sample materials were obtained. The Rugotest No. 3, with surfaces whose roughness values ranged between $0.8\ \mu\text{m}$ and $25\ \mu\text{m}$, and the Paint Comparator, with surface whose roughness values ranged between $25\ \mu\text{m}$ and $100\ \mu\text{m}$, were experimented with. Different surface groups, combining different surfaces from the two samples, were created. Through the use of softwares Matlab and MVTec's Halcon, conclusions were drawn out regarding the legitimacy of the proposed technique. The linear regressions R-squared values, that describe how close to the data points the approximation is, were evaluated for every surface group. The results from the surface groups that contained only surfaces from the same samples were satisfactory, always obtaining R-squared values above 0.95 for at least one of the evaluated Haralick's parameters, but the attempts to combine the two samples' surfaces lowered the result quality, with only one Haralick's parameter obtaining results higher than 0.90, with the others' best values going as low as 0.70. Diverse factors were attributed to this quality drop, such as surface composition or state of conservation.

As such, it is concluded that this method is better for surfaces from the same material, and whose production period and conservation states are quite similar.

After the results' showcase, an automated version of this system was proposed, in order to cut calibration measurements' time, and to reduce human interaction with the system, as it only results in component displacement, subverting the previous measurements and causing inaccurate measurements.

Thus, the proposed method is a viable alternative to the other surface roughness measurement techniques, providing accurate results. As it is an optical method, it does not require any type of contact with the sample, and is able to perform a full surface scan, instead of obtaining information from only one line profile of the surface. Were the system to be adapted and automated, it would

be able to be employed in an industrial environment, as long as it's correctly calibrated. This calibration, although advised, is dispensable, as long as it's not a high-end application. As it was concluded in the results' showcase, in most of the cases, the optimal distance is around 8cm, the iris range should be set to F22, and the Haralick's parameter that should be analysed would be Energy.

6.1 Future Work

Finalizing this thesis, and having acquired satisfactory results from the proposed technique, rendering this method a viable one, further work would definitely be beneficial, as to refine the procedures.

For the proposed technique, further experimentation around the distance between sample and camera of 8cm would definitely help in locating the optimal distance between sample and camera. As it's been demonstrated, all the best results fluctuated around the distance of 8cm. As the increments between distances were 2cm, reducing down these increments to 0.5cm or even 0.25cm would be a good change in order to find the general best distance. Further experimentation by testing the method in different settings would also be helpful, as to conclude if the optimal distance fluctuating around the 8cm mark is a result of the setting, or if it holds true for other environments.

A combination of the proposed technique and the originally established technique would also be an interesting approach. The methodology would be, instead of only obtaining information from the surface from one surface's capture, to include in the overall surface group, rotating the sample to obtain a second capture, and then introducing the comparison between captures in the surface group would probably fine-tune the method, allowing even better results. This could be accomplished by means of a precision micro-movement rotation table.

Mostly out of curiosity, the analysis of the peak of 'good' results spread out between the distances should be studied. In the results' showcase, it was highlighted that, after the usual peak around the distance between camera and sample of 8cm, some parameters also peaked randomly in other distances. A further study to understand if these are due to surface capture quality, or if it has any relation to the light beam, or its properties, such as wavelength, would be interesting as to understand what conditions the optimal distance for these measurements. It is a known fact that different materials reflect or absorb light differently, which may influence the parameters under study.

It has been referred that, for low-end applications, a combination of settings like the ones presented in Chapter 5 should be enough for a good estimate of the surface roughness values. However, for applications in which an accurate measurement is necessary, it is better to perform an analysis of the combinations of settings, such as the one performed in the development in the project, presented in the Methodology chapter.

For these procedures, it is necessary to move both the samples and the camera, and also change the iris range. Software manipulation is also necessary, as the captures are taken using a software, and the captured images names' must be changed and the images put in the right folder. Finally,

the analysis is performed using either Matlab or MVTec's Halcon, and the comparison for the R-squared values is done in an Excel, where the data will be exported to. These procedures are quite a dull and slow task. An operator might take up to a day to finish all these measurements, due to all the different steps, which will be repeated throughout the methodology.

Due to the stated reasons, an automated system that would completely realize the procedures is proposed. It is possible for the mechanism responsible for the moving of the parts and image capture to be automated, as it is possible for the softwares to be prepared in a way that would allow the complete analysis to be performed, without the need of manually renaming the images or putting them in the right folder or further move data between software packages, developing the entire application under a single software package and deploying it in the industrial setting.

As such, the following sections will describe a rough planning for the automated system. This planning was made with a Rugotest No. 3 measurement's calibration in mind. As such, only 8 surfaces will be captured (N6, N7, N8, N9a, N9b, N10a, N10b, N11a, and N11b). The distance between camera and sample range is from 4cm to 12cm, with 1cm intervals in between (4cm, 5cm, 6cm, 7cm, 8cm, 9cm, 10cm, 11cm, and 12cm), performing a total of 9 different distances. The iris range settings are, as in the performed experimentation, F16, F22, and the maximum allowed.

The following section will review each component needed for the system to be constructed.

6.1.1 Components

This section is initiated with the discussion of type of system that will be used, between hydraulic, pneumatic and servo-electrical.

An hydraulic system would be excessive, as the only moved components are the camera and the samples, whose mass should be relatively low and, as such, there isn't a need for elevated force capacity. Another problem is that hydraulic systems are relatively slow and, for this application, speeds higher than what hydraulic systems are able to provide are needed.

Between pneumatic and servo-electrical, the latter is clearly chosen due to ease of use and no further need of additional installations, as pneumatic would need an additional pressured air circulation system to be connected to the actuators, and unwanted vibrations would have to be accommodated, a task seldom easy to perform. Added to the ease of use, servo-electrical components, obviously depending on their quality, bring a higher degree of precision for their movements.

The first components which will be presented are the linear axis actuators needed for the movement of both the camera and the sample. These are self-explanatory, as they would perform the linear movements of the camera, forwards and backwards as needed, as to change the distance between camera and sample, and move the sample to the left and right, in order to capture the focus of the laser in the multiple surfaces in Rugotest No. 3. Instead of an horizontal movement, a vertical linear axis is also possible for the sample surface, performing the sample's movement in the vertical instead of the horizontal. In fact, a combination of the two might also be a good option.

For the linear axis, it is recommended to use a servomotor, with the adequate drivers, for their precision. As it's been referred, a precise movement is necessary to accurately perform the measurements on the samples and, as such, the servomotors are capable of this precision's degree.

Other components that might be considered are rotating axis, for both the laser, the sample and the camera to be mounted on. This way, another degree of movement is added, allowing for a wider variety of distances and angles between components, to further explore the measurements' results. As with the linear axis, micro-controlled precision rotary stages are recommended, for exactly the same reasons.

Depending on the degree of automation required, something that will be discussed further ahead, an automatic shutter system for the camera might be considered, or an automatic system for the variation of the iris range. Such a camera might be acquired, or a camera that has support for these kind of systems. This way, with the automatic shutter system, no human action is needed in order to capture the surface's topology, or to change the iris range of the camera.

Obviously, for the system to work as envisaged, all the components referred in the Methodology chapter need to be present. The ones presented in this section are purely to turn the manual system into an automated system.

6.1.2 System operation

A brief description of the system operation is due. For the project of the automated system, as it's been referred, only nine different distances are considered, with the nine different surfaces on Rugotest No. 3. Also, only the iris range settings of F16, F22 and the maximum allowed are considered.

A schematic of the system's operation can be observed in Figure 6.1, under the form of a GRAFCET.

In the GRAFCET, three different variables are used to store the information of the three settings in the system:

- i stores the information of which sample's surface is to be captured next, in the form of linear axis position for the camera to focus on said sample's surface;
- j stores the iris range settings;
- k stores the distances between camera and sample.

In this case, i stores the information for the nine different surfaces, assigning a linear axis position to each of them; j stores the information of the three different iris range settings; k stores the information of the nine distances between camera and sample.

As such, when the system is initiated, these variables are reset, with the assignment of the value 1 to each variable.

After Button 1 is pressed, the system begins its operation. The camera moves to the first set distance between sample and camera, which is 4cm, in this case; the Rugotest No. 3 is moved to a

position in which the capture of the surface N6 is possible; and the iris range, in this specific case, is manually changed to the setting F16.

When the sample is at position i , and the iris range is set at j , a picture is taken by the picture capturing system. In this case, it's the operator that takes the picture, with the indicated software. Once the picture is stored, a verification is ran: in case the last Rugotest's surface has been captured, i.e., i has the value 9, the iris range must be changed to its next setting. As such, when the iris range has been manually changed, Button 2 is pressed, the variable i is reset, the variable j changes its value, and a new surface capturing is performed.

After the iris range is changed, and button 2 is pressed, after the variable j , another verification occurs. If the captures have already been done with the three iris settings, i.e., j has the value 3, the camera moves, and the surface capture procedure is followed yet again, resetting j 's value, and the variable k changes its value.

Every time the captures are performed with the three different iris range settings, a third verification is done for the camera position variable. Once the captures are done with all the camera distances, i.e., the variable k has the value 9, the system shuts down.

For a complete shutdown, the OFF button must be pressed. For another rerun, the ON Button is pressed, and then Button 1 again.

Thus, the explanation of the system's operation has been performed. This system is semi-automated, with some manual operations still included, such as the capture of the pictures, and the change of the iris range setting, done by an operator. Additionally, the images must still be renamed to a name that easily is recognized by the software, and the same software must also be run by the same operator.

Although this solution offers a semi-automated system, if necessary, the system may be automated to a higher degree. A few steps for achieving a higher automation degree will be demonstrated.

The first step would be to make the image capturing an automatic process. This can be either achieved with an automatic shutter system that is attached to the camera, programmed to trigger at the right times, to capture the surfaces; or an additional software that is connected to the camera, such as MV Tec Halcon, that allows the programming of automatic image capture. Thus, the image capture no longer depends of an operator.

An obvious second step would be the preparation of the captured images. By preparation, it means storing them in the appropriate place, and automatically renaming them to be analysed in the main software. This might be achieved with additional software.

The final step, is the automatic change of the iris range setting. This is possible with an additional system, an automatic aperture control device. This way, it is no longer necessary for a manual change in the iris range setting.

The individual functioning of every component must be assured, but the coordination of all these different devices and components is also something to keep in mind. A master device must be considered, that is able to receive and send signals, from and to every device, as to regulate the functioning of every component. Only with a master device is the functioning of the system

secured as a whole, as it acts as the communication bridge between every device, organizing each component's functions.

Even though quite a multitude of devices is needed to fully automate the system, it should still be more economically affordable than any other previously mentioned method.

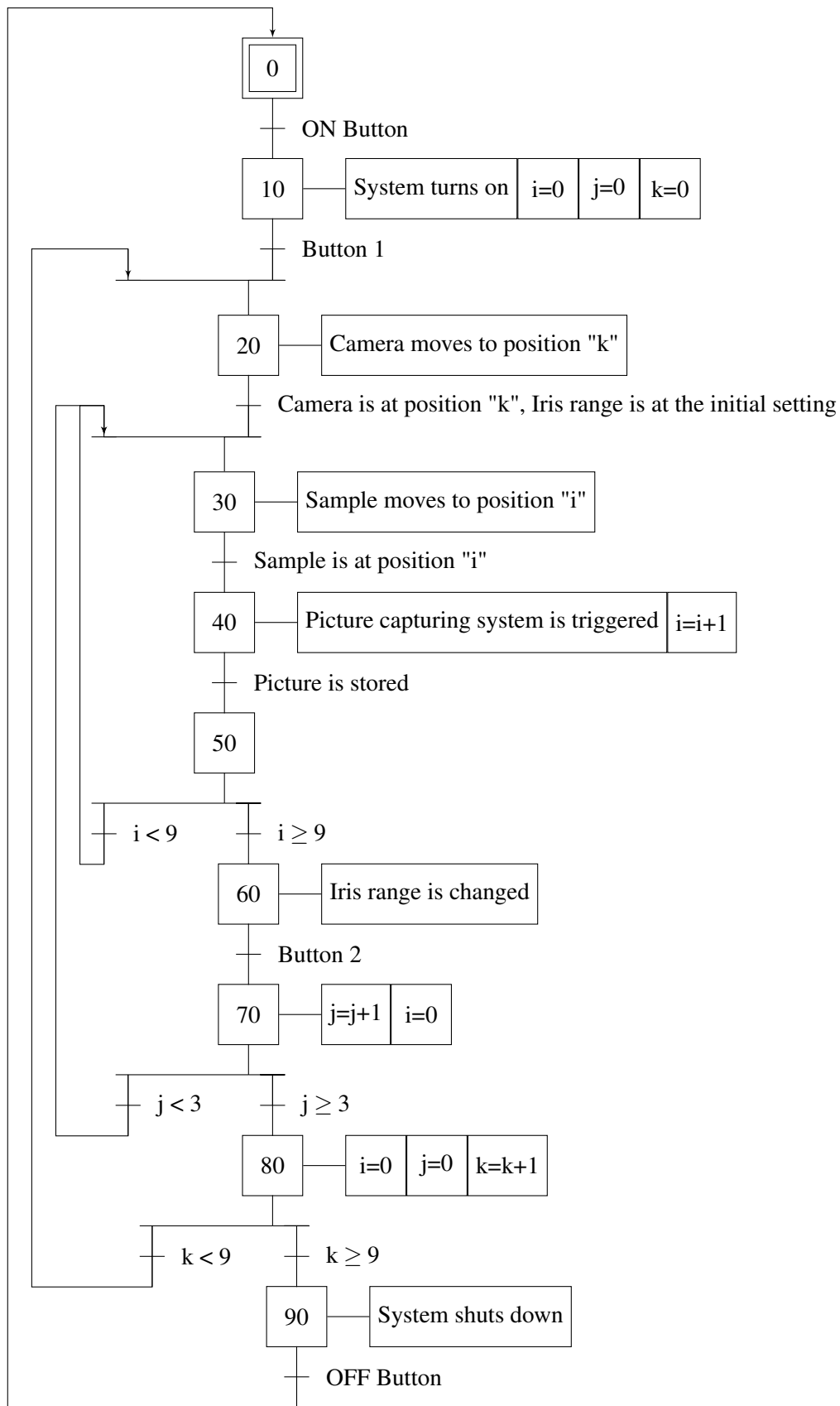


Figure 6.1: Rough sketch of a behavioral GRAFCET that describes the functioning of the system.

References

- [1] Hassan A. Abdulhadi, Syarifah N. Aqida, and Izwan Ismail. Tool failure in die casting. In *Reference Module in Materials Science and Materials Engineering*. Elsevier, 2019.
- [2] M.S.H. Bhuiyan and I.A. Choudhury. 13.22 - review of sensor applications in tool condition monitoring in machining. In Saleem Hashmi, Gilmar Ferreira Batalha, Chester J. Van Tyne, and Bekir Yilbas, editors, *Comprehensive Materials Processing*, pages 539 – 569. Elsevier, Oxford, 2014.
- [3] A. Curtis and M. Dalby. 17 - cell response to nanofeatures in biomaterials. In Lucy Di Silvio, editor, *Cellular Response to Biomaterials*, Woodhead Publishing Series in Biomaterials, pages 429 – 461. Woodhead Publishing, 2009.
- [4] Christina Freyman, Bo Zhao, and Yip-Wah Chung. 18 - suppression of moisture sensitivity of friction in carbon-based coatings. In Ali Erdemir and Jean-Michel Martin, editors, *Superlubricity*, pages 295 – 310. Elsevier Science B.V., Amsterdam, 2007.
- [5] Yujing Jiang, Bo Li, and Yosihiko Tanabashi. Estimating the relation between surface roughness and mechanical properties of rock joints. *International Journal of Rock Mechanics and Mining Sciences*, 43(6):837 – 846, 2006.
- [6] Eliseu Münchow, Marcos Correa, Fabrício Ogliari, Evandro Piva, and Cesar Zanchi. Correlation between surface roughness and microhardness of experimental composites with varying filler concentration. *The journal of contemporary dental practice*, 13:299–304, 2012.
- [7] D.J. Whitehouse. Comparison between stylus and optical methods for measuring surfaces. *CIRP Annals*, 37(2):649 – 653, 1988.
- [8] Yuxuan Gong, Jian Xu, and Relva Buchanan. Surface roughness: A review of its measurement at micro-/nano-scale. *Physical Sciences Reviews*, 3, 01 2018.
- [9] Vladimir Lyukshin, Dmitry Shatko, and Pavel Strelnikov. Methods and approaches to the surface roughness assessment. *Materials Today: Proceedings*, 2020.
- [10] M.B. Kiran, B. Ramamoorthy, and V. Radhakrishnan. Evaluation of surface roughness by vision system. *International Journal of Machine Tools and Manufacture*, 38(5):685 – 690, 1998. International Conference on Metrology and Properties of Engineering Surfaces.

- [11] Robert A. Sprague. Surface roughness measurement using white light speckle. *Appl. Opt.*, 11(12):2811–2816, 1972.
- [12] T. Asakura. *Surface roughness measurement*, pages 11–49. Elsevier, 1978.
- [13] R. Erf. *Speckle Metrology*. Quantum Electronics–Principles and Applications. Elsevier Science, 2012.
- [14] B. Bhushan. *Principles and Applications of Tribology*. A Wiley interscience publication. Wiley, 1999.
- [15] D.J. Whitehouse. *Handbook of Surface Metrology*. Taylor & Francis, 1994.
- [16] Hy D. Tran. Measuring and characterizing surface topography. 5 2016.
- [17] B. Bhushan. *Modern Tribology Handbook, Two Volume Set*. Mechanics & Materials Science. CRC Press, 2000.
- [18] ASME B46.1. *Surface Texture (Surface Roughness, Waviness, and Lay)*. ASME, 2019.
- [19] J. Raja, B. Muralikrishnan, and Shengyu Fu. Recent advances in separation of roughness, waviness and form. *Precision Engineering*, 26(2):222 – 235, 2002.
- [20] N.O. Myers. Characterization of surface roughness. *Wear*, 5(3):182 – 189, 1962.
- [21] Mark C. Malburg. A unified methodology for the application of surface metrology. 1996.
- [22] E.S. Gadelmawla, M.M. Koura, T.M.A. Maksoud, I.M. Elewa, and H.H. Soliman. Roughness parameters. *Journal of Materials Processing Technology*, 123(1):133 – 145, 2002.
- [23] T.R. Thomas. Characterization of surface roughness. *Precision Engineering*, 3(2):97 – 104, 1981.
- [24] Robert N. Wenzel. Surface roughness and contact angle. *The Journal of Physical and Colloid Chemistry*, 53(9):1466–1467, 1949.
- [25] G. Gold and K. Helmreich. A physical surface roughness model and its applications. *IEEE Transactions on Microwave Theory and Techniques*, 65(10):3720–3732, 2017.
- [26] Aitor Cazón, Paz Morer, and Luis Matey. Polyjet technology for product prototyping: Tensile strength and surface roughness properties. *Proceedings of the Institution of Mechanical Engineers, Part B: Journal of Engineering Manufacture*, 228(12):1664–1675, 2014.
- [27] Monchai Suraratchai, Jérôme Limido, Catherine Mabru, and Rémy Chieragatti. Modelling the influence of machined surface roughness on the fatigue life of aluminium alloy. *International Journal of fatigue*, 30(12):2119–2126, 2008.
- [28] S. Suresh and R. O. Ritchie. A geometric model for fatigue crack closure induced by fracture surface roughness. *Metallurgical Transactions A*, 13(9):1627–1631, 1982.

- [29] D. Greitemeier, C. Dalle Donne, F. Syassen, J. Eufinger, and T. Melz. Effect of surface roughness on fatigue performance of additive manufactured ti-6al-4v. *Materials Science and Technology*, 32(7):629–634, 2016.
- [30] Yukitaka Murakami. 16 - effect of surface roughness on fatigue strength. In Yukitaka Murakami, editor, *Metal Fatigue (Second Edition)*, pages 407 – 430. Academic Press, second edition edition, 2019.
- [31] DAVID E. PACKHAM. Chapter 7 - surface roughness and adhesion. In D.A. Dillard, A.V. Pocius, and M. Chaudhury, editors, *Adhesion Science and Engineering*, pages 317 – 349. Elsevier Science B.V., Amsterdam, 2002.
- [32] David E Packham. Surface energy, surface topography and adhesion. *International Journal of Adhesion and Adhesives*, 23(6):437–448, 2003.
- [33] A Luke. Pool boiling heat transfer from horizontal tubes with different surface roughness. *International Journal of Refrigeration*, 20(8):561 – 574, 1997. Special Issue: New Developments in Pool Boiling.
- [34] Vipin B. Gawande, A.S. Dhoble, and D.B. Zodpe. Effect of roughness geometries on heat transfer enhancement in solar thermal systems – a review. *Renewable and Sustainable Energy Reviews*, 32:347 – 378, 2014.
- [35] Gabriela Díaz and Miguel José-Yacamán. Advanced characterization of nanoparticles: experimental evidence of surface roughness. *Materials Chemistry and Physics*, 41(4):240 – 244, 1995.
- [36] V.B. Svetovoy and G. Palasantzas. Influence of surface roughness on dispersion forces. *Advances in Colloid and Interface Science*, 216:1 – 19, 2015.
- [37] Mark W. Smith. Roughness in the earth sciences. *Earth-Science Reviews*, 136:202 – 225, 2014.
- [38] Yao Zhang and Junrui Chai. Effect of surface morphology on fluid flow in rough fractures: A review. *Journal of Natural Gas Science and Engineering*, 79:103343, 2020.
- [39] J M Bennett. Recent developments in surface roughness characterization. *Measurement Science and Technology*, 3(12):1119–1127, dec 1992.
- [40] R. Wiesendanger and W. Roland. *Scanning Probe Microscopy and Spectroscopy: Methods and Applications*. Scanning Probe Microscopy and Spectroscopy: Methods and Applications. Cambridge University Press, 1994.
- [41] S. M. SALAPAKA and M. V. SALAPAKA. Scanning probe microscopy. *IEEE Control Systems Magazine*, 28(2):65–83, 2008.

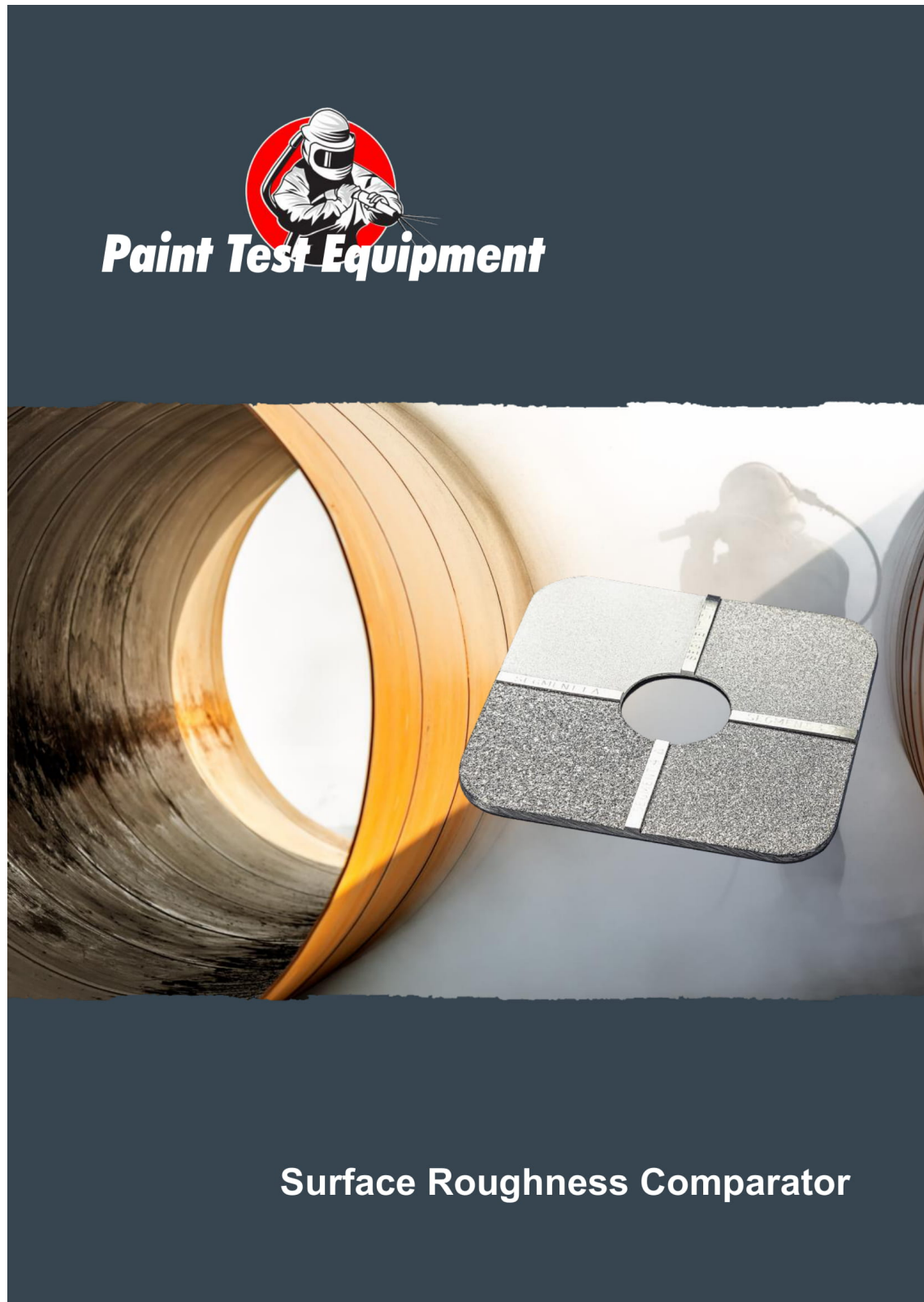
- [42] Ivar Giaever. Electron tunneling between two superconductors. *Phys. Rev. Lett.*, 5:464–466, Nov 1960.
- [43] G. Binnig, H. Rohrer, Ch. Gerber, and E. Weibel. Surface studies by scanning tunneling microscopy. *Phys. Rev. Lett.*, 49:57–61, Jul 1982.
- [44] G. Binnig and H. Rohrer. Scanning tunneling microscopy. *Surface Science*, 126(1):236 – 244, 1983.
- [45] Gerd Binnig, Calvin F Quate, and Ch Gerber. Atomic force microscope. *Physical review letters*, 56(9):930, 1986.
- [46] Duncan T Moore. *Tutorials in Optics*.
- [47] M. P. Schultz and A. Myerz. Comparison of three roughness function determination methods. *Experiments in Fluids*, 35:372–379, Oct 2003.
- [48] Ronald W. Woolley. Pneumatic method for making fast, higher resolution, noncontacting measurement of surface topography. In Lionel R. Baker, editor, *Commercial Applications of Precision Manufacturing at the Sub-Micron Level*, volume 1573, pages 205 – 215. International Society for Optics and Photonics, SPIE, 1992.
- [49] Y-P Zhao, G-C Wang, T-M Lu, Georgios Palasantzas, and J Th M De Hosson. Surface-roughness effect on capacitance and leakage current of an insulating film. *Physical review B*, 60(12):9157, 1999.
- [50] David R. McMurtry and David K. Thomas. Probe for measuring surface roughness by sensing fringe field capacitance effects, Dec 1993.
- [51] J. S. Halliday. Surface examination by reflection electron microscopy. *Proceedings of the Institution of Mechanical Engineers*, 169(1):777–787, 1955.
- [52] Koichi Tozawa, Hisayoshi Sato, and Masanori O-Hori. A new method for the measurement of the straightness of machine tools and machined work. *Journal of Mechanical Design, Transactions Of the ASME*, 104(3):587–592, July 1982.
- [53] James A. Holzer and C. C. Sung. Scattering of electromagnetic waves from a rough surface. ii. *Journal of Applied Physics*, 49(3):1002–1011, 1978.
- [54] Suting Chen, Rui Feng, Chuang Zhang, and Yanyan Zhang. Surface roughness measurement method based on multi-parameter modeling learning. *Measurement*, 129:664 – 676, 2018.
- [55] H. E. Bennett and J. O. Porteus. Relation between surface roughness and specular reflectance at normal incidence. *J. Opt. Soc. Am.*, 51(2):123–129, Feb 1961.
- [56] Russell Loughridge and Daniel Abramovitch. A tutorial on laser interferometry for precision measurements. pages 3686–3703, 06 2013.

- [57] Katherine Creath and James C. Wyant. Absolute measurement of surface roughness. *Appl. Opt.*, 29(26):3823–3827, Sep 1990.
- [58] Katherine Creath. V phase-measurement interferometry techniques. In E. Wolf, editor, *Progress in Optics*, volume 26, pages 349 – 393. Elsevier, 1988.
- [59] S. Tolansky. *An Introduction to Interferometry*. A Halsted Press book. Longman, 1973.
- [60] Sergey I. Bozhevolnyi, Valentyn S. Volkov, Eloïse Devaux, Jean-Yves Laluet, and Thomas W. Ebbesen. Channel plasmon subwavelength waveguide components including interferometers and ring resonators. *Nature*, 440:508–511, Mar 2006.
- [61] R. M. Haralick, K. Shanmugam, and I. Dinstein. Textural features for image classification. *IEEE Transactions on Systems, Man, and Cybernetics*, SMC-3(6):610–621, 1973.
- [62] HR Nelson. Taper sectioning as a means of describing the surface contour of metals. In *Proc. Conf. on Friction and Surface Finish*, pages 217–237. Massachusetts Institute of Technology Press Cambridge, MA, 1969.
- [63] Suting Chen, Rui Feng, Chuang Zhang, and Yanyan Zhang. An evaluation of surface roughness as measured by the brush surface analyzer and the schmaltz optical cut. 1967.
- [64] G. Schmaltz. *Technische oberflächenkunde: feingestalt und eigenschaften von grenzflächen technischer Körper, insbesondere der maschinenteile*. J. Springer, 1936.
- [65] Petr Beckmann and Andre Spizzichino. The scattering of electromagnetic waves from rough surfaces. *Norwood*, 1987.
- [66] Joseph Koleske. *Paint and Coating Testing Manual: 15th. Edition of the Gardner-Sward Handbook*. ASTM International, 2012.
- [67] E. Hecht, A. Zajac, and A. Zając. *Optics*. Addison-Wesley series in physics. Addison-Wesley Publishing Company, 1974.
- [68] W Timothy Liu. Progress in scatterometer application. *Journal of Oceanography*, 58(1):121–136, 2002.
- [69] John C. Stover, Marvin L. Bernt, and Tod F. Schiff. TIS uniformity maps of wafers, disks, and other samples. In John C. Stover, editor, *Optical Scattering in the Optics, Semiconductor, and Computer Disk Industries*, volume 2541, pages 21 – 25. International Society for Optics and Photonics, SPIE, 1995.
- [70] Harold Earl Bennett. Scattering characteristics of optical materials. *Optical Engineering*, 17(5):175480, 1978.
- [71] C. J. Peters. Light depolarizer. *Appl. Opt.*, 3(12):1502–1503, Dec 1964.

- [72] G.M. Clarke and T.R. Thomas. Roughness measurement with a laser scanning analyser. *Wear*, 57(1):107 – 116, 1979.
- [73] E. L. Church, T. V. Vorburger, and J. C. Wyant. Direct Comparison Of Mechanical And Optical Measurements Of The Finish Of Precision Machined Optical Surfaces. In Donald P. Brehm, editor, *Production Aspects of Single Point Machined Optics*, volume 0508, pages 71 – 82. International Society for Optics and Photonics, SPIE, 1984.
- [74] Guiseppe Schirripa Spagnolo, Domenica Paoletti, Alfonso Paoletti, and Dario Ambrosini. Roughness measurement by electronic speckle correlation and mechanical profilometry. *Measurement*, 20(4):243 – 249, 1997.
- [75] Lisa C Leonard and Vincent Toal. Roughness measurement of metallic surfaces based on the laser speckle contrast method. *Optics and Lasers in Engineering*, 30(5):433 – 440, 1998.
- [76] Rong-Sheng Lu, Gui-Yun Tian, Duke Gledhill, and Steve Ward. Grinding surface roughness measurement based on the co-occurrence matrix of speckle pattern texture. *Applied Optics*, 45(35):8839–8847, 2006.
- [77] Peter Lehmann. Surface-roughness measurement based on the intensity correlation function of scattered light under speckle-pattern illumination. *Applied Optics*, 38(7):1144–1152, 1999.
- [78] J. H. Bruning, D. R. Herriott, J. E. Gallagher, D. P. Rosenfeld, A. D. White, and D. J. Brangaccio. Digital wavefront measuring interferometer for testing optical surfaces and lenses. *Appl. Opt.*, 13(11):2693–2703, Nov 1974.
- [79] J. C. Wyant. Use of an ac heterodyne lateral shear interferometer with real-time wavefront correction systems. *Appl. Opt.*, 14(11):2622–2626, Nov 1975.
- [80] Klaus Freischlad and Chris L. Koliopoulos. Fourier description of digital phase-measuring interferometry. *J. Opt. Soc. Am. A*, 7(4):542–551, Apr 1990.
- [81] Paul Kumar Upputuri, Krishna Nandigana, and Mahendra Kothiyal. Single-shot interferometry techniques for optical testing. *Asian Journal of Physics*, 24:1317–1338, 10 2015.
- [82] Dennis C Ghiglia and Mark D Pritt. *Two-dimensional phase unwrapping: theory, algorithms, and software*, volume 4. Wiley New York, 1998.
- [83] Paul J. Caber. Interferometric profiler for rough surfaces. *Appl. Opt.*, 32(19):3438–3441, Jul 1993.
- [84] James C. Wyant. White light interferometry. In H. John Caulfield, editor, *Holography: A Tribute to Yuri Denisyuk and Emmett Leith*, volume 4737, pages 98 – 107. International Society for Optics and Photonics, SPIE, 2002.

Appendix A

Technical Datasheet for the Paint Comparator





Paint Test Equipment

Roughness Comparator

A precision nickel Comparator plate for grit and shot-blast surface roughness comparison measurement.



When steel has been blast-cleaned, the surface consists of random irregularities with peaks and valleys that are not easily characterised. Because of this random nature, experts have recommended that the profile should be identified as either angular (where grit abrasives have been used) or dimpled (where shot abrasives have been used) and that they should be graded as fine, medium or coarse with each grade being defined by limits specified in ISO 8503.

The Roughness Comparator method is applicable to steel surfaces that have been blast-cleaned with either metallic or non-metallic abrasives to grades Sa 2½ and Sa 3.

When a mixture of shot and grit abrasives are used to blast-clean a substrate, the Grit Surface Roughness Comparator should be used.

Specification

Profile Segment 1: Grit 25µm. Shot 25µm.

Profile Segment 2: Grit 60µm. Shot 40µm.

Profile Segment 3: Grit 100µm. Shot 70µm.

Profile Segment 4: Grit 150µm. Shot 100µm.

Compliance

ISO 8503-1, ISO 8503-2 and ASTM D4417.



Supply

The Roughness Comparator is supplied in a protective Wallet.

A X5 Illuminated Magnifier for viewing the Comparator is available as an optional extra.



Ordering

R2006	Roughness Comparator Grit
R2007	Roughness Comparator Shot
RA001	Illuminated Magnifier X5. Includes Carrying Case
NRC01	Roughness Comparator Conformance Certificate



Instructions

Evaluation

Remove all loose dirt and debris from the test surface.
 Select the appropriate surface profile reference Comparator. The Grit Comparator is for Comparing profiles after blast-cleaning with grit abrasives, and the Shot Comparator is for comparing profiles after blast-cleaning with shot abrasives.



Place the selected Comparator against an area of the test surface. Compare in turn the test surface with the four segments of the Comparator, using the Illuminated Magnifier if necessary. If the Illuminated Magnifier is used, place it so that the test surface is viewed simultaneously with a segment of the Comparator.

Assess the profiles on the Comparator that are nearest to the profile of the test surface and determine its grade from the following:

Fine-grade profiles equal to segment 1 and up to but excluding segment 2

Medium-grade profiles equal to segment 2 and up to but excluding segment 3.

Coarse-grade profiles equal to segment 3 and up to but excluding segment 4.

If any profile is assessed as below the lower limit for the fine grading, assess this grading as finer than fine.

If any profile is assessed as greater than the upper limit for the coarse grading, assess this grading as coarser than coarse.

Care

Never place the Comparator face down on a rough surface. Keep the Comparator in the protective Wallet provided when not in use.

If the Comparator becomes tarnished, wash with a Dilute detergent solution and soft brush and dry with soft tissue.

About Us

Paint Test Equipment is a global leader in the manufacture of specialist test equipment specifically for the industrial painting and coating industries for the protection of steel assets from corrosion, mainly in the oil, renewables and steel construction sectors. We have over 30 years experience and extensive knowledge in delivering practical solutions in supporting our customers with world class products for corrosion prevention.

Prevention of corrosion on steel is essential to extend the asset lifetime, optimise performance and minimise downtime for expensive maintenance work. Using Paint Test Equipment products ensures that industrial coatings are applied to the highest achievable quality standards of ISO compliance.

We supply small, medium and multinational companies with the full range of technologies and innovations in our unrivalled portfolio of products for our customers to grow their business and enhance profits through cost effective corrosion management equipment.

Paint Test Equipment is committed to providing proactive and innovative solutions to meet customer requirements for the highest quality, user friendly inspection equipment. Paint Test Equipment is the partner of choice.

Paint Test Equipment reserves the right to alter specifications without prior notice.
Copyright Paint Test Equipment 2021.



Paint Test Equipment

www.paint-test-equipment.com

Tel: +44 (0)1260 275614
e-mail: sales@paint-test-equipment.com

Appendix B

Technical Datasheet for the Rugotest No. 3



Vision on quality
www.tqc.eu

RUGOTEST NO.3 – SURFACE ROUGHNESS COMPARATOR

LD6010

MANUAL

1 PRODUCT DESCRIPTION

Surface finish specimens for testing surface roughness by the sight and touch method.

Registered design L.C.A. – C.E.A.

The Sight and Touch method

The specimens have been assembled so as to represent, for the most commonly-used machining methods, the limiting values of surface finish quality arranged in a geometrical progression in accordance with factor 2. These values were chosen among those recommended for the criterion "Ra" in the ISO standards 2632/I-1975 and 2632/II-1977.

Experience shows that the method of comparing a machined surface with a known sample, by sight and touch, enables the quality of the finish of this surface to be estimated with remarkable accuracy.

The remotest method is particularly convenient when specifying surface finish for components which feature in sub-contracting arrangements, sales contracts, etc.

The samples supplied are for use only in sight and touch comparisons, not as references for calibrating surface finish measuring instruments of any type.

Although the **Rugotest** is a simple and inexpensive tool, the reliability of the results it provides makes it highly useful at the levels of any manufacturing industry.

When opened, the left-hand page gives the most important information for the design office, the workshop and the classroom, as well as a summary of the relevant ISO standards for surface finish and the graph showing the relationship between production cost and surface finish.



1.1 Specifications

Surface roughness comparison standard, model RUG 3 for shot- and grit blasting.

Material : High-nickel test plate

Width : 90mm

Length : 118mm

2 STANDARDS

Complies with standards NF/E05-051, ASTM D 4417/A, ISO 2632 / I 1975, ISO 2632/II 1977

Look up the appropriate standard for a correct execution of the test.

3 WHAT'S IN THE BOX?

The surface roughness comparison standard comes with table, manual and leather pouch.

1 |

TQC B.V.
Nijverheidscentrum 14

2761 JP Zevenhuizen
The Netherlands

T 31(0)180 - 63 13 44
F 31(0)180 - 63 29 17

E info@tqc.eu
W www.tqc.eu

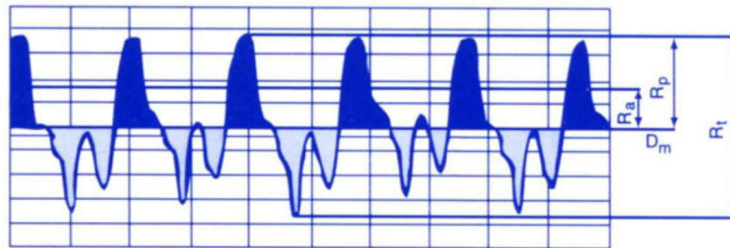


Vision on quality
www.tqc.eu

4 PERFORM A MEASUREMENT

- By positioning the comparing standard onto the test surface a comparison to the reference examples of the comparison standard is made.
- Assess the profile of the comparison standard most closely to match that of the test area and determine the result to the class: **A** for Shot and **B** for Grit.
- The fineness of the abrasive medium is further divided into: **a** for coarse grain or **b** for fine grain.
- Comparison of average roughness R_a value is found in the table were $N_6=0,8$ $N_7=1,6$ $N_8=3,3$ $N_9=6,3$ $N_{10}=12,5$ and $N_{11}=25 \mu\text{m}$.

5 EXPLANATION AND SUMMARY OF ROUGHNESS CRITERIA



D_m – Mean line of the surface profile:

The line parallel to the direction of the sampling length, which divides the surface profile such that the sum of the areas enclosed by itself and the profile are equal above and below it.

R_a – Arithmetical mean deviation of the profile:

The arithmetical mean of the absolute values of the profile departure.

R_p – Flattening depth:

Distance between the highest point of the peaks and the average line.

R_t – Maximum height of the profile:

The distance between the line of peaks of the profile and the line of valleys of the profile.

R_z – Ten point height of irregularities:

The average value of the absolute values of heights of five maximum profile peaks and the depths of five maximum profile valleys.

R – Average depth:

Mean of the peaks/depths distances.

Note: criteria's complete definitions can be found in the NF E 05-015 standards



Vision on quality
www.tqc.eu

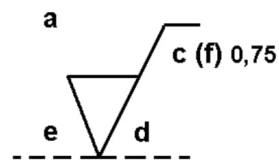
6 INDICATION ON DRAWINGS

Example

- a:** Roughness value Ra in micrometers or microinches or Roughness grade number N1 to N11
b: Production method. Treatment or coating.
c: Sampling length
d: Direction of lay
e: Machining allowance
f: Other roughness values (in brackets)

Ra = 1,6

b milled



7 MAINTENANCE

- Though robust in design and made of nickel treat it with care.
- Clean the instrument using a soft dry cloth or a little soap. Never clean the instrument by any mechanical means such as a wire brush or abrasive paper. This may cause, just like the use of aggressive cleaning agents, permanent damage.
- Always keep the instrument in its case when not in use.

8 DISCLAIMER

The information given in this manual is not intended to be exhaustive and any person using the product for any purpose other than that specifically recommended in this manual without first obtaining written confirmation from us as to the suitability of the product for the intended purpose does so at his own risk. Whilst we endeavour to ensure that all advice we give about the product (whether in this manual or otherwise) is correct we have no control over either the quality or condition of the product or the many factors affecting the use and application of the product. Therefore, unless we specifically agree in writing to do so, we do not accept any liability whatsoever or howsoever arising for the performance of the product or for any loss or damage (other than death or personal injury resulting from our negligence) arising out of the use of the product. The information contained in this manual is liable to modification from time to time in the light of experience and our policy of continuous product development.

Appendix C

Developed scripts for Matlab's image analysis

The present Appendix is meant to showcase the script that was developed for the image analysis performed in software Matlab.

```
1 clear ;
2 close all ;
3 %% Variable declaration
4 M = 256; %GLCM Matrix dimension
5 Roughness = [0.8; 1.6; 3.2; 6.3; 12.5; 25; 25; 40; 70; 100];
   %For Comparator + Rugotest (Fine/Coarse)
6 Roughness_Comp = Roughness(7:10); %For Comparator
7 Roughness_RugF = Roughness(1:6); %For Rugotest (Fine)
8 Roughness_RugC = Roughness(1:6); %For Rugotest (Coarse)
9 %% Image Introduction
10 I1r = imread('1.bmp');
11 I2r = imread('2.bmp');
12 I3r = imread('3.bmp');
13 I4r = imread('4.bmp');
14 I6r = imread('6.bmp');
15 I7r = imread('7.bmp');
16 I8r = imread('8.bmp');
17 I9ar = imread('9a.bmp');
18 I9br = imread('9b.bmp');
19 I10ar = imread('10a.bmp');
20 I10br = imread('10b.bmp');
21 I11ar = imread('11a.bmp');
22 I11br = imread('11b.bmp');
23 %% Image Cropping
```

```
24 targetsize = [0 0 825 1050];
25 I1 = imcrop(I1r , targetsize);
26 I2 = imcrop(I2r , targetsize);
27 I3 = imcrop(I3r , targetsize);
28 I4 = imcrop(I4r , targetsize);
29 I6 = imcrop(I6r , targetsize);
30 I7 = imcrop(I7r , targetsize);
31 I8 = imcrop(I8r , targetsize);
32 I9a = imcrop(I9ar , targetsize);
33 I9b = imcrop(I9br , targetsize);
34 I10a = imcrop(I10ar , targetsize);
35 I10b = imcrop(I10br , targetsize);
36 I11a = imcrop(I11ar , targetsize);
37 I11b = imcrop(I11br , targetsize);
38 %% Intensity Calculation
39 Intensity1 = mean2(I1);
40 Intensity2 = mean2(I2);
41 Intensity3 = mean2(I3);
42 Intensity4 = mean2(I4);
43 Intensity6 = mean2(I6);
44 Intensity7 = mean2(I7);
45 Intensity8 = mean2(I8);
46 Intensity9a = mean2(I9a);
47 Intensity9b = mean2(I9b);
48 Intensity10a = mean2(I10a);
49 Intensity10b = mean2(I10b);
50 Intensity11a = mean2(I11a);
51 Intensity11b = mean2(I11b);
52 %% GLCM Creation
53 offsets = [0 1; -1 1; -1 0; -1 -1];
54 glcm1 = graycomatrix(I1 , 'GrayLimits' , [0 255] , 'NumLevels' , M,
    'Offset' , offsets);
55 glcm2 = graycomatrix(I2 , 'GrayLimits' , [0 255] , 'NumLevels' , M,
    'Offset' , offsets);
56 glcm3 = graycomatrix(I3 , 'GrayLimits' , [0 255] , 'NumLevels' , M,
    'Offset' , offsets);
57 glcm4 = graycomatrix(I4 , 'GrayLimits' , [0 255] , 'NumLevels' , M,
    'Offset' , offsets);
58 glcm6 = graycomatrix(I6 , 'GrayLimits' , [0 255] , 'NumLevels' , M,
    'Offset' , offsets);
```



```
59 glcm7 = graycomatrix(I7, 'GrayLimits', [0 255], 'NumLevels', M,  
    'Offset', offsets);  
60 glcm8 = graycomatrix(I8, 'GrayLimits', [0 255], 'NumLevels', M,  
    'Offset', offsets);  
61 glcm9a = graycomatrix(I9a, 'GrayLimits', [0 255], 'NumLevels', M,  
    'Offset', offsets);  
62 glcm9b = graycomatrix(I9b, 'GrayLimits', [0 255], 'NumLevels', M,  
    'Offset', offsets);  
63 glcm10a = graycomatrix(I10a, 'GrayLimits', [0 255], 'NumLevels',  
    M, 'Offset', offsets);  
64 glcm10b = graycomatrix(I10b, 'GrayLimits', [0 255], 'NumLevels',  
    M, 'Offset', offsets);  
65 glcm11a = graycomatrix(I11a, 'GrayLimits', [0 255], 'NumLevels',  
    M, 'Offset', offsets);  
66 glcm11b = graycomatrix(I11b, 'GrayLimits', [0 255], 'NumLevels',  
    M, 'Offset', offsets);  
67 %% Contrast Calculation  
68 Contrast1 = (graycoprops(glcm1(:, :, 1)).Contrast +  
    graycoprops(glcm1(:, :, 2)).Contrast +  
    graycoprops(glcm1(:, :, 3)).Contrast +  
    graycoprops(glcm1(:, :, 4)).Contrast) ./4;  
69 Contrast2 = (graycoprops(glcm2(:, :, 1)).Contrast +  
    graycoprops(glcm2(:, :, 2)).Contrast +  
    graycoprops(glcm2(:, :, 3)).Contrast +  
    graycoprops(glcm2(:, :, 4)).Contrast) ./4;  
70 Contrast3 = (graycoprops(glcm3(:, :, 1)).Contrast +  
    graycoprops(glcm3(:, :, 2)).Contrast +  
    graycoprops(glcm3(:, :, 3)).Contrast +  
    graycoprops(glcm3(:, :, 4)).Contrast) ./4;  
71 Contrast4 = (graycoprops(glcm4(:, :, 1)).Contrast +  
    graycoprops(glcm4(:, :, 2)).Contrast +  
    graycoprops(glcm4(:, :, 3)).Contrast +  
    graycoprops(glcm4(:, :, 4)).Contrast) ./4;  
72 Contrast6 = (graycoprops(glcm6(:, :, 1)).Contrast +  
    graycoprops(glcm6(:, :, 2)).Contrast +  
    graycoprops(glcm6(:, :, 3)).Contrast +  
    graycoprops(glcm6(:, :, 4)).Contrast) ./4;  
73 Contrast7 = (graycoprops(glcm7(:, :, 1)).Contrast +  
    graycoprops(glcm7(:, :, 2)).Contrast +
```

```

    graycoprops(glcm7(:,:,3)).Contrast +
    graycoprops(glcm7(:,:,4)).Contrast)./4;
74 Contrast8 = (graycoprops(glcm8(:,:,1)).Contrast +
    graycoprops(glcm8(:,:,2)).Contrast +
    graycoprops(glcm8(:,:,3)).Contrast +
    graycoprops(glcm8(:,:,4)).Contrast)./4;
75 Contrast9a = (graycoprops(glcm9a(:,:,1)).Contrast +
    graycoprops(glcm9a(:,:,2)).Contrast +
    graycoprops(glcm9a(:,:,3)).Contrast +
    graycoprops(glcm9a(:,:,4)).Contrast)./4;
76 Contrast9b = (graycoprops(glcm9b(:,:,1)).Contrast +
    graycoprops(glcm9b(:,:,2)).Contrast +
    graycoprops(glcm9b(:,:,3)).Contrast +
    graycoprops(glcm9b(:,:,4)).Contrast)./4;
77 Contrast10a = (graycoprops(glcm10a(:,:,1)).Contrast +
    graycoprops(glcm10a(:,:,2)).Contrast +
    graycoprops(glcm10a(:,:,3)).Contrast +
    graycoprops(glcm10a(:,:,4)).Contrast)./4;
78 Contrast10b = (graycoprops(glcm10b(:,:,1)).Contrast +
    graycoprops(glcm10b(:,:,2)).Contrast +
    graycoprops(glcm10b(:,:,3)).Contrast +
    graycoprops(glcm10b(:,:,4)).Contrast)./4;
79 Contrast11a = (graycoprops(glcm11a(:,:,1)).Contrast +
    graycoprops(glcm11a(:,:,2)).Contrast +
    graycoprops(glcm11a(:,:,3)).Contrast +
    graycoprops(glcm11a(:,:,4)).Contrast)./4;
80 Contrast11b = (graycoprops(glcm11b(:,:,1)).Contrast +
    graycoprops(glcm11b(:,:,2)).Contrast +
    graycoprops(glcm11b(:,:,3)).Contrast +
    graycoprops(glcm11b(:,:,4)).Contrast)./4;
81 %% Energy Calculation
82 Energy1 = (graycoprops(glcm1(:,:,1)).Energy +
    graycoprops(glcm1(:,:,2)).Energy +
    graycoprops(glcm1(:,:,3)).Energy +
    graycoprops(glcm1(:,:,4)).Energy)./4;
83 Energy2 = (graycoprops(glcm2(:,:,1)).Energy +
    graycoprops(glcm2(:,:,2)).Energy +
    graycoprops(glcm2(:,:,3)).Energy +
    graycoprops(glcm2(:,:,4)).Energy)./4;

```

```
84 Energy3 = (graycoprops(glcm3(:,:,1)).Energy +  
    graycoprops(glcm3(:,:,2)).Energy +  
    graycoprops(glcm3(:,:,3)).Energy +  
    graycoprops(glcm3(:,:,4)).Energy) ./4;  
85 Energy4 = (graycoprops(glcm4(:,:,1)).Energy +  
    graycoprops(glcm4(:,:,2)).Energy +  
    graycoprops(glcm4(:,:,3)).Energy +  
    graycoprops(glcm4(:,:,4)).Energy) ./4;  
86 Energy6 = (graycoprops(glcm6(:,:,1)).Energy +  
    graycoprops(glcm6(:,:,2)).Energy +  
    graycoprops(glcm6(:,:,3)).Energy +  
    graycoprops(glcm6(:,:,4)).Energy) ./4;  
87 Energy7 = (graycoprops(glcm7(:,:,1)).Energy +  
    graycoprops(glcm7(:,:,2)).Energy +  
    graycoprops(glcm7(:,:,3)).Energy +  
    graycoprops(glcm7(:,:,4)).Energy) ./4;  
88 Energy8 = (graycoprops(glcm8(:,:,1)).Energy +  
    graycoprops(glcm8(:,:,2)).Energy +  
    graycoprops(glcm8(:,:,3)).Energy +  
    graycoprops(glcm8(:,:,4)).Energy) ./4;  
89 Energy9a = (graycoprops(glcm9a(:,:,1)).Energy +  
    graycoprops(glcm9a(:,:,2)).Energy +  
    graycoprops(glcm9a(:,:,3)).Energy +  
    graycoprops(glcm9a(:,:,4)).Energy) ./4;  
90 Energy9b = (graycoprops(glcm9b(:,:,1)).Energy +  
    graycoprops(glcm9b(:,:,2)).Energy +  
    graycoprops(glcm9b(:,:,3)).Energy +  
    graycoprops(glcm9b(:,:,4)).Energy) ./4;  
91 Energy10a = (graycoprops(glcm10a(:,:,1)).Energy +  
    graycoprops(glcm10a(:,:,2)).Energy +  
    graycoprops(glcm10a(:,:,3)).Energy +  
    graycoprops(glcm10a(:,:,4)).Energy) ./4;  
92 Energy10b = (graycoprops(glcm10b(:,:,1)).Energy +  
    graycoprops(glcm10b(:,:,2)).Energy +  
    graycoprops(glcm10b(:,:,3)).Energy +  
    graycoprops(glcm10b(:,:,4)).Energy) ./4;  
93 Energy11a = (graycoprops(glcm11a(:,:,1)).Energy +  
    graycoprops(glcm11a(:,:,2)).Energy +  
    graycoprops(glcm11a(:,:,3)).Energy +  
    graycoprops(glcm11a(:,:,4)).Energy) ./4;
```

```

94 Energy11b = (graycoprops(glcm11b(:, :, 1)).Energy +
    graycoprops(glcm11b(:, :, 2)).Energy +
    graycoprops(glcm11b(:, :, 3)).Energy +
    graycoprops(glcm11b(:, :, 4)).Energy) ./ 4;
95 %% Intensity Vector Concatenation
96 Intensity_Comp = [Intensity1; Intensity2; Intensity3;
    Intensity4];
97 Intensity_RugC = [Intensity6; Intensity7; Intensity8;
    Intensity9a; Intensity10a; Intensity11a];
98 Intensity_RugF = [Intensity6; Intensity7; Intensity8;
    Intensity9b; Intensity10b; Intensity11b];
99 Intensity_Comp_RugF = [Intensity_RugF; Intensity_Comp];
100 Intensity_Comp_RugC = [Intensity_RugC; Intensity_Comp];
101 %% Contrast Vector Concatenation
102 Contrast_Comp = [Contrast1; Contrast2; Contrast3; Contrast4];
103 Contrast_RugC = [Contrast6; Contrast7; Contrast8; Contrast9a;
    Contrast10a; Contrast11a];
104 Contrast_RugF = [Contrast6; Contrast7; Contrast8; Contrast9b;
    Contrast10b; Contrast11b];
105 Contrast_Comp_RugF = [Contrast_RugF; Contrast_Comp];
106 Contrast_Comp_RugC = [Contrast_RugC; Contrast_Comp];
107 %% Energy Vector Concatenation
108 Energy_Comp = [Energy1; Energy2; Energy3; Energy4];
109 Energy_RugC = [Energy6; Energy7; Energy8; Energy9a; Energy10a;
    Energy11a];
110 Energy_RugF = [Energy6; Energy7; Energy8; Energy9b; Energy10b;
    Energy11b];
111 Energy_Comp_RugF = [Energy_RugF; Energy_Comp];
112 Energy_Comp_RugC = [Energy_RugC; Energy_Comp];
113 %% Roughness - Intensity Graph Plot
114 figure (1)
115 plot(Roughness_Comp, Intensity_Comp);
116 xlabel('Roughness');
117 ylabel('Intensity');
118 title('Comparator: Roughness - Intensity');
119 figure (2)
120 plot(Roughness_RugC, Intensity_RugC);
121 xlabel('Roughness');
122 ylabel('Intensity');
123 title('Rugotest, Coarse: Roughness - Intensity');

```

```
124 figure(3)
125 plot(Roughness_RugF, Intensity_RugF);
126 xlabel('Roughness');
127 ylabel('Intensity');
128 title('Rugotest, Fine: Roughness - Intensity');
129 figure(4)
130 plot(Roughness, Intensity_Comp_RugC);
131 xlabel('Roughness');
132 ylabel('Intensity');
133 title('Comparator + Rugotest, Coarse: Roughness - Intensity');
134 figure(5)
135 plot(Roughness, Intensity_Comp_RugF);
136 xlabel('Roughness');
137 ylabel('Intensity');
138 title('Comparator + Rugotest, Fine: Roughness - Intensity');
139 %% Roughness - Contrast Graph Plot
140 figure(5)
141 plot(Roughness_Comp, Contrast_Comp);
142 xlabel('Roughness');
143 ylabel('Contrast');
144 title('Comparator: Roughness - Contrast');
145 figure(6)
146 plot(Roughness_RugC, Contrast_RugC);
147 xlabel('Roughness');
148 ylabel('Contrast');
149 title('Rugotest, Coarse: Roughness - Contrast');
150 figure(7)
151 plot(Roughness_RugF, Contrast_RugF);
152 xlabel('Roughness');
153 ylabel('Contrast');
154 title('Rugotest, Fine: Roughness - Contrast');
155 figure(8)
156 plot(Roughness, Contrast_Comp_RugC);
157 xlabel('Roughness');
158 ylabel('Contrast');
159 title('Comparator + Rugotest, Coarse: Roughness - Contrast');
160 figure(9)
161 plot(Roughness, Contrast_Comp_RugF);
162 xlabel('Roughness');
163 ylabel('Contrast');
```

```
164 title('Comparator + Rugotest , Fine: Roughness - Contrast');
165 %% Roughness - Energy Graph Plot
166 figure(10)
167 plot(Roughness_Comp , Energy_Comp);
168 xlabel('Roughness');
169 ylabel('Energy');
170 title('Comparator: Roughness - Energy');
171 figure(11)
172 plot(Roughness_RugC , Energy_RugC);
173 xlabel('Roughness');
174 ylabel('Energy');
175 title('Rugotest , Coarse: Roughness - Energy');
176 figure(12)
177 plot(Roughness_RugF , Energy_RugF);
178 xlabel('Roughness');
179 ylabel('Energy');
180 title('Rugotest , Fine: Roughness - Energy');
181 figure(13)
182 plot(Roughness , Energy_Comp_RugC);
183 xlabel('Roughness');
184 ylabel('Energy');
185 title('Comparator + Rugotest , Coarse: Roughness - Energy');
186 figure(14)
187 plot(Roughness , Energy_Comp_RugF);
188 xlabel('Roughness');
189 ylabel('Energy');
190 title('Comparator + Rugotest , Fine: Roughness - Energy');
191 %% Linear Regression Analysis for Comparator
192 % Contrast
193 X_Comp1 = [ones(length(Roughness_Comp),1) Roughness_Comp];
194 b_Comp1 = X_Comp1\Contrast_Comp;
195 yCalc_Comp1 = X_Comp1*b_Comp1;
196 figure(15)
197 scatter(Roughness_Comp , Contrast_Comp);
198 hold on
199 plot(Roughness_Comp , yCalc_Comp1);
200 xlabel('Roughness');
201 ylabel('Contrast');
202 title('Roughness-Contrast');
203 grid on
```

```

204 R_Comp1 = 1 - sum((Contrast_Comp - yCalc_Comp1).^2) /
      sum((Contrast_Comp - mean(Contrast_Comp)).^2);
205 % Energy
206 X_Comp2 = [ones(length(Roughness_Comp),1) Roughness_Comp];
207 b_Comp2 = X_Comp2 \ Energy_Comp;
208 yCalc_Comp2 = X_Comp2 * b_Comp2;
209 figure(16)
210 scatter(Roughness_Comp, Energy_Comp);
211 hold on
212 plot(Roughness_Comp, yCalc_Comp2);
213 xlabel('Roughness');
214 ylabel('Energy');
215 title('Roughness-Energy');
216 grid on
217 R_Comp2 = 1 - sum((Energy_Comp - yCalc_Comp2).^2) /
      sum((Energy_Comp - mean(Energy_Comp)).^2);
218 % Intensity
219 X_Comp3 = [ones(length(Roughness_Comp),1) Roughness_Comp];
220 b_Comp3 = X_Comp3 \ Intensity_Comp;
221 yCalc_Comp3 = X_Comp3 * b_Comp3;
222 figure(17)
223 scatter(Roughness_Comp, Intensity_Comp);
224 hold on
225 plot(Roughness_Comp, yCalc_Comp3);
226 xlabel('Roughness');
227 ylabel('Intensity');
228 title('Roughness-Intensity');
229 grid on
230 R_Comp3 = 1 - sum((Intensity_Comp - yCalc_Comp3).^2) /
      sum((Intensity_Comp - mean(Intensity_Comp)).^2);
231 R_Comp = [R_Comp1, R_Comp2, R_Comp3];
232 %% Linear Regression Analysis for Rugotest Fine
233 % Contrast
234 X_RugF1 = [ones(length(Roughness_RugF),1) Roughness_RugF];
235 b_RugF1 = X_RugF1 \ Contrast_RugF;
236 yCalc_RugF1 = X_RugF1 * b_RugF1;
237 figure(18)
238 scatter(Roughness_RugF, Contrast_RugF);
239 hold on
240 plot(Roughness_RugF, yCalc_RugF1);

```

```

241 xlabel('Roughness');
242 ylabel('Contrast');
243 title('Roughness-Contrast');
244 grid on
245 R_RugF1 = 1 - sum((Contrast_RugF - yCalc_RugF1).^2) /
    sum((Contrast_RugF - mean(Contrast_RugF)).^2);
246 % Energy
247 X_RugF2 = [ones(length(Roughness_RugF),1) Roughness_RugF];
248 b_RugF2 = X_RugF2\Energy_RugF;
249 yCalc_RugF2 = X_RugF2*b_RugF2;
250 figure(19)
251 scatter(Roughness_RugF, Energy_RugF);
252 hold on
253 plot(Roughness_RugF, yCalc_RugF2);
254 xlabel('Roughness');
255 ylabel('Energy');
256 title('Roughness-Energy');
257 grid on
258 R_RugF2 = 1 - sum((Energy_RugF - yCalc_RugF2).^2) /
    sum((Energy_RugF - mean(Energy_RugF)).^2);
259 %Intensity
260 X_RugF3 = [ones(length(Roughness_RugF),1) Roughness_RugF];
261 b_RugF3 = X_RugF3\Intensity_RugF;
262 yCalc_RugF3 = X_RugF3*b_RugF3;
263 figure(20)
264 scatter(Roughness_RugF, Intensity_RugF);
265 hold on
266 plot(Roughness_RugF, yCalc_RugF3);
267 xlabel('Roughness');
268 ylabel('Intensity');
269 title('Roughness-Intensity');
270 grid on
271 R_RugF3 = 1 - sum((Intensity_RugF - yCalc_RugF3).^2) /
    sum((Intensity_RugF - mean(Intensity_RugF)).^2);
272 R_RugF = [R_RugF1, R_RugF2, R_RugF3];
273 %% Linear Regression Analysis for Rugotest Coarse
274 % Contrast
275 X_RugC1 = [ones(length(Roughness_RugC),1) Roughness_RugC];
276 b_RugC1 = X_RugC1\Contrast_RugC;
277 yCalc_RugC1 = X_RugC1*b_RugC1;

```



```

278 figure(21)
279 scatter(Roughness_RugC, Contrast_RugC);
280 hold on
281 plot(Roughness_RugC, yCalc_RugC1);
282 xlabel('Roughness');
283 ylabel('Contrast');
284 title('Roughness-Contrast');
285 grid on
286 R_RugC1 = 1 - sum((Contrast_RugC - yCalc_RugC1).^2) /
    sum((Contrast_RugC - mean(Contrast_RugC)).^2);
287 % Energy
288 X_RugC2 = [ones(length(Roughness_RugC),1) Roughness_RugC];
289 b_RugC2 = X_RugC2 \ Energy_RugC;
290 yCalc_RugC2 = X_RugC2 * b_RugC2;
291 figure(22)
292 scatter(Roughness_RugC, Energy_RugC);
293 hold on
294 plot(Roughness_RugC, yCalc_RugC2);
295 xlabel('Roughness');
296 ylabel('Energy');
297 title('Roughness-Energy');
298 grid on
299 R_RugC2 = 1 - sum((Energy_RugC - yCalc_RugC2).^2) /
    sum((Energy_RugC - mean(Energy_RugC)).^2);
300 %Intensity
301 X_RugC3 = [ones(length(Roughness_RugC),1) Roughness_RugC];
302 b_RugC3 = X_RugC3 \ Intensity_RugC;
303 yCalc_RugC3 = X_RugC3 * b_RugC3;
304 figure(23)
305 scatter(Roughness_RugC, Intensity_RugC);
306 hold on
307 plot(Roughness_RugC, yCalc_RugC3);
308 xlabel('Roughness');
309 ylabel('Intensity');
310 title('Roughness-Intensity');
311 grid on
312 R_RugC3 = 1 - sum((Intensity_RugC - yCalc_RugC3).^2) /
    sum((Intensity_RugC - mean(Intensity_RugC)).^2);
313 R_RugC = [R_RugC1, R_RugC2, R_RugC3];
314 %% Linear Regression Analysis for Comparator + Rugotest Fine

```

```

315 % Contrast
316 X_Comp_RugF1 = [ones(length(Roughness),1) Roughness];
317 b_Comp_RugF1 = X_Comp_RugF1 \ Contrast_Comp_RugF;
318 yCalc_Comp_RugF1 = X_Comp_RugF1 * b_Comp_RugF1;
319 figure(24)
320 scatter(Roughness, Contrast_Comp_RugF);
321 hold on
322 plot(Roughness, yCalc_Comp_RugF1);
323 xlabel('Roughness');
324 ylabel('Contrast');
325 title('Roughness-Contrast');
326 grid on
327 R_Comp_RugF1 = 1 - sum((Contrast_Comp_RugF -
    yCalc_Comp_RugF1).^2) / sum((Contrast_Comp_RugF -
    mean(Contrast_Comp_RugF)).^2);
328 % Energy
329 X_Comp_RugF2 = [ones(length(Roughness),1) Roughness];
330 b_Comp_RugF2 = X_Comp_RugF2 \ Energy_Comp_RugF;
331 yCalc_Comp_RugF2 = X_Comp_RugF2 * b_Comp_RugF2;
332 figure(25)
333 scatter(Roughness, Energy_Comp_RugF);
334 hold on
335 plot(Roughness_Comp_RugF, yCalc_Comp_RugF2);
336 xlabel('Roughness');
337 ylabel('Energy');
338 title('Roughness-Energy');
339 grid on
340 R_Comp_RugF2 = 1 - sum((Energy_Comp_RugF -
    yCalc_Comp_RugF2).^2) / sum((Energy_Comp_RugF -
    mean(Energy_Comp_RugF)).^2);
341 % Intensity
342 X_Comp_RugF3 = [ones(length(Roughness),1) Roughness];
343 b_Comp_RugF3 = X_Comp_RugF3 \ Intensity_Comp_RugF;
344 yCalc_Comp_RugF3 = X_Comp_RugF3 * b_Comp_RugF3;
345 figure(26)
346 scatter(Roughness, Intensity_Comp_RugF);
347 hold on
348 plot(Roughness_Comp_RugF, yCalc_Comp_RugF3);
349 xlabel('Roughness');
350 ylabel('Intensity');

```

```

351 title('Roughness-Intensity');
352 grid on
353 R_Comp_RugF3 = 1 - sum((Intensity_Comp_RugF -
    yCalc_Comp_RugF3).^2) / sum((Intensity_Comp_RugF -
    mean(Intensity_Comp_RugF)).^2);
354 R_Comp_RugF = [R_Comp_RugF1, R_Comp_RugF2, R_Comp_RugF3];
355 %% Linear Regression Analysis for Comparator + Rugotest Coarse
356 % Contrast
357 X_Comp_RugC1 = [ones(length(Roughness),1) Roughness];
358 b_Comp_RugC1 = X_Comp_RugC1 \ Contrast_Comp_RugC;
359 yCalc_Comp_RugC1 = X_Comp_RugC1 * b_Comp_RugC1;
360 figure(27)
361 scatter(Roughness, Contrast_Comp_RugC);
362 hold on
363 plot(Roughness, yCalc_Comp_RugC1);
364 xlabel('Roughness');
365 ylabel('Contrast');
366 title('Roughness-Contrast');
367 grid on
368 R_Comp_RugC1 = 1 - sum((Contrast_Comp_RugC -
    yCalc_Comp_RugC1).^2) / sum((Contrast_Comp_RugC -
    mean(Contrast_Comp_RugC)).^2);
369 % Energy
370 X_Comp_RugC2 = [ones(length(Roughness),1) Roughness];
371 b_Comp_RugC2 = X_Comp_RugC2 \ Energy_Comp_RugC;
372 yCalc_Comp_RugC2 = X_Comp_RugC2 * b_Comp_RugC2;
373 figure(28)
374 scatter(Roughness, Energy_Comp_RugC);
375 hold on
376 plot(Roughness_Comp_RugC, yCalc_Comp_RugC2);
377 xlabel('Roughness');
378 ylabel('Energy');
379 title('Roughness-Energy');
380 grid on
381 R_Comp_RugC2 = 1 - sum((Energy_Comp_RugC -
    yCalc_Comp_RugC2).^2) / sum((Energy_Comp_RugC -
    mean(Energy_Comp_RugC)).^2);
382 % Intensity
383 X_Comp_RugC3 = [ones(length(Roughness),1) Roughness];
384 b_Comp_RugC3 = X_Comp_RugC3 \ Intensity_Comp_RugC;

```

```
385 yCalc_Comp_RugC3 = X_Comp_RugC3*b_Comp_RugC3;
386 figure(29)
387 scatter(Roughness, Intensity_Comp_RugC);
388 hold on
389 plot(Roughness_Comp_RugC, yCalc_Comp_RugC3);
390 xlabel('Roughness');
391 ylabel('Intensity');
392 title('Roughness-Intensity');
393 grid on
394 R_Comp_RugC3 = 1 - sum((Intensity_Comp_RugC -
    yCalc_Comp_RugC3).^2) / sum((Intensity_Comp_RugC -
    mean(Intensity_Comp_RugC)).^2);
395 R_Comp_RugC = [R_Comp_RugC1, R_Comp_RugC2, R_Comp_RugC3];
396 R1 = [R_Comp;R_RugF;R_RugC;R_Comp_RugF;R_Comp_RugC];
397 header1 = {'Comp'; 'RugF'; 'RugC'; 'Comp+RugF'; 'Comp+RugC'};
398 header2 = {' ', 'Contrast', 'Energy', 'Intensity'};
399 R = [header2; header1, num2cell(R1)];
```

Algorithm C.1: Matlab script in its entirety for Matlab analysis

Appendix D

Developed scripts for MVTec Halcon's image analysis

The present Appendix is meant to showcase the scripts that were developed for the image analysis performed in software MVTec Halcon. As it's been referred, two separate scripts were developed, one in Halcon for the image parameter's calculations, and one in Matlab for algebraic manipulation of the extracted image data.

D.1 MVTec Halcon's script

```
1 read_image (Image1 , ' 1.bmp ' )
2 read_image (Image2 , ' 2.bmp ' )
3 read_image (Image3 , ' 3.bmp ' )
4 read_image (Image4 , ' 4.bmp ' )
5 read_image (Image6 , ' 6.bmp ' )
6 read_image (Image7 , ' 7.bmp ' )
7 read_image (Image8 , ' 8.bmp ' )
8 read_image (Image9a , ' 9a.bmp ' )
9 read_image (Image9b , ' 9b.bmp ' )
10 read_image (Image10a , ' 10a.bmp ' )
11 read_image (Image10b , ' 10b.bmp ' )
12 read_image (Image11a , ' 11a.bmp ' )
13 read_image (Image11b , ' 11b.bmp ' )
14 gen_rectangle1 (Rectangle , 0.0 , 0.0 , 1050 , 800)
15 reduce_domain (Image1 , Rectangle , Mask1)
16 emphasize (Mask1 , Emphasize1 , 9 , 9 , 1.0)
17 reduce_domain (Image2 , Rectangle , Mask2)
18 emphasize (Mask2 , Emphasize2 , 9 , 9 , 1.0)
19 reduce_domain (Image3 , Rectangle , Mask3)
```

```
20 emphasize (Mask3 , Emphasize3 ,9 ,9 ,1.0)
21 reduce_domain (Image4 ,Rectangle ,Mask4)
22 emphasize (Mask4 , Emphasize4 ,9 ,9 ,1.0)
23 reduce_domain (Image6 ,Rectangle ,Mask6)
24 emphasize (Mask6 , Emphasize6 ,9 ,9 ,1.0)
25 reduce_domain (Image7 ,Rectangle ,Mask7)
26 emphasize (Mask7 , Emphasize7 ,9 ,9 ,1.0)
27 reduce_domain (Image8 ,Rectangle ,Mask8)
28 emphasize (Mask8 , Emphasize8 ,9 ,9 ,1.0)
29 reduce_domain (Image9a ,Rectangle ,Mask9a)
30 emphasize (Mask9a , Emphasize9a ,9 ,9 ,1.0)
31 reduce_domain (Image9b ,Rectangle ,Mask9b)
32 emphasize (Mask9b , Emphasize9b ,9 ,9 ,1.0)
33 reduce_domain (Image10a ,Rectangle ,Mask10a)
34 emphasize (Mask10a , Emphasize10a ,9 ,9 ,1.0)
35 reduce_domain (Image10b ,Rectangle ,Mask10b)
36 emphasize (Mask10b , Emphasize10b ,9 ,9 ,1.0)
37 reduce_domain (Image11a ,Rectangle ,Mask11a)
38 emphasize (Mask11a , Emphasize11a ,9 ,9 ,1.0)
39 reduce_domain (Image11b ,Rectangle ,Mask11b)
40 emphasize (Mask11b , Emphasize11b ,9 ,9 ,1.0)
41 intensity (Rectangle , Image1 , Mean1 , Deviation1)
42 intensity (Rectangle , Image2 , Mean2 , Deviation2)
43 intensity (Rectangle , Image3 , Mean3 , Deviation3)
44 intensity (Rectangle , Image4 , Mean4 , Deviation4)
45 intensity (Rectangle , Image6 , Mean6 , Deviation6)
46 intensity (Rectangle , Image7 , Mean7 , Deviation7)
47 intensity (Rectangle , Image8 , Mean8 , Deviation8)
48 intensity (Rectangle , Image9a , Mean9a , Deviation9a)
49 intensity (Rectangle , Image9b , Mean9b , Deviation9b)
50 intensity (Rectangle , Image10a , Mean10a , Deviation10a)
51 intensity (Rectangle , Image10b , Mean10b , Deviation10b)
52 intensity (Rectangle , Image11a , Mean11a , Deviation11a)
53 intensity (Rectangle , Image11b , Mean11b , Deviation11b)
54 gen_cooc_matrix (Rectangle , Image1 , Matrix01 , 8 , 0)
55 cooc_feature_matrix (Matrix01 , Energy01 , Correlation01 ,
    Homogeneity01 , Contrast01)
56 gen_cooc_matrix (Rectangle , Image1 , Matrix451 , 8 , 45)
57 cooc_feature_matrix (Matrix451 , Energy451 , Correlation451 ,
    Homogeneity451 , Contrast451)
```

```
58 gen_cooc_matrix(Rectangle , Image1 , Matrix901 , 8 , 90)
59 cooc_feature_matrix(Matrix901 , Energy901 , Correlation901 ,
    Homogeneity901 , Contrast901 )
60 gen_cooc_matrix(Rectangle , Image1 , Matrix1351 , 8 , 135)
61 cooc_feature_matrix(Matrix1351 , Energy1351 , Correlation1351 ,
    Homogeneity1351 , Contrast1351 )
62 Energy1 := (Energy01 + Energy451 + Energy901 + Energy1351)/4
63 Contrast1 := (Contrast01 + Contrast451 + Contrast901 +
    Contrast1351)/4
64 gen_cooc_matrix(Rectangle , Image2 , Matrix02 , 8 , 0)
65 cooc_feature_matrix(Matrix02 , Energy02 , Correlation02 ,
    Homogeneity02 , Contrast02 )
66 gen_cooc_matrix(Rectangle , Image2 , Matrix452 , 8 , 45)
67 cooc_feature_matrix(Matrix452 , Energy452 , Correlation452 ,
    Homogeneity452 , Contrast452 )
68 gen_cooc_matrix(Rectangle , Image2 , Matrix902 , 8 , 90)
69 cooc_feature_matrix(Matrix902 , Energy902 , Correlation902 ,
    Homogeneity902 , Contrast902 )
70 gen_cooc_matrix(Rectangle , Image2 , Matrix1352 , 8 , 135)
71 cooc_feature_matrix(Matrix1352 , Energy1352 , Correlation1352 ,
    Homogeneity1352 , Contrast1352 )
72 Energy2 := (Energy02 + Energy452 + Energy902 + Energy1352)/4
73 Contrast2 := (Contrast02 + Contrast452 + Contrast902 +
    Contrast1352)/4
74 gen_cooc_matrix(Rectangle , Image3 , Matrix03 , 8 , 0)
75 cooc_feature_matrix(Matrix03 , Energy03 , Correlation03 ,
    Homogeneity03 , Contrast03 )
76 gen_cooc_matrix(Rectangle , Image3 , Matrix453 , 8 , 45)
77 cooc_feature_matrix(Matrix453 , Energy453 , Correlation453 ,
    Homogeneity453 , Contrast453 )
78 gen_cooc_matrix(Rectangle , Image3 , Matrix903 , 8 , 90)
79 cooc_feature_matrix(Matrix903 , Energy903 , Correlation903 ,
    Homogeneity903 , Contrast903 )
80 gen_cooc_matrix(Rectangle , Image3 , Matrix1353 , 8 , 135)
81 cooc_feature_matrix(Matrix1353 , Energy1353 , Correlation1353 ,
    Homogeneity1353 , Contrast1353 )
82 Energy3 := (Energy03 + Energy453 + Energy903 + Energy1353)/4
83 Contrast3 := (Contrast03 + Contrast453 + Contrast903 +
    Contrast1353)/4
84 gen_cooc_matrix(Rectangle , Image4 , Matrix04 , 8 , 0)
```

```
85 cooc_feature_matrix(Matrix04 , Energy04 , Correlation04 ,  
    Homogeneity04 , Contrast04 )  
86 gen_cooc_matrix( Rectangle , Image4 , Matrix454 , 8 , 45 )  
87 cooc_feature_matrix(Matrix454 , Energy454 , Correlation454 ,  
    Homogeneity454 , Contrast454 )  
88 gen_cooc_matrix( Rectangle , Image4 , Matrix904 , 8 , 90 )  
89 cooc_feature_matrix(Matrix904 , Energy904 , Correlation904 ,  
    Homogeneity904 , Contrast904 )  
90 gen_cooc_matrix( Rectangle , Image4 , Matrix1354 , 8 , 135 )  
91 cooc_feature_matrix(Matrix1354 , Energy1354 , Correlation1354 ,  
    Homogeneity1354 , Contrast1354 )  
92 Energy4 := ( Energy04 + Energy454 + Energy904 + Energy1354 )/4  
93 Contrast4 := ( Contrast04 + Contrast451 + Contrast901 +  
    Contrast1351 )/4  
94 gen_cooc_matrix( Rectangle , Image6 , Matrix06 , 8 , 0 )  
95 cooc_feature_matrix(Matrix06 , Energy06 , Correlation06 ,  
    Homogeneity06 , Contrast06 )  
96 gen_cooc_matrix( Rectangle , Image6 , Matrix456 , 8 , 45 )  
97 cooc_feature_matrix(Matrix456 , Energy456 , Correlation456 ,  
    Homogeneity456 , Contrast456 )  
98 gen_cooc_matrix( Rectangle , Image6 , Matrix906 , 8 , 90 )  
99 cooc_feature_matrix(Matrix906 , Energy906 , Correlation906 ,  
    Homogeneity906 , Contrast906 )  
100 gen_cooc_matrix( Rectangle , Image6 , Matrix1356 , 8 , 135 )  
101 cooc_feature_matrix(Matrix1356 , Energy1356 , Correlation1356 ,  
    Homogeneity1356 , Contrast1356 )  
102 Energy6 := ( Energy06 + Energy456 + Energy906 + Energy1356 )/4  
103 Contrast6 := ( Contrast06 + Contrast456 + Contrast906 +  
    Contrast1356 )/4  
104 gen_cooc_matrix( Rectangle , Image7 , Matrix07 , 8 , 0 )  
105 cooc_feature_matrix(Matrix07 , Energy07 , Correlation07 ,  
    Homogeneity07 , Contrast07 )  
106 gen_cooc_matrix( Rectangle , Image7 , Matrix457 , 8 , 45 )  
107 cooc_feature_matrix(Matrix457 , Energy457 , Correlation457 ,  
    Homogeneity457 , Contrast457 )  
108 gen_cooc_matrix( Rectangle , Image7 , Matrix907 , 8 , 90 )  
109 cooc_feature_matrix(Matrix907 , Energy907 , Correlation907 ,  
    Homogeneity907 , Contrast907 )  
110 gen_cooc_matrix( Rectangle , Image7 , Matrix1357 , 8 , 135 )
```



```
111 cooc_feature_matrix(Matrix1357, Energy1357, Correlation1357,
    Homogeneity1357, Contrast1357)
112 Energy7 := (Energy07 + Energy457 + Energy907 + Energy1357)/4
113 Contrast7 := (Contrast07 + Contrast457 + Contrast907 +
    Contrast1357)/4
114 gen_cooc_matrix(Rectangle, Image8, Matrix08, 8, 0)
115 cooc_feature_matrix(Matrix08, Energy08, Correlation08,
    Homogeneity08, Contrast08)
116 gen_cooc_matrix(Rectangle, Image8, Matrix458, 8, 45)
117 cooc_feature_matrix(Matrix458, Energy458, Correlation458,
    Homogeneity458, Contrast458)
118 gen_cooc_matrix(Rectangle, Image8, Matrix908, 8, 90)
119 cooc_feature_matrix(Matrix908, Energy908, Correlation908,
    Homogeneity908, Contrast908)
120 gen_cooc_matrix(Rectangle, Image8, Matrix1358, 8, 135)
121 cooc_feature_matrix(Matrix1358, Energy1358, Correlation1358,
    Homogeneity1358, Contrast1358)
122 Energy8 := (Energy08 + Energy458 + Energy908 + Energy1358)/4
123 Contrast8 := (Contrast08 + Contrast458 + Contrast908 +
    Contrast1358)/4
124 gen_cooc_matrix(Rectangle, Image9a, Matrix09a, 8, 0)
125 cooc_feature_matrix(Matrix09a, Energy09a, Correlation09a,
    Homogeneity09a, Contrast09a)
126 gen_cooc_matrix(Rectangle, Image9a, Matrix459a, 8, 45)
127 cooc_feature_matrix(Matrix459a, Energy459a, Correlation459a,
    Homogeneity459a, Contrast459a)
128 gen_cooc_matrix(Rectangle, Image9a, Matrix909a, 8, 90)
129 cooc_feature_matrix(Matrix909a, Energy909a, Correlation909a,
    Homogeneity909a, Contrast909a)
130 gen_cooc_matrix(Rectangle, Image9a, Matrix1359a, 8, 135)
131 cooc_feature_matrix(Matrix1359a, Energy1359a, Correlation1359a,
    Homogeneity1359a, Contrast1359a)
132 Energy9a := (Energy09a + Energy459a + Energy909a +
    Energy1359a)/4
133 Contrast9a := (Contrast09a + Contrast459a + Contrast909a +
    Contrast1359a)/4
134 gen_cooc_matrix(Rectangle, Image9b, Matrix09b, 8, 0)
135 cooc_feature_matrix(Matrix09b, Energy09b, Correlation09b,
    Homogeneity09b, Contrast09b)
136 gen_cooc_matrix(Rectangle, Image9b, Matrix459b, 8, 45)
```

```
137 cooc_feature_matrix(Matrix459b, Energy459b, Correlation459b ,  
    Homogeneity459b, Contrast459b)  
138 gen_cooc_matrix(Rectangle, Image9b, Matrix909b, 8, 90)  
139 cooc_feature_matrix(Matrix909b, Energy909b, Correlation909b ,  
    Homogeneity909b, Contrast909b)  
140 gen_cooc_matrix(Rectangle, Image9b, Matrix1359b, 8, 135)  
141 cooc_feature_matrix(Matrix1359b, Energy1359b, Correlation1359b ,  
    Homogeneity1359b, Contrast1359b)  
142 Energy9b := (Energy09b + Energy459b + Energy909b +  
    Energy1359b)/4  
143 Contrast9b := (Contrast09b + Contrast459b + Contrast909b +  
    Contrast1359b)/4  
144 gen_cooc_matrix(Rectangle, Image10a, Matrix010a, 8, 0)  
145 cooc_feature_matrix(Matrix010a, Energy010a, Correlation010a ,  
    Homogeneity010a, Contrast010a)  
146 gen_cooc_matrix(Rectangle, Image10a, Matrix4510a, 8, 45)  
147 cooc_feature_matrix(Matrix4510a, Energy4510a, Correlation4510a ,  
    Homogeneity4510a, Contrast4510a)  
148 gen_cooc_matrix(Rectangle, Image10a, Matrix9010a, 8, 90)  
149 cooc_feature_matrix(Matrix9010a, Energy9010a, Correlation9010a ,  
    Homogeneity9010a, Contrast9010a)  
150 gen_cooc_matrix(Rectangle, Image10a, Matrix13510a, 8, 135)  
151 cooc_feature_matrix(Matrix13510a, Energy13510a ,  
    Correlation13510a, Homogeneity13510a, Contrast13510a)  
152 Energy10a := (Energy010a + Energy4510a + Energy9010a +  
    Energy13510a)/4  
153 Contrast10a := (Contrast010a + Contrast4510a + Contrast9010a +  
    Contrast13510a)/4  
154 gen_cooc_matrix(Rectangle, Image10b, Matrix010b, 8, 0)  
155 cooc_feature_matrix(Matrix010b, Energy010b, Correlation010b ,  
    Homogeneity010b, Contrast010b)  
156 gen_cooc_matrix(Rectangle, Image10b, Matrix4510b, 8, 45)  
157 cooc_feature_matrix(Matrix4510b, Energy4510b, Correlation4510b ,  
    Homogeneity4510b, Contrast4510b)  
158 gen_cooc_matrix(Rectangle, Image10b, Matrix9010b, 8, 90)  
159 cooc_feature_matrix(Matrix9010b, Energy9010b, Correlation9010b ,  
    Homogeneity9010b, Contrast9010b)  
160 gen_cooc_matrix(Rectangle, Image10b, Matrix13510b, 8, 135)  
161 cooc_feature_matrix(Matrix13510b, Energy13510b ,  
    Correlation13510b, Homogeneity13510b, Contrast13510b)
```

```
162 Energy10b := (Energy010b + Energy4510b + Energy9010b +
    Energy13510b)/4
163 Contrast10b := (Contrast010b + Contrast4510b + Contrast9010b +
    Contrast13510b)/4
164 gen_cooc_matrix(Rectangle, Image11a, Matrix011a, 8, 0)
165 cooc_feature_matrix(Matrix011a, Energy011a, Correlation011a,
    Homogeneity011a, Contrast011a)
166 gen_cooc_matrix(Rectangle, Image11a, Matrix4511a, 8, 45)
167 cooc_feature_matrix(Matrix4511a, Energy4511a, Correlation4511a,
    Homogeneity4511a, Contrast4511a)
168 gen_cooc_matrix(Rectangle, Image11a, Matrix9011a, 8, 90)
169 cooc_feature_matrix(Matrix9011a, Energy9011a, Correlation9011a,
    Homogeneity9011a, Contrast9011a)
170 gen_cooc_matrix(Rectangle, Image11a, Matrix13511a, 8, 135)
171 cooc_feature_matrix(Matrix13511a, Energy13511a,
    Correlation13511a, Homogeneity13511a, Contrast13511a)
172 Energy11a := (Energy011a + Energy4511a + Energy9011a +
    Energy13511a)/4
173 Contrast11a := (Contrast011a + Contrast4511a + Contrast9011a +
    Contrast13511a)/4
174 gen_cooc_matrix(Rectangle, Image11b, Matrix011b, 8, 0)
175 cooc_feature_matrix(Matrix011b, Energy011b, Correlation011b,
    Homogeneity011b, Contrast011b)
176 gen_cooc_matrix(Rectangle, Image11b, Matrix4511b, 8, 45)
177 cooc_feature_matrix(Matrix4511b, Energy4511b, Correlation4511b,
    Homogeneity4511b, Contrast4511b)
178 gen_cooc_matrix(Rectangle, Image11b, Matrix9011b, 8, 90)
179 cooc_feature_matrix(Matrix9011b, Energy9011b, Correlation9011b,
    Homogeneity9011b, Contrast9011b)
180 gen_cooc_matrix(Rectangle, Image11b, Matrix13511b, 8, 135)
181 cooc_feature_matrix(Matrix13511b, Energy13511b,
    Correlation13511b, Homogeneity13511b, Contrast13511b)
182 Energy11b := (Energy011b + Energy4511b + Energy9011b +
    Energy13511b)/4
183 Contrast11b := (Contrast011b + Contrast4511b + Contrast9011b +
    Contrast13511b)/4
184 Energy := [Energy1, Energy2, Energy3, Energy4, Energy6,
    Energy7, Energy8, Energy9a, Energy9b, Energy10a, Energy10b,
    Energy11a, Energy11b]
185 write_tuple(Energy, 'Energy')
```

```

186 Contrast := [Contrast1 , Contrast2 , Contrast3 , Contrast4 ,
              Contrast6 , Contrast7 , Contrast8 , Contrast9a , Contrast9b ,
              Contrast10a , Contrast10b , Contrast11a , Contrast11b]
187 write_tuple(Contrast , 'Contrast')
188 Intensity := [Mean1 , Mean2 , Mean3 , Mean4 , Mean6 , Mean7 , Mean8 ,
              Mean9a , Mean9b , Mean10a , Mean10b , Mean11a , Mean11b]
189 write_tuple(Intensity , 'Intensity')

```

Algorithm D.1: Halcon script in its entirety for MVTec's Halcon analysis

D.2 Matlab's script

```

1 %%
2 clear ;
3 close ;
4 %% Copy of the Halcon generated files
5 formatSpec = '%f';
6 fileID1 = fopen('Contrast', 'r');
7 sizeContrast_1 = [2 Inf];
8 Contrast_1 = fscanf(fileID1 ,formatSpec ,sizeContrast_1);
9 Contrast_1 = Contrast_1';
10 fclose(fileID1);
11 fileID2 = fopen('Energy', 'r');
12 sizeEnergy_1 = [2 Inf];
13 Energy_1 = fscanf(fileID2 ,formatSpec ,sizeEnergy_1);
14 Energy_1 = Energy_1';
15 fclose(fileID2);
16 fileID3 = fopen('Intensity', 'r');
17 sizeIntensity_1 = [2 Inf];
18 Intensity_1 = fscanf(fileID3 ,formatSpec ,sizeIntensity_1);
19 Intensity_1 = Intensity_1';
20 fclose(fileID3);
21 %% Parameter's values extraction
22 Contrast = Contrast_1(2:14,1);
23 Energy = Energy_1(2:14,1);
24 Intensity = Intensity_1(2:14,1);
25 Roughness = [0.8; 1.6; 3.2; 6.3; 12.5; 25; 25; 40; 70; 100];
26 Roughness_Comp = Roughness(6:9);
27 Roughness_RugF = Roughness(1:6);
28 Roughness_RugC = Roughness(1:6);
29 %% Concatenating Parameter Vectors

```

```

30 % Contrast
31 Contrast_Comp = Contrast(1:4,:); % Comparator
32 Contrast_RugC = [Contrast(5); Contrast(6); Contrast(7);
    Contrast(8); Contrast(10); Contrast(12)]; % Rugotest Coarse
33 Contrast_RugF = [Contrast(5); Contrast(6); Contrast(7);
    Contrast(9); Contrast(11); Contrast(13)]; % Rugotest Fine
34 Contrast_Comp_RugC = [Contrast_RugC; Contrast_Comp]; %
    Comparator + Rugotest Coarse
35 Contrast_Comp_RugF = [Contrast_RugF; Contrast_Comp]; %
    Comparator + Rugotest Fine
36 % Energy
37 Energy_Comp = Energy(1:4,:); % Comparator
38 Energy_RugC = [Energy(5); Energy(6); Energy(7); Energy(8);
    Energy(10); Energy(12)]; % Rugotest Coarse
39 Energy_RugF = [Energy(5); Energy(6); Energy(7); Energy(9);
    Energy(11); Energy(13)]; % Rugotest Fine
40 Energy_Comp_RugC = [Energy_RugC; Energy_Comp]; % Comparator +
    Rugotest Coarse
41 Energy_Comp_RugF = [Energy_RugF; Energy_Comp]; % Comparator +
    Rugotest Fine
42 % Intensity
43 Intensity_Comp = Intensity(1:4,:); % Comparator
44 Intensity_RugC = [Intensity(5); Intensity(6); Intensity(7);
    Intensity(8); Intensity(10); Intensity(12)]; % Rugotest
    Coarse
45 Intensity_RugF = [Intensity(5); Intensity(6); Intensity(7);
    Intensity(9); Intensity(11); Intensity(13)]; % Rugotest Fine
46 Intensity_Comp_RugC = [Intensity_RugC; Intensity_Comp]; %
    Comparator + Rugotest Coarse
47 Intensity_Comp_RugF = [Intensity_RugF; Intensity_Comp]; %
    Comparator + Rugotest Fine
48 %% Roughness - Intensity Graph Plot
49 figure(1)
50 plot(Roughness_Comp, Intensity_Comp);
51 xlabel('Roughness');
52 ylabel('Intensity');
53 title('Comparator: Roughness - Intensity');
54 figure(2)
55 plot(Roughness_RugC, Intensity_RugC);
56 xlabel('Roughness');

```

```
57 ylabel('Intensity');
58 title('Rugotest, Coarse: Roughness - Intensity');
59 figure(3)
60 plot(Roughness_RugF, Intensity_RugF);
61 xlabel('Roughness');
62 ylabel('Intensity');
63 title('Rugotest, Fine: Roughness - Intensity');
64 figure(4)
65 plot(Roughness, Intensity_Comp_RugC);
66 xlabel('Roughness');
67 ylabel('Intensity');
68 title('Comparator + Rugotest, Coarse: Roughness - Intensity');
69 figure(5)
70 plot(Roughness, Intensity_Comp_RugF);
71 xlabel('Roughness');
72 ylabel('Intensity');
73 title('Comparator + Rugotest, Fine: Roughness - Intensity');
74 %% Roughness - Contrast Graph Plot
75 figure(5)
76 plot(Roughness_Comp, Contrast_Comp);
77 xlabel('Roughness');
78 ylabel('Contrast');
79 title('Comparator: Roughness - Contrast');
80 figure(6)
81 plot(Roughness_RugC, Contrast_RugC);
82 xlabel('Roughness');
83 ylabel('Contrast');
84 title('Rugotest, Coarse: Roughness - Contrast');
85 figure(7)
86 plot(Roughness_RugF, Contrast_RugF);
87 xlabel('Roughness');
88 ylabel('Contrast');
89 title('Rugotest, Fine: Roughness - Contrast');
90 figure(8)
91 plot(Roughness, Contrast_Comp_RugC);
92 xlabel('Roughness');
93 ylabel('Contrast');
94 title('Comparator + Rugotest, Coarse: Roughness - Contrast');
95 figure(9)
96 plot(Roughness, Contrast_Comp_RugF);
```

```
97 xlabel('Roughness');
98 ylabel('Contrast');
99 title('Comparator + Rugotest, Fine: Roughness - Contrast');
100 %% Roughness - Energy Graph Plot
101 figure(10)
102 plot(Roughness_Comp, Energy_Comp);
103 xlabel('Roughness');
104 ylabel('Energy');
105 title('Comparator: Roughness - Energy');
106 figure(11)
107 plot(Roughness_RugC, Energy_RugC);
108 xlabel('Roughness');
109 ylabel('Energy');
110 title('Rugotest, Coarse: Roughness - Energy');
111 figure(12)
112 plot(Roughness_RugF, Energy_RugF);
113 xlabel('Roughness');
114 ylabel('Energy');
115 title('Rugotest, Fine: Roughness - Energy');
116 figure(13)
117 plot(Roughness, Energy_Comp_RugC);
118 xlabel('Roughness');
119 ylabel('Energy');
120 title('Comparator + Rugotest, Coarse: Roughness - Energy');
121 figure(14)
122 plot(Roughness, Energy_Comp_RugF);
123 xlabel('Roughness');
124 ylabel('Energy');
125 title('Comparator + Rugotest, Fine: Roughness - Energy');
126 %% Linear Regression Analysis for Comparator
127 % Contrast
128 X_Comp1 = [ones(length(Roughness_Comp),1) Roughness_Comp];
129 b_Comp1 = X_Comp1 \ Contrast_Comp;
130 yCalc_Comp1 = X_Comp1 * b_Comp1;
131 figure(15)
132 scatter(Roughness_Comp, Contrast_Comp);
133 hold on
134 plot(Roughness_Comp, yCalc_Comp1);
135 xlabel('Roughness');
136 ylabel('Contrast');
```

```

137 title('Roughness-Contrast');
138 grid on
139 R_Comp1 = 1 - sum((Contrast_Comp - yCalc_Comp1).^2) /
    sum((Contrast_Comp - mean(Contrast_Comp)).^2);
140 % Energy
141 X_Comp2 = [ones(length(Roughness_Comp),1) Roughness_Comp];
142 b_Comp2 = X_Comp2\Energy_Comp;
143 yCalc_Comp2 = X_Comp2*b_Comp2;
144 figure(16)
145 scatter(Roughness_Comp, Energy_Comp);
146 hold on
147 plot(Roughness_Comp, yCalc_Comp2);
148 xlabel('Roughness');
149 ylabel('Energy');
150 title('Roughness-Energy');
151 grid on
152 R_Comp2 = 1 - sum((Energy_Comp - yCalc_Comp2).^2) /
    sum((Energy_Comp - mean(Energy_Comp)).^2);
153 % Intensity
154 X_Comp3 = [ones(length(Roughness_Comp),1) Roughness_Comp];
155 b_Comp3 = X_Comp3\Intensity_Comp;
156 yCalc_Comp3 = X_Comp3*b_Comp3;
157 figure(17)
158 scatter(Roughness_Comp, Intensity_Comp);
159 hold on
160 plot(Roughness_Comp, yCalc_Comp3);
161 xlabel('Roughness');
162 ylabel('Intensity');
163 title('Roughness-Intensity');
164 grid on
165 R_Comp3 = 1 - sum((Intensity_Comp - yCalc_Comp3).^2) /
    sum((Intensity_Comp - mean(Intensity_Comp)).^2);
166 R_Comp = [R_Comp1, R_Comp2, R_Comp3];
167 %% Linear Regression Analysis for Rugotest Fine
168 % Contrast
169 X_RugF1 = [ones(length(Roughness_RugF),1) Roughness_RugF];
170 b_RugF1 = X_RugF1\Contrast_RugF;
171 yCalc_RugF1 = X_RugF1*b_RugF1;
172 figure(18)
173 scatter(Roughness_RugF, Contrast_RugF);

```



```

174 hold on
175 plot(Roughness_RugF , yCalc_RugF1);
176 xlabel('Roughness');
177 ylabel('Contrast');
178 title('Roughness-Contrast');
179 grid on
180 R_RugF1 = 1 - sum((Contrast_RugF - yCalc_RugF1).^2) /
    sum((Contrast_RugF - mean(Contrast_RugF)).^2);
181 % Energy
182 X_RugF2 = [ones(length(Roughness_RugF),1) Roughness_RugF];
183 b_RugF2 = X_RugF2\Energy_RugF;
184 yCalc_RugF2 = X_RugF2*b_RugF2;
185 figure(19)
186 scatter(Roughness_RugF , Energy_RugF);
187 hold on
188 plot(Roughness_RugF , yCalc_RugF2);
189 xlabel('Roughness');
190 ylabel('Energy');
191 title('Roughness-Energy');
192 grid on
193 R_RugF2 = 1 - sum((Energy_RugF - yCalc_RugF2).^2) /
    sum((Energy_RugF - mean(Energy_RugF)).^2);
194 %Intensity
195 X_RugF3 = [ones(length(Roughness_RugF),1) Roughness_RugF];
196 b_RugF3 = X_RugF3\Intensity_RugF;
197 yCalc_RugF3 = X_RugF3*b_RugF3;
198 figure(20)
199 scatter(Roughness_RugF , Intensity_RugF);
200 hold on
201 plot(Roughness_RugF , yCalc_RugF3);
202 xlabel('Roughness');
203 ylabel('Intensity');
204 title('Roughness-Intensity');
205 grid on
206 R_RugF3 = 1 - sum((Intensity_RugF - yCalc_RugF3).^2) /
    sum((Intensity_RugF - mean(Intensity_RugF)).^2);
207 R_RugF = [R_RugF1, R_RugF2, R_RugF3];
208 %% Linear Regression Analysis for Rugotest Coarse
209 % Contrast
210 X_RugC1 = [ones(length(Roughness_RugC),1) Roughness_RugC];

```

```
211 b_RugC1 = X_RugC1\Contrast_RugC ;
212 yCalc_RugC1 = X_RugC1*b_RugC1;
213 figure (21)
214 scatter (Roughness_RugC , Contrast_RugC );
215 hold on
216 plot (Roughness_RugC , yCalc_RugC1);
217 xlabel ( 'Roughness' );
218 ylabel ( 'Contrast' );
219 title ( 'Roughness-Contrast' );
220 grid on
221 R_RugC1 = 1 - sum((Contrast_RugC - yCalc_RugC1).^2) /
    sum((Contrast_RugC - mean(Contrast_RugC)).^2);
222 % Energy
223 X_RugC2 = [ones(length(Roughness_RugC),1) Roughness_RugC];
224 b_RugC2 = X_RugC2\Energy_RugC;
225 yCalc_RugC2 = X_RugC2*b_RugC2;
226 figure (22)
227 scatter (Roughness_RugC , Energy_RugC );
228 hold on
229 plot (Roughness_RugC , yCalc_RugC2);
230 xlabel ( 'Roughness' );
231 ylabel ( 'Energy' );
232 title ( 'Roughness-Energy' );
233 grid on
234 R_RugC2 = 1 - sum((Energy_RugC - yCalc_RugC2).^2) /
    sum((Energy_RugC - mean(Energy_RugC)).^2);
235 %Intensity
236 X_RugC3 = [ones(length(Roughness_RugC),1) Roughness_RugC];
237 b_RugC3 = X_RugC3\Intensity_RugC;
238 yCalc_RugC3 = X_RugC3*b_RugC3;
239 figure (23)
240 scatter (Roughness_RugC , Intensity_RugC );
241 hold on
242 plot (Roughness_RugC , yCalc_RugC3);
243 xlabel ( 'Roughness' );
244 ylabel ( 'Intensity' );
245 title ( 'Roughness-Intensity' );
246 grid on
247 R_RugC3 = 1 - sum((Intensity_RugC - yCalc_RugC3).^2) /
    sum((Intensity_RugC - mean(Intensity_RugC)).^2);
```

```

248 R_RugC = [R_RugC1, R_RugC2, R_RugC3];
249 %% Linear Regression Analysis for Comparator + Rugotest Fine
250 % Contrast
251 X_Comp_RugF1 = [ones(length(Roughness),1) Roughness];
252 b_Comp_RugF1 = X_Comp_RugF1 \ Contrast_Comp_RugF;
253 yCalc_Comp_RugF1 = X_Comp_RugF1 * b_Comp_RugF1;
254 figure(24)
255 scatter(Roughness, Contrast_Comp_RugF);
256 hold on
257 plot(Roughness, yCalc_Comp_RugF1);
258 xlabel('Roughness');
259 ylabel('Contrast');
260 title('Roughness-Contrast');
261 grid on
262 R_Comp_RugF1 = 1 - sum((Contrast_Comp_RugF -
    yCalc_Comp_RugF1).^2) / sum((Contrast_Comp_RugF -
    mean(Contrast_Comp_RugF)).^2);
263 % Energy
264 X_Comp_RugF2 = [ones(length(Roughness),1) Roughness];
265 b_Comp_RugF2 = X_Comp_RugF2 \ Energy_Comp_RugF;
266 yCalc_Comp_RugF2 = X_Comp_RugF2 * b_Comp_RugF2;
267 figure(25)
268 scatter(Roughness, Energy_Comp_RugF);
269 hold on
270 plot(Roughness_Comp_RugF, yCalc_Comp_RugF2);
271 xlabel('Roughness');
272 ylabel('Energy');
273 title('Roughness-Energy');
274 grid on
275 R_Comp_RugF2 = 1 - sum((Energy_Comp_RugF -
    yCalc_Comp_RugF2).^2) / sum((Energy_Comp_RugF -
    mean(Energy_Comp_RugF)).^2);
276 % Intensity
277 X_Comp_RugF3 = [ones(length(Roughness),1) Roughness];
278 b_Comp_RugF3 = X_Comp_RugF3 \ Intensity_Comp_RugF;
279 yCalc_Comp_RugF3 = X_Comp_RugF3 * b_Comp_RugF3;
280 figure(26)
281 scatter(Roughness, Intensity_Comp_RugF);
282 hold on
283 plot(Roughness_Comp_RugF, yCalc_Comp_RugF3);

```

```

284 xlabel('Roughness');
285 ylabel('Intensity');
286 title('Roughness-Intensity');
287 grid on
288 R_Comp_RugF3 = 1 - sum((Intensity_Comp_RugF -
    yCalc_Comp_RugF3).^2) / sum((Intensity_Comp_RugF -
    mean(Intensity_Comp_RugF)).^2);
289 R_Comp_RugF = [R_Comp_RugF1, R_Comp_RugF2, R_Comp_RugF3];
290 %% Linear Regression Analysis for Comparator + Rugotest Coarse
291 % Contrast
292 X_Comp_RugC1 = [ones(length(Roughness),1) Roughness];
293 b_Comp_RugC1 = X_Comp_RugC1 \ Contrast_Comp_RugC;
294 yCalc_Comp_RugC1 = X_Comp_RugC1 * b_Comp_RugC1;
295 figure(27)
296 scatter(Roughness, Contrast_Comp_RugC);
297 hold on
298 plot(Roughness, yCalc_Comp_RugC1);
299 xlabel('Roughness');
300 ylabel('Contrast');
301 title('Roughness-Contrast');
302 grid on
303 R_Comp_RugC1 = 1 - sum((Contrast_Comp_RugC -
    yCalc_Comp_RugC1).^2) / sum((Contrast_Comp_RugC -
    mean(Contrast_Comp_RugC)).^2);
304 % Energy
305 X_Comp_RugC2 = [ones(length(Roughness),1) Roughness];
306 b_Comp_RugC2 = X_Comp_RugC2 \ Energy_Comp_RugC;
307 yCalc_Comp_RugC2 = X_Comp_RugC2 * b_Comp_RugC2;
308 figure(28)
309 scatter(Roughness, Energy_Comp_RugC);
310 hold on
311 plot(Roughness_Comp_RugC, yCalc_Comp_RugC2);
312 xlabel('Roughness');
313 ylabel('Energy');
314 title('Roughness-Energy');
315 grid on
316 R_Comp_RugC2 = 1 - sum((Energy_Comp_RugC -
    yCalc_Comp_RugC2).^2) / sum((Energy_Comp_RugC -
    mean(Energy_Comp_RugC)).^2);
317 % Intensity

```

```
318 X_Comp_RugC3 = [ones(length(Roughness),1) Roughness];
319 b_Comp_RugC3 = X_Comp_RugC3 \ Intensity_Comp_RugC;
320 yCalc_Comp_RugC3 = X_Comp_RugC3 * b_Comp_RugC3;
321 figure(29)
322 scatter(Roughness, Intensity_Comp_RugC);
323 hold on
324 plot(Roughness_Comp_RugC, yCalc_Comp_RugC3);
325 xlabel('Roughness');
326 ylabel('Intensity');
327 title('Roughness-Intensity');
328 grid on
329 R_Comp_RugC3 = 1 - sum((Intensity_Comp_RugC -
    yCalc_Comp_RugC3).^2) / sum((Intensity_Comp_RugC -
    mean(Intensity_Comp_RugC)).^2);
330 R_Comp_RugC = [R_Comp_RugC1, R_Comp_RugC2, R_Comp_RugC3];
331 R1 = [R_Comp; R_RugF; R_RugC; R_Comp_RugF; R_Comp_RugC];
332 header1 = {'Comp'; 'RugF'; 'RugC'; 'Comp+RugF'; 'Comp+RugC'};
333 header2 = {' ', 'Contrast', 'Energy', 'Intensity'};
334 R = [header2; header1, num2cell(R1)];
```

Algorithm D.2: Matlab script in its entirety for MVTec's Halcon analysis